Interactive comment on "Mobile MAX-DOAS observations of tropospheric NO_2 and HCHO during summer over the Three Rivers' Source region in China" *by* Siyang Cheng et al.: Authors' Response

We thank the editor for handing this manuscript and the two anonymous referees for their insightful comments and constructive suggestions on our manuscript. Below are our point-to-point responses to the comments from each referee. Also enclosed is the revised version of the manuscript, marked up using revision track. Note that the Sections 4.2 (Temporal variation) and 4.3 (Spatial distribution) in the original manuscript were reorganized into Section 4.2 (Spatio-temporal variation) in the revised manuscript, suggested by Referee #2. This change is not marked up using revision track in order to keep the manuscript clear to read.

Interactive comment on "Mobile MAX-DOAS observations of tropospheric NO_2 and HCHO during summer over the Three Rivers' Source region in China" *by* Siyang Cheng et al.: Reply to Anonymous Referee #1

Referee comments are in black. Author responses are in blue.

This manuscript describes mobile MAX-DOAS measurements recorded on drives around the Tibetan Plateau. The measurements are used to quantify the column of NO_2 and HCHO along circular drive paths on the Plateau. The measurements are compared to TROPOMI satellite products. The manuscript represents a valuable contribution to the literature and reports ground truth around this relatively remote and high-altitude region. The manuscript uses the geometric method to retrieve tropospheric vertical column densities from differential slant column densities measured on the vehicle. This method, while lacking the refinement of one using radiative transfer calculations, is reasonable for this purpose. However there are some details on the method that should be discussed further and it would be valuable for other groups to understand how to optimize the measurements to get the most measurements from such studies. Concerns on the method are described below, followed by specific comments. If the concerns regarding the method can be addressed, this manuscript would be acceptable for publication in ACP.

Reply: First of all, we appreciate the reviewer's positive comments on our manuscript. In response to the reviewer's comments and suggestions, we have made relevant revisions to the manuscript. Listed below are our responses and the corresponding changes made to the manuscript according to the suggestions given by the reviewer. Note that the Sections 4.2 (Temporal variation) and 4.3 (Spatial distribution) in the original manuscript were reorganized into Section 4.2 (Spatio-temporal variation) in the revised manuscript. This change is not marked up using revision track in order to keep the manuscript clear to read.

Were the elevation angles recorded relative to the mobile vehicle or to gravity? If they were gravitationally referenced, was a gyroscope used? If they are relative to the road, how is the local horizon taken into consideration? I think lines 260-265 indicate that the angles are with respect to the vehicle, and that is a reason to use

higher elevation angles, but the text is not very clear to this regard. Can the authors be more clear about how the view geometry is defined?

Reply: The elevation angles were recorded relative to the mobile vehicle. We didn't use a gyroscope. During our deployment strategies, we designed a partial system recording the attitude angles of the mobile vehicle to correct the elevation angle of MAX-DOAS measurements. However, it did not work well and couldn't be used for this study. To reduce the influences of local non-horizontal road on the un-corrected elevation angle, we used the DSCDs at larger elevation angles. Also, the VCDs were further filtered based on the absolute difference and the relative difference of VCDs between 15 ° and 20 °. The definition of elevation angle has been added to the text in Section 2.1 of the revised manuscript.

As is pointed out by the authors, the higher altitude and lower aerosol extinction conditions of a sparsely populated plateau make the geometric approach more tenable. However, clouds or aerosol-particle-rich pollution plumes (which may accompany NO2) may affect this assumption. Therefore, it seems reasonable to check this assumption by using O4 observations. The authors could calculate the O4 VCD above the vehicle from the altitude (which they know) and pressures at meteorological stations (or better soundings if available). They can then use the mobile-measured geometrically calculated O4 VCD_15 to compare to the meteorologically calculated one. Due to radiative transfer effects, particularly the relative azimuth angle to the sun, these quantities won't be perfect, but times when there is a large amount of aerosol or clouds or the view azimuth happened to be close to the sun, one could tell that the NO2 and HCHO data are being affected by these confounding effects. This check should help to assure that the geometric method is working for NO2 and HCHO.

Reply: Many thanks for your suggestions. The procedures of O_4 VCDs derived from MAX-DOAS measurements and calculations are as the following.

(1) The O_4 DSCDs were retrieved from MAX-DOAS spectra in the wavelength interval of 351-390 nm using a sequential FRS and are then filtered by the conditions of SZA <80 °, RMS < 0.005, offset (constant) between ± 0.03. The O_4 VCDs obtained by the geometric approximation method at 15 ° elevation angle were further filtered by the differences of the O_4 VCDs between 15 ° and 20 °. The O_4 VCDs were kept if the

absolute difference of VCDs between 15 ° and 20 ° is < 1×10^{42} molec^2 cm^{-5} or the relative difference is <10%.

(2) During the procedure of the O_4 VCD calculation, we used the air temperature and pressure profiles of hourly ERA5 with 0.25 °×0.25 ° grid above the altitude of the driving route. Firstly, we extracted the profiles of temperature and pressure matched with each measurement at the same grid cell and the same hour. Then we calculated the O_2 concentrations from the surface to 30 km at each altitude with a vertical interval of 50m. The O_4 concentrations were assumed as the square of the O_2 concentrations at each vertical grid cell and integrated as O_4 VCDs from the surface to 30 km (Wagner et al., 2019).

The results of O_4 VCDs derived from the MAX-DOAS measurements and calculated from ERA5 data are shown in the figure below. The main finding is that the measured O_4 VCDs are systematically lower than the calculated ones. Part of the underestimation is probably related to clouds, but a strong underestimation is also found for measurements for clear skies.

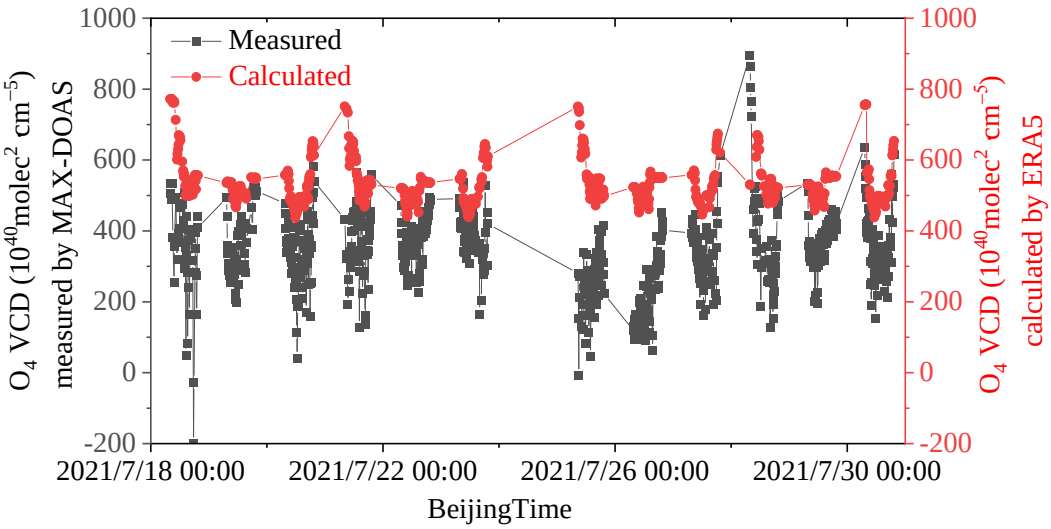

Hence we further explored the applicability of the geometric approximation method by radiative transfer simulations. According to the AODs from the AERONET website (https://aeronet.gsfc.nasa.gov, last access: 2 December 2022) at three sites (Mt_WLG, NAM_CO, QOMS_CAS) over the Tibetan Plateau, we estimate the AODs

around 0.1 during our field campaign. But similar results are also found for AODs of 0.05 and 0.2. The simulation scheme is as the following.

Parameters	O_4	NO_2	HCHO
Wavelength (nm)	340	440	340
Layer height (km)	US standard atmosphere	0-1; 0-2	0-1; 0-2
Aerosol height (km)	0-1	same as trace gases	
AOD	0; 0.05; 0.1; 0.2	0; 0.05; 0.1; 0.2	0; 0.05; 0.1; 0.2
SZA (°)	20, 40, 60, 70, 80		
RAA (°)	10, 30, 60, 90, 180		
Elevation angle (°)	15		
Terrain height (km)	2, 3, 4, 5		

The VCD ratios of the RTM simulations and the geometric approximation for 15° elevation angle under the condition of AOD=0.1 can be obtained for O_4, NO_2, and HCHO, respectively. The DAMF ratios' means and standard deviations for all geometries (blue symbols) and RAA=10°, SZA=60° and RAA=10°, SZA=70° excluded (red symbols, for these rare measurement scenarios the strongest errors occur) are shown below. The main findings are: (1) The typical errors of the geometric approximation are <20% for NO_2 and HCHO; (2) The errors of the geometric approximation are much larger for O_4 with a systematic underestimation between about 40% and 60%, which are in overall agreement with the comparison of the measured and calculated O_4 VCDs above; (3) The large underestimation of the O_4 VCDs indicates that O_4 can not be used for the test if the geometric approximation is justified or not for an individual measurement of NO_2 and HCHO.

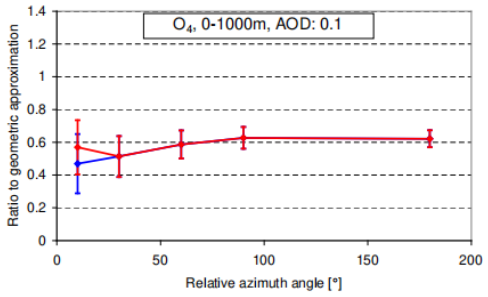

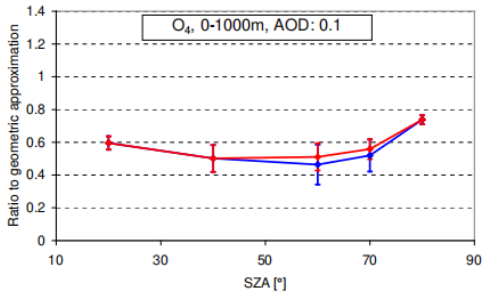

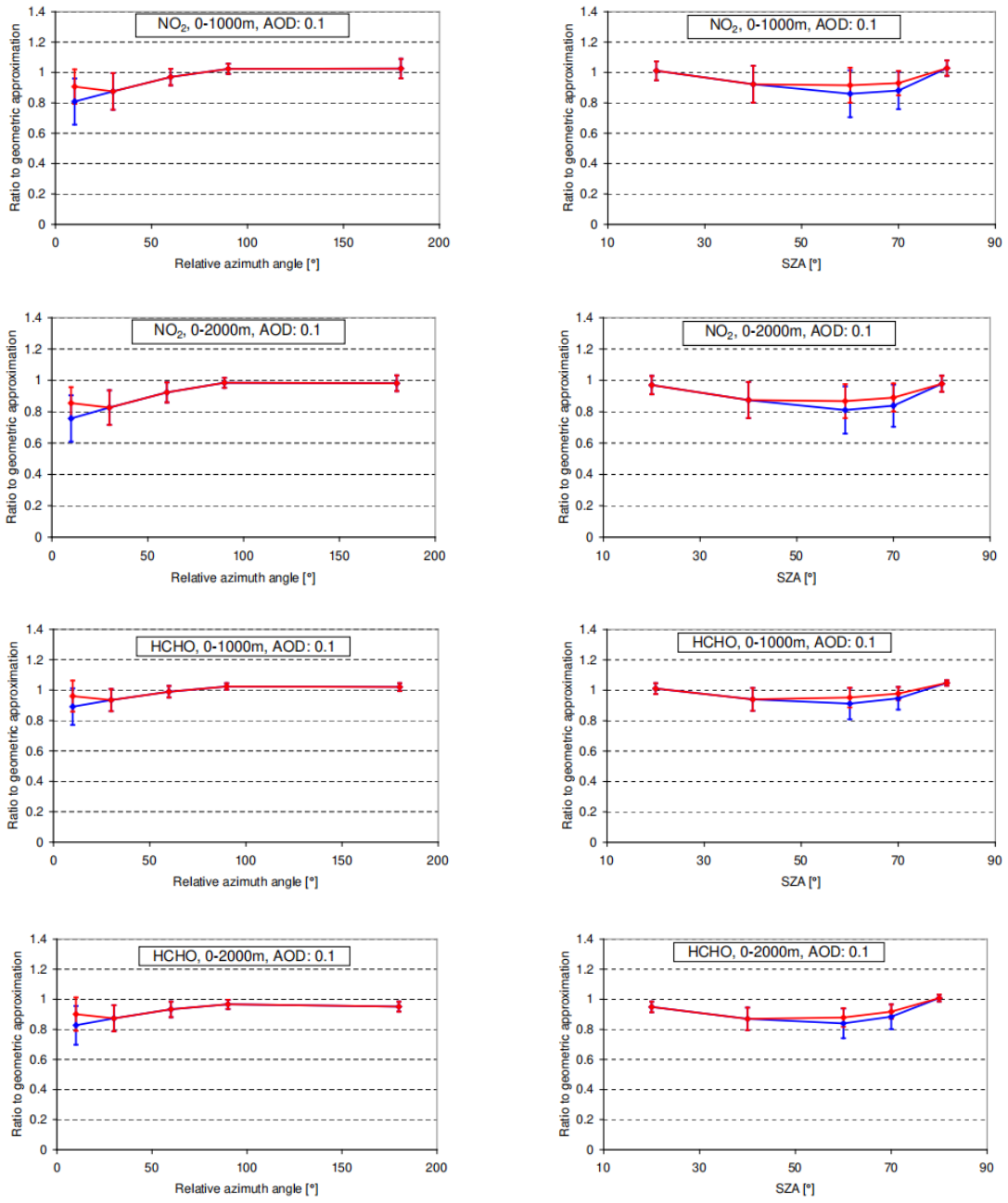

Figure S1 in the revised supplement

Reference:

Wagner, T., Beirle, S., Benavent, N., Bösch, T., Chan, K. L., Donner, S., Dörner, S., Fayt, C., Frieß, U., García-Nieto, D., Gielen, C., González-Bartolome, D., Gomez, L., Hendrick, F., Henzing, B., Jin, J. L., Lampel, J., Ma, J., Mies, K., Navarro, M., Peters, E., Pinardi, G., Puentedura, O., Puķīte, J., Remmers, J., Richter, A., Saiz-Lopez, A., Shaiganfar, R., Sihler, H., Van Roozendael, M., Wang, Y., and Yela, M.: Is a scaling factor required to obtain closure between measured and modelled atmospheric O_4 absorptions? An assessment of uncertainties of measurements and radiative transfer

simulations for 2 selected days during the MAD-CAT campaign, Atmospheric Measurement Techniques, 12, 2745-2817, 10.5194/amt-12-2745-2019, 2019.

It seems like data were recorded at 7 elevation angles, but only four of them were used, and then the 15 degree angle was selected, so only two (15 and 90) were used for the final determination of tropospheric VCD. Therefore, the scan pattern seems inefficient. The authors should discuss good practices for mobile DOAS deriving from this experience. It seems like the upper elevation angles are useful to tell that 15 degrees is not biased compared to other angles, but the lower elevation angles are affected both by road tilt (if the geometry is based upon the vehicle -- see above) and obstructions (e.g. buildings, canyon walls, etc.). Can the authors discuss this issue and give advice for future studies?

Reply: Many thanks for your good comments and suggestions. Because this is the first practice of mobile MAX-DOAS observations over the Tibetan Plateau, we didn't know which elevation angle was the best for measuring the tropospheric VCDs of trace gases in the background atmosphere over mountain terrain before this campaign. Therefore, we made the telescope scanning at 7 elevation angles. In future studies on observing tropospheric NO_2 and HCHO VCDs by mobile DOAS, we suggest to measure at 15°, 20°, 90° elevation angles. There are at least two reasons: (1) The larger elevation angles were less influenced by the road tilt and obstructions; (2) The measurements at 15° and 20° elevation angles have an enhanced sensitivity to tropospheric trace gases (increase of sensitivity compared to 90° elevation is about a factor 3.8 and 2.9, respectively). The increased sensitivity is especially important for measurements of the rather low trace gas concentrations in the background atmosphere. We have added the suggestion to the text at the end of Section 3.2 in revised manuscript from our experiences in this study.

The writing of this manuscript is readable, but in places it could be condensed regarding details that don't seem relevant to the study. For instance, description of the study region seems to include details not really related to the purpose of the study. In places some phrases may also need minor English language editing to read more clearly.

Reply: Many thanks for your kind suggestions. The paragraph about the study

region has been refined. We also improved the English language in the revised manuscript.

Specific comments:

Units -- ACP uses SI units, which indicate that ppb and ppt are language dependent, so they prefer mixing ratios in nmol mol^-1 or pmol mol^-1.

Reply: Agreed. We have checked the units in this paper and revisions have been made.

Line 117: Maybe a transition here to say that although there are challenges, it is useful for reasons...

Reply: Agreed. The description has been modified as "Although there are challenges in measuring NO_2 and HCHO concentrations by mobile MAX-DOAS over the Tibetan Plateau, they are useful for studies on the spatio-temporal evolution of the atmospheric composition in the background atmosphere, validation and improvement of satellite products over mountain terrain, and evaluation of the simulation results of atmospheric chemistry models over the Tibetan Plateau.".

Line 150: Were the angles with respect to gravity or with respect to the mobile platform? How where they corrected to be with respect to gravity?

Reply: The angles were with respect to the mobile platform. We use the uncorrected elevation angles in this study. Originally we planned to use the platform attitude angle to correct the elevation angles. It is a pity that the partial system of the attitude angles of the mobile vehicle did not work well during the field campaign. Nevertheless, we estimated the uncertainties for measurements on tilted roads and found them very small (~1%) for the average of several measurements (for more details see below).

Line 152: What company manufactured the spectrometer?

Reply: AVANTES. This information and model number (AvaSpec-ULS2048x64-USB2) have been added to the revised manuscript.

Lines 162 to 174: Some of this repeats information in the introduction, and some are a bit challenging to read (e.g. what does "four indistinct seasons" mean?). I'd suggest making this section more directly relevant to the mobile campaigns.

Reply: Many thanks for your kind suggestions. This paragraph has been refined.

Line 202: I found this sentence confusing. You could possibly reword or add the word "respectively" after "... can be neglected or cancels out". I think you mean that if a species has no stratospheric part, you can neglect the SCD_stra, or in the other case, if a species has a stratospheric part and there is no light scattering in the stratosphere (thus the light path in the stratosphere is the same independent of alpha) that SCD_stra appears in both SCDs and will then cancel out.

Reply: Per your suggestion, we have added the word “respectively”. You understood this sentence correctly.

Line 209: I presume the interpolation is in time at which the off-zenith spectrum occurs weighting the two neighboring zenith spectra. Can you clarify?

Reply: Yes, the “sequential FRS” are defined as the time interpolated spectra between two zenith spectra measured before and after the measurement time of the current off-zenith elevation angle. We have amended the description in the revised manuscript.

Line 266: I think that the authors should estimate the effect of the elevation angle error. Presuming that the view is relative to the car, one could use an estimate of road grade angle to calculate the magnitude of this error. In the US, interstate highways are allowed to be up to 6% grade (angle = arctan(0.06) = 3.4 °). It would be good to quantify the magnitude of this error, and while I expect it to be small compared to others, the authors should show that it "can be neglected".

Reply: Many thanks for your kind suggestion. we estimate the error of the elevation angle to be about 2.3 °, based on the median of the mobile platform attitude angle

during the effective MAX-DOAS measurement period. The corresponding error of an individual measurement will be up to about 21%. However, it should be noted that on average the positive and negative deviations of the elevation angle will almost cancel each other. Thus the errors of individual measurements will be usually much smaller (except for measurements on continuous strong slopes). For averages of several measurements the errors of the elevation angles lead to much smaller VCD errors with a magnitude smaller than 1% when using geometric approximation method (equation 6):

$\alpha = 15° - 2.3° = 12.7°$, VCD=0.2818×DSCD;

$\alpha = 15°$, VCD=0.3492×DSCD;

$\alpha = 15° + 2.3° = 17.7°$, VCD=0.4232×DSCD;

[(0.2818×DSCD+0.4232×DSCD)÷2-0.3492DSCD] ÷(0.3492×DSCD)×100 =1%

Line 270: I think that this implies that "the geometric approximation method is self consistent", but not that it "has high accuracy". The test done by the authors is only a test of how consistent their data at one elevation angle is compared to another of their elevation angles. If there were aerosol light extinction that reduced pathlengths on each view, the results would still be correlated, but would be affected and not be accurate.

Reply: Agreed. The description has been amended as “the geometric approximation method is self-consistent”.

Line 320: I think the wording "This implies that..." is a bit too strong. The HCHO data are consistent with increasing temperature leading to more BVOC emissions, but they could also be affected by the temperature of the photochemical sources and sinks of HCHO.

Reply: Many thanks for your suggestion. The description of “This implies that” has been amended to “Probably” in the revised manuscript.

Around line 341: Could the U-shape for NO2 also be affected by the city at the start and end of each daily journey?

Reply: Yes. The U-shape of NO_2 VCD diurnal variation was affected by several factors. From our findings we conclude that the NO_2 diurnal variations were primarily caused by enhanced pollution in the morning and evening when the mobile observation vehicle was located in or close to the cities or county town. An additional effect on the diurnal variation is probably caused by the enhanced NO_2 photolysis around noon.

Line 394: Are these figure numbers right? I'm not sure how I can tell about the telescope direction from these maps. Possibly some better annotation on the maps (e.g. an arrow or special marker) would help. I'm not sure what "vehicle flowrate was less" means.

Reply: We checked the figure numbers again and they are correct. According to the explanations of the driving routes in Table 1, we added the marks (‘XD’, ‘DY’, ‘YX’) of the driving routes in figure 11 and figure 12 (of the original manuscript) to indicate the driving direction. The telescope pointed backwards of the driving direction, which was illustrated in Section 2.1. We have amended the description of "vehicle flowrate was less" to “traffic flow was lower” in the revised manuscript.

Line 465: It is of note that there is a large positive offset on the TROPOMI HCHO. It appears that this offset is larger than the MAX-DOAS observed typical column. Discussion of the offset in addition to the correlation would be appropriate.

Reply: Many thanks for your comments. Previous studies found that the offsets of the TROPOMI HCHO were dependent on the HCHO concentration levels and presented to be positive at remote sites (Vigouroux et al., 2020). The larger positive offsets of the TROPOMI HCHO in this study were probably related to the HCHO horizontal inhomogeneity, caused by mountain terrains and varying local microclimates over the Tibetan Plateau. This discussion has been added in revised manuscript.

Reference:

Vigouroux, C., Langerock, B., Aquino, C. A. B., Blumenstock, T., Cheng, Z., Mazière, M. D., Smedt, I. D., Grutter, M., Hannigan, J. W., Jones, N., Kivi, R., Loyola, D., Lutsch, E., Mahieu, E., Makarova, M., Metzger, J.-M., Morino, I., Murata, I., Nagahama, T., Notholt, J., Ortega, I., Palm, M., Pinardi, G., Röhling, A., Smale, D., Stremme, W., Strong, K., Sussmann, R., Té, Y., Roozendael, M. v., Wang, P., and Winkler, H.: TROPOMI–Sentinel-5 Precursor formaldehyde validation using an extensive network of ground-based Fourier-transform infrared stations, Atmos. Meas. Tech., 13, 3751–3767, 10.5194/amt-13-3751-2020, 2020.

Figures 9 and 10: It would be useful for Figure 9 vertical axes to say that NO2 VCD is plotted, and for Figure 10 to say HCHO VCD on the axis.

Reply: Per your suggestion, the title of the vertical axes in Figure 9 and Figure 10 (of the original manuscript) has been amended as "NO_2 VCD" and "HCHO VCD", respectively.

Interactive comment on "Mobile MAX-DOAS observations of tropospheric NO_2 and HCHO during summer over the Three Rivers' Source region in China" *by* Siyang Cheng et al.: Reply to Anonymous Referee #2

Referee comments are in black. Author responses are in blue.

This paper presents mobile MAX-DOAS measurement of tropospheric nitrogen dioxide (NO2) and formaldehyde (HCHO) during summer months over the Tibetan plateau. Mobile MAX-DOAS made four closed loop journeys each spanning 3 days. Measurements of slant column densities (SCDs) at 15 degrees elevation angles (EA) are converted to vertical column densities (VCDs) using geometric approximation. The paper presents diurnal variation, and spatial variation of NO2 and HCHO VCDs in the Tibetan plateau. Using the terrain altitude of the drive track, it also presents the vertical profile of NO2 and HCHO VCDs over this remote background region. Finally, the measured NO2 and HCHO VCDs are used to validate TROPOMI measurements over the region. This paper provides a rare measurement over a data scarce region and hence is worthy of publication to ACP. However, major revision is needed, focused on characterizing the instrument detection limit and measurement uncertainty, and justifying some of the conclusions of the paper before it is accepted for publication.

Reply: First of all, we appreciate the reviewer's positive comments on our manuscript. In response to the reviewer's comments and suggestions, major revisions have been made in the revised manuscript. Listed below are our responses and the corresponding changes made to the manuscript according to the suggestions given by the reviewer.

Major Comments:

The main focus of the paper is providing measurements over a data scarce remote background region. However, the paper lacks discussion of the instrument detection limit and measurement uncertainty. Proper characterization of the detection limit and measurement uncertainty is very important so that the data presented in the paper are properly utilized in the future. Please include discussion of the instrument detection limit and measurement uncertainty. Based on the presented RMS values, most of the measurement appears to be close to or below the detection limits of the instrument.

Please comment on the frequency of measurement at or below the detection limits, and how this impacts the reported background values for NO2 and HCHO of 4 x 1014 and 2.27 x 1015 molecule/cm2 respectively. Uncertainty due to geometric approximation also needs to be better characterized with some radiative transfer calculations and using measurements at different EA. Right now measurements at different EA are only being used to filter data. Absolute difference in VCDs between 15 and 20 EA of 1 x 1015 molecule/cm2 for NO2 and 2 x 1015 molecule/cm2 for HCHO is used as one of the filtering criterias. This is a factor of 1-2 higher than the mean background value so the measured VCDs could have error >100%.

Reply: Many thanks for your comments. Per your suggestions, we have added the discussion of instrument detection limit and measurement uncertainty in Section 3.1 of the revised manuscript. Based on the spectral fit errors corresponding to filtered NO_2 and HCHO DSCDs, twice the medians of the spectral fit errors were estimated as the instrument detection limits for NO_2 and HCHO, which are 0.68×10^{15} and 2.11×10^{15} molec cm^{-2}, respectively. According to the DSCD detection limits divided by the DAMF for 15° elevation angle, the VCD detection limits were estimated to be about 0.24×10^{15} molec cm^{-2} for NO_2 and 0.74×10^{15} molec cm^{-2} for HCHO, respectively. These values are very similar to the estimation of the background levels for NO_2 and HCHO VCDs estimated by the maximum frequency method: the half widths at half maximum of the fitted curves were estimated to be their uncertainties ($\pm0.23\times10^{15}$ molec cm^{-2} for NO_2 and $\pm0.96\times10^{15}$ molec cm^{-2} for HCHO), respectively (Section 4.1).

There are 17% and 15% of the retrieved NO_2 and HCHO DSCDs below the detection limits, respectively. Based on the spectral fit errors, we can also calculate the relative errors for each NO_2 and HCHO DSCD. Then the mean relative errors (uncertainties) of NO_2 and HCHO DSCDs were about 21% and 12%, respectively.

It is a good suggestion to compare the geometric approximation and the atmospheric radiative transfer simulation. However, we lack necessary data during the field campaign to simulate the correct NO_2 and HCHO AMFs. For example, the varying azimuth angle and shelter situation in these viewing direction are not known exactly along the driving routes. Thus we compare and filter NO_2 and HCHO VCDs at different elevation angles, referring to previous study (Brinksma et al., 2008). In

this study, we used both absolute difference and relative difference as the filters, and data would be kept if at least one of both filters was fulfilled. The reason for choosing the absolute difference is to avoid to skip many measurements with low VCDs. With the condition of using two filters in this study, the means of the absolute differences and relative differences in the VCDs between 15° and 20° elevation angles are 5.48×10^{13} molec cm^{-2} and 11% for NO_2 and 3.02×10^{14} molec cm^{-2} and 7% for HCHO respectively.

We also tested the applicability of the geometric approximation method by radiative transfer simulations using typical parameters. According to the AODs from the AERONET website (https://aeronet.gsfc.nasa.gov, last access: 2 December 2022) at three sites (Mt_WLG, NAM_CO, QOMS_CAS) over the Tibetan Plateau, we estimate the AODs around 0.1 during our field campaign. But similar results are also found for AODs of 0.05 and 0.2. The simulation scheme is as the following.

Parameters	NO_2	HCHO
Wavelength (nm)	440	340
Layer height (km)	0-1; 0-2	0-1; 0-2
Aerosol height (km)	same as trace gases	
AOD	0; 0.05; 0.1; 0.2	
SZA (°)	20, 40, 60, 70, 80	
RAA (°)	10, 30, 60, 90, 180	
Elevation angle (°)	15	
Terrain height (km)	2, 3, 4, 5	

The VCD ratios of the RTM simulations and the geometric approximation for 15° elevation angle under the condition of AOD=0.1 can be obtained for NO_2 and HCHO, respectively. The DAMF ratios' means and standard deviations for all geometries (blue symbols) and RAA=10°, SZA=60° and RAA=10°, SZA=70° excluded (red symbols, for these rare measurement scenarios the strongest errors occur) are shown below. The main findings are that the typical errors of the geometric approximation are <20% for NO_2 and HCHO.

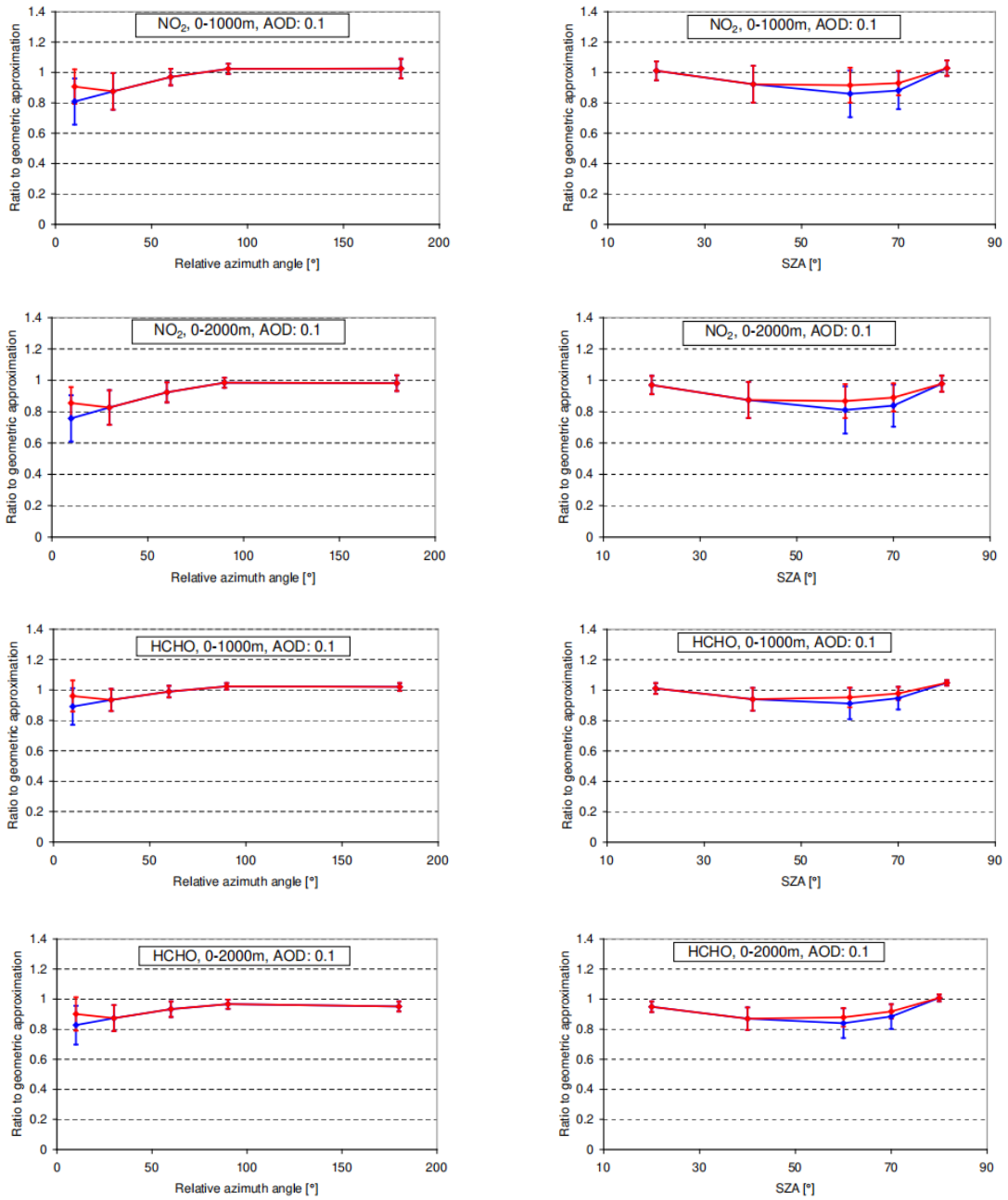

Figure S1 in the revised supplement

References:

Brinksma, E. J., Pinardi, G., Volten, H., Braak, R., Richter, A., Schönhardt, A., van Roozendael, M., Fayt, C., Hermans, C., Dirksen, R. J., Vlemmix, T., Berkhout, A. J. C., Swart, D. P. J., Oetjen, H., Wittrock, F., Wagner, T., Ibrahim, O. W., de Leeuw, G., Moerman, M., Curier, R. L., Celarier, E. A., Cede, A., Knap, W. H., Veefkind, J. P., Eskes, H. J., Allaart, M., Rothe, R., Piters, A. J. M., and Levelt, P. F.: The 2005 and 2006 DANDELIONS NO_2 and aerosol intercomparison campaigns, Journal of Geophysical Research, 113, D16S46, 10.1029/2007jd008808, 2008.

A large portion of the manuscript is dedicated to characterizing the temporal variation of the NO2 and HCHO even though the mobile MAX-DOAS drives covered large spatial region. The temporal variation analysis assumes there is a little to no spatial variation in these species along the drive track. However, this is not the case as shown in the spatial analysis plots. There is spatial variability as well as day to day variability along the drive track. Assuming the drives started at around the same time each day and reached the same locations around similar time during the drives, the diurnal variation presented here represents spatial variation and not temporal variation. This is also the likely reason for the W shape in HCHO diurnal variation, and U shape in NO2. So, it might be best not to include the temporal variation section in the paper or may be present it as spatial variation.

Reply: Many thanks for your suggestions. Yes, the NO_2 and HCHO VCDs, measured by mobile MAX-DOAS, reflected their combined spatio-temporal variations. From the findings in this study, we infer that the variable diurnal patterns of HCHO were connected with the secondary photochemical formation of active VOCs at different locations. We conclude that the 'U' shape of the NO_2 diurnal variations were primarily caused by enhanced pollution in the morning and evening when the mobile observation vehicle was located in or close to the cities or county town. An additional effect on the NO_2 diurnal variation is probably caused by the enhanced NO_2 photolysis around noon.

Therefore, as you suggested, we combined the Section 4.2 (Temporal variation) and 4.3 (Spatial distribution) in the original manuscript together, which were reorganized into Section 4.2 (Spatio-temporal variation) in the revised manuscript. This change is not marked up using revision track in order to keep the manuscript clear to read.

The paper talks about making measurements at high spatial resolution, but there is no information about the spatial resolution of the measurements in the paper. The only spatial information about the data is presented at 0.25 degree resolution. Please include the spatial resolution of the data. Further TROPOMI data is also gridded into 0.25 x 0.25 degree cells (~ 25 km x 25 km). This suggests that the mobile MAX-DOAS data is only available at 25 km spatial resolution. Please include reasoning for not averaging the MAX-DOAS data to the TROPOMI grid (~ 5km)?

Reply: It spent about 8 min for measurements at two adjacent 15 ° elevation angle.

The corresponding spatial resolution can be estimated as ~8 km at a speed of ~60 km/h of the mobile vehicle. Assuming that the trace gas is located in the lowest 1000m above the surface, we can also estimate the horizontal extent of the line of sight through that layer. For measurements at 15 °elevation angle, this extent is about 4km.

However, for the comparison with TROPOMI observations, we use the means of typically 2-3 data points (approximate 25 km) at a specific grid in order to reduce the uncertainties of the VCDs from both mobile MAX-DOAS and TROPOMI. In addition, the chosen grid cell matches the finest mesh of the ERA5 meteorological data. The spatial resolution of measurements and the reason for using the 0.25 °×0.25 °grid have been added in the Section 3.2 and 4.3 of revised manuscript.

We also tried to match the individual MAX-DOAS measurement with TROPOMI Level-2 NO_2 and HCHO products (5.5 km ×3.5 km). Both data sets are combined under the conditions of Δlongitude<0.05° & Δlatitude<0.05° & ΔTime < 1.5h (or on the same day), which was referred to '$\Delta T_{1.5}$' ('All') in the figure below. The finer (0.05 °×0.05 °) spatial distributions of TROPOMI NO_2 and HCHO are also shown in the following. From the results with fine (0.05 °×0.05 °) and coarse (0.25 °×0.25 °) spatial resolutions, the conclusions drawn in this paper were almost the same. Thus we did not change the comparison results in the paper.

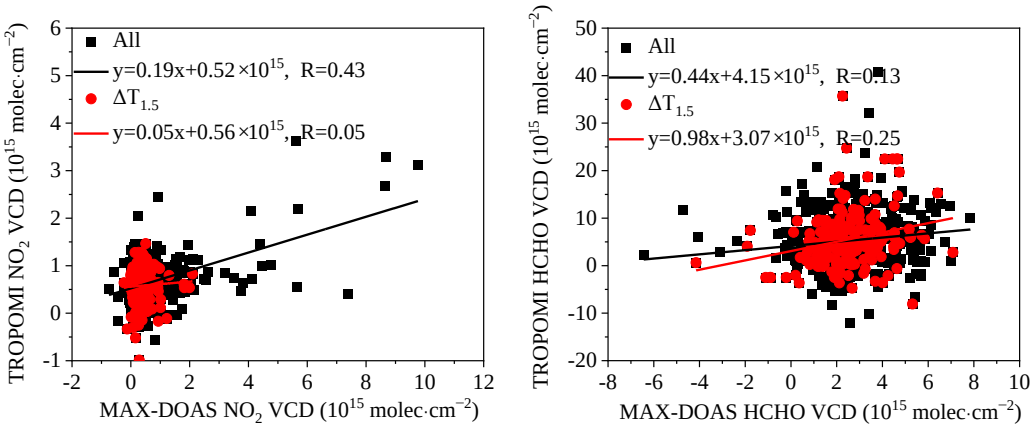

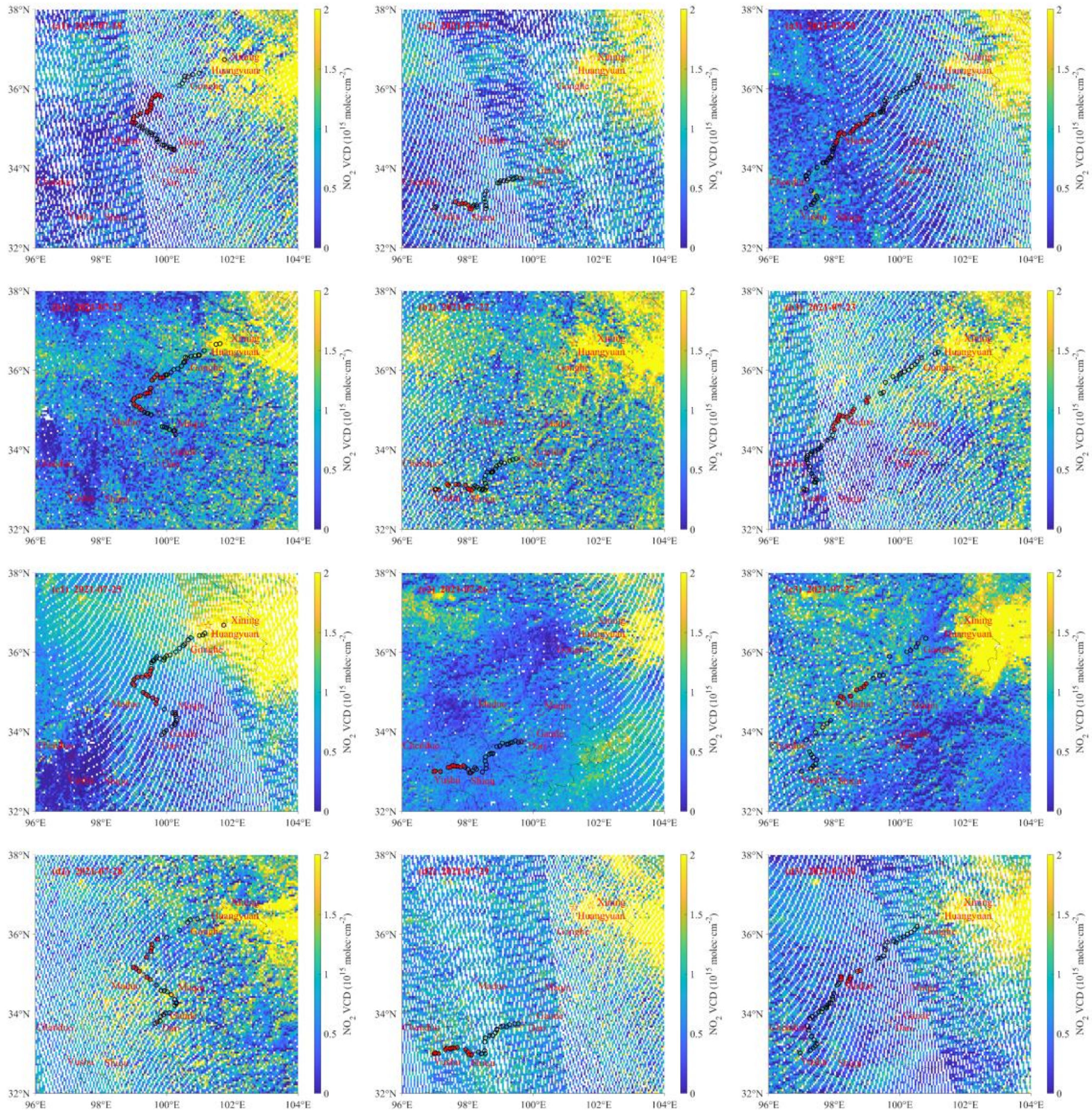
38°N
36°N
34°N
32°N
96°E
98°E
100°E
102°E
104°E
NO2 VCD (10^15 molec·cm^-2)
0
0.5
1
1.5
2
Xining
Huangyuan
Gonghe

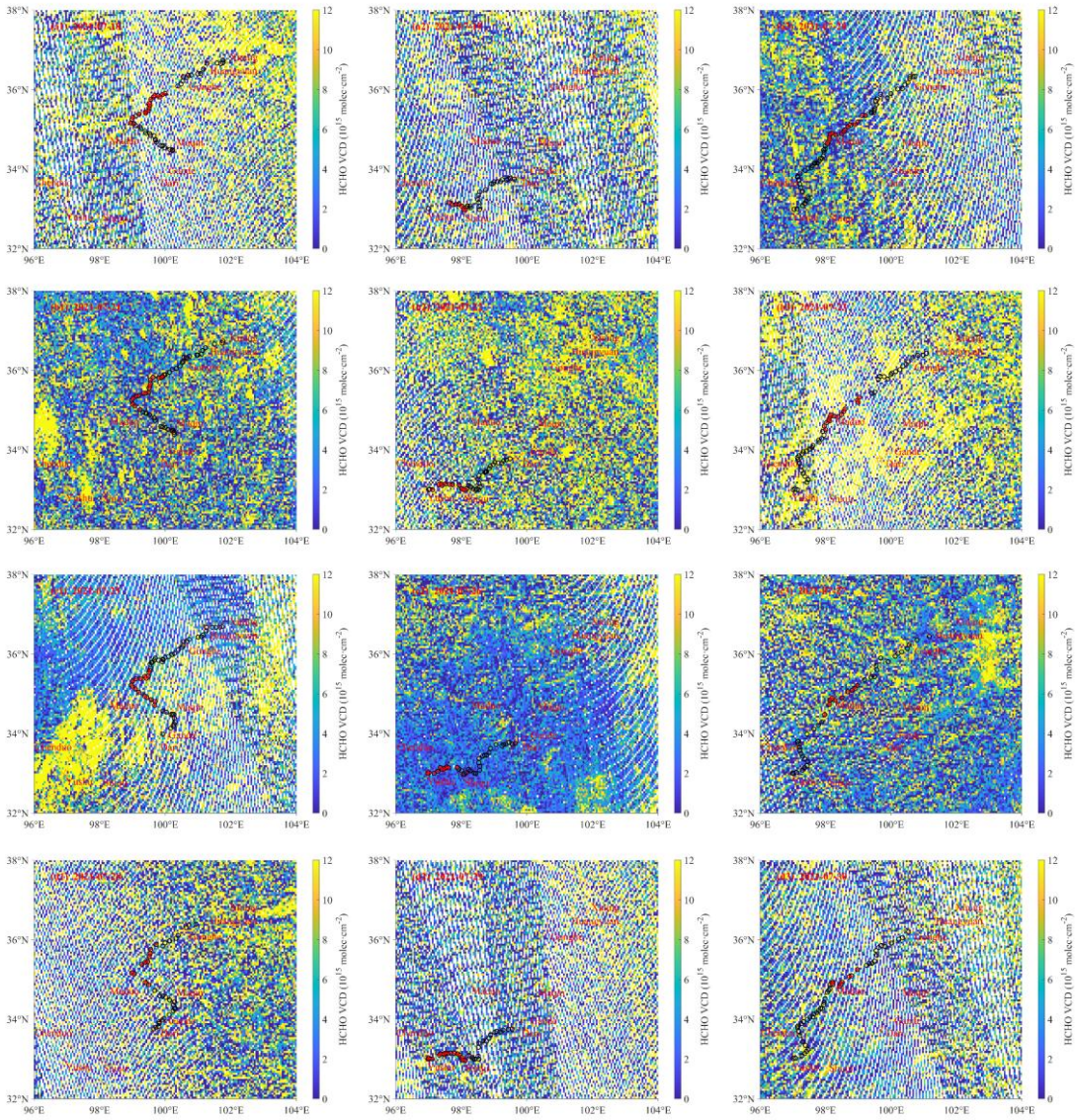

It is not clear how the authors came to the conclusion that "TROPOMI can't identify the fine scale spatial variability in the tropospheric NO2 VCDs in the background atmosphere over the Tibetan Plateau". TROPOMI data is not even being used at its native resolution for this analysis. Same with HCHO fine-scale and temporal variations.

Reply: Many thanks for your comments. Originally, we want to say: 'The elevated trends of the tropospheric NO_2 VCDs around the counties, which are clearly observed by the mobile MAX-DOAS, are nearly not captured by TROPOMI'. This conclusion has been deleted in revised manuscript.

I don’t think regression analysis is appropriate tool for evaluating the TROPOMI satellite products over remote background region where the dynamic range of the data is very small. It is not clear how linear regression helps validate fine-scale variability in tropospheric NO2 and HCHO VCDs? The lower TROPOMI NO2 VCDs over the cities might be related to the difference in timing of the measurements between mobile MAX-DOAS measurements and TROPOMI measurements. Mobile MAX-DOAS generally measured higher NO2 over the cities in the morning during the start of the drive, whereas TROPOMI make measurements at mid-day when NO2 abundances are lowest. I suggest the authors focus on bias in TROPOMI data in the background region rather than correlation.

Reply: Although the regression analysis is limited by the dynamic range of NO_2 and HCHO levels, it is still a common method to compare ground-based observation with satellite products and correlation coefficients are usually small at a remote site (Vigouroux et al., 2020; Verhoelst et al., 2021). For NO_2, both mobile MAX-DOAS and TROPOMI present clear differences between Xining city and the main area of the Three Rivers’ Source, although there are differences in measurement time in Xining city between the two methods. However, the elevated trends of the tropospheric NO_2 VCDs around the counties over the main area of the Three Rivers’ Source, which are clearly observed by the mobile MAX-DOAS, are nearly not captured by TROPOMI. These differences of the NO_2 spatial distribution are reflected in the different correlation coefficients by the regression analysis for the situations of ‘All’ and ‘$\Delta T_{1.5}$’, respectively. The regression analysis for the HCHO VCDs also partly showed the similarities and differences of the HCHO spatio-temporal variations between mobile MAX-DOAS and TROPOMI. For example, the higher TROPOMI HCHO VCDs appear more in the second circling journey and the lower HCHO VCDs in the third and fourth circling journey, consistent with the results derived from mobile MAX-DOAS. Therefore, we find it very useful to retain the results of the regression analyses. Of course, comparing the bias between two data sets, which is significant over the background region, has been added in revised manuscript.

References:

Vigouroux, C., Langerock, B., Aquino, C. A. B., Blumenstock, T., Cheng, Z., Mazière, M. D., Smedt, I. D., Grutter, M., Hannigan, J. W., Jones, N., Kivi, R., Loyola, D., Lutsch, E., Mahieu, E., Makarova, M., Metzger, J.-M., Morino, I., Murata,

I., Nagahama, T., Notholt, J., Ortega, I., Palm, M., Pinardi, G., Röhling, A., Smale, D., Stremme, W., Strong, K., Sussmann, R., Té, Y., Roozendael, M. v., Wang, P., and Winkler, H.: TROPOMI–Sentinel-5 Precursor formaldehyde validation using an extensive network of ground-based Fourier-transform infrared stations, Atmos. Meas. Tech., 13, 3751–3767, 10.5194/amt-13-3751-2020, 2020.

Verhoelst, T., Compernolle, S., Pinardi, G., Lambert, J.-C., Eskes, H. J., Eichmann, K.-U., Fjæraa, A. M., Granville, J., Niemeijer, S., Cede, A., Tiefengraber, M., Hendrick, F., Pazmiño, A., Bais, A., Bazureau, A., Boersma, K. F., Bognar, K., Dehn, A., Donner, S., Elokhov, A., Gebetsberger, M., Goutail, F., Grutter de la Mora, M., Gruzdev, A., Gratsea, M., Hansen, G. H., Irie, H., Jepsen, N., Kanaya, Y., Karagkiozidis, D., Kivi, R., Kreher, K., Levelt, P. F., Liu, C., Müller, M., Navarro Comas, M., Piters, A. J. M., Pommereau, J.-P., Portafaix, T., Prados-Roman, C., Puentedura, O., Querel, R., Remmers, J., Richter, A., Rimmer, J., Rivera Cárdenas, C., Saavedra de Miguel, L., Sinyakov, V. P., Stremme, W., Strong, K., Van Roozendael, M., Veefkind, J. P., Wagner, T., Wittrock, F., Yela González, M., and Zehner, C.: Ground-based validation of the Copernicus Sentinel-5P TROPOMI NO_2 measurements with the NDACC ZSL-DOAS, MAX-DOAS and Pandonia global networks, Atmospheric Measurement Techniques, 14, 481-510, 10.5194/amt-14-481-2021, 2021.

The spectral analysis or the method section has no references other than Platt and Stutz (2008). There are lots of papers describing MAX-DOAS measurements, retrievals, pros and cons of fixed vs sequential FRS. So, please add references to appropriate paper.

Reply: Many thanks for your kind suggestions. Several references have been added in the revised manuscript.

Minor Comments:

It would be great to show the VCD profiles as mixing ratio profiles. Temperature and pressure from the ERA5 reanalysis could be used for this purpose as well. This would very likely provide greater utility of the dataset. It would also be very useful to have the vertical profiles that does not include anthropogenic influenced values from Xining.

Reply: Many thanks for your suggestions. We have amended the profiles of the NO_2 and HCHO VCDs along the driving route altitude (Figure 6b in revised manuscript), which were used to derive the profiles of the NO_2 and HCHO mixing

ratios (VMRs, Figure S2 in the revised supplement, also shown below). During the calculation process of the NO_2 and HCHO VMRs, we firstly obtained the differences of the VCDs (ΔVCD) between two adjacent vertical intervals. Then we utilized hourly surface air pressure and temperature at 2 m above the land surface from ERA5 (with the 0.25 °×0.25 ° resolution) to calculate the mean temperatures and pressures at each altitude interval. In addition, it should be noted that the conversion of the ΔVCDs to VMRs was based on an assumption, i.e. the abundances of the trace gases at the same altitude are independent on measurement location. But this assumption may be not quite fulfilled. Therefore, the profiles of NO_2 and HCHO VMRs were just approximate estimation values and we tend to put them in the supplement.

The data points at the grid cell of 2000-2500 m represent the conditions around Xining. We prefer to keep the measurement point at this grid cell in order to clearly show the differences between Xining city and background region.

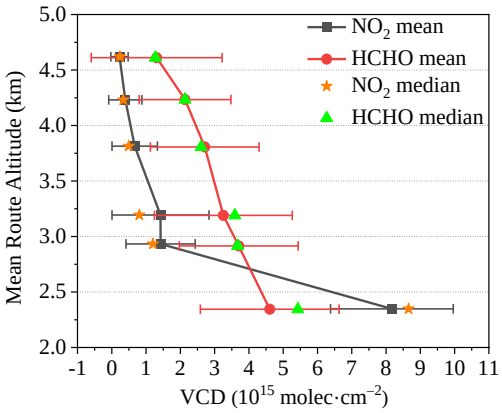

Figure 6b in the revised manuscript

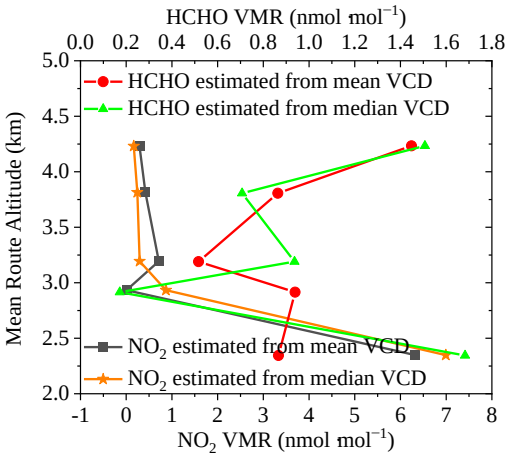

Figure S2 in the revised supplement

How is ERA5 reanalysis temperature and solar radiation at the surface (SSRD) used to calculate daily temperature and SSRD? Do you interpolate it to each VCD measurements and then calculate the average for each day?

Reply: Yes, the air temperature at 2 m above the land surface and the downward solar radiation at the surface (SSRD) from ERA5 are firstly matched with each measured HCHO VCD. Then the daily averages of temperature and SSRD were calculated. The description has been made more clear in the revised manuscript.

It is not clear how relatively large noise in the TROPOMI satellite product results in small correlation coefficient between two data sets. Is the uncertainty in measurements included in the regression analysis?

Reply: The rather low signal-to-noise ratio of the TROPOMI HCHO VCDs will result in a partly random distribution, which will lead to a smaller correlation coefficient of the HCHO VCDs between mobile MAX-DOAS and TROPOMI. However, the noise level of the TROPOMI VCDs is difficult to estimate, because it not only depends on the spectral analysis, but also on the applied tropospheric AMF, which is in particular influenced by partial clouds and varying surface elevation. Therefore, the measurement uncertainties were not included during the process of the regression analysis in Figure 15. This information has been amended in the revised

manuscript.

I wonder why the authors decided not to simply do zenith DOAS measurements. It would remove some of the challenges associated with MAX-DOAS measurement such as signal blockage. I assume this is to leverage the air mass factor. This needs to be made clear. Since data from all EAs are not used, I also suggest the authors include some discussion on need for different EA measurements. This will be very helpful for future mobile MAX-DOAS measurements.

Reply: Many thanks for your comments and suggestions. The tropospheric light path is shorter at the zenith view, compared with the off-axis view. Especially for the background atmosphere with typically low concentration levels, the weak absorptions of the trace gases can be enhanced using longer light paths in the troposphere in order to enhance the detection limit. In addition, because this is the first practice of mobile MAX-DOAS observations over the Tibetan Plateau, we didn't know which elevation angle was the best for measuring the tropospheric VCDs of trace gases in the background atmosphere over mountain terrain before this campaign. Therefore, we made the telescope scanning at 7 elevation angles. In future studies on observations of tropospheric NO_2 and HCHO VCDs by mobile MAX-DOAS, we suggest to measure at 15°, 20°, 90° elevation angles. There are at least two reasons: (1) The larger elevation angles are less influenced by the road tilt and obstructions; (2) The measurements at 15° and 20° elevation angles with longer light path have a higher sensitivity (by about a factor of 2.9 for 20°, and 3.8 for 15° elevation angle, respectively) for tropospheric trace gases in the background atmosphere. We have added this information to the text at the end of Section 3.2 in revised manuscript from our experiences in this study.

Specific Comments:

Line 48: "grinding environment" – not sure what you mean by that. May be replace with complex terrain?

Reply: The description of "grinding environment" has been deleted in revised

manuscript.

Line 49: What do you mean by the sparseness of effective techniques and methods? Do you mean most methods don't work due to high altitude environment?

Reply: Yes. We mean that some instruments don't work due to special environment (such as lower pressure) over the Tibetan Plateau.

Line 93-96: Please provide more information about the methods. Right now it is very vague.

Reply: Many thanks for your suggestions. More information about the sampling observation methods and surface in-situ measurement methods has been added in the revised manuscript.

Line 135: Are there any other measurements on the vehicle?

Reply: Yes. The other measurements for the purpose of improving weather forecasts were performed by other groups and will be reported in another study.

Line 142: consider replacing "complex" with "difficult"

Reply: Agreed. Done.

Line 146: Is there a reference for the Tube MAX-DOAS instrument?

Reply: Yes. We have added some references for the Tube MAX-DOAS instrument.

Line 157: DC and OS are collected at night. Does the instrument need to be operating at night every day or can you use single DC and OS files?

Reply: The instrument recorded spectra of dark current (DC) and electronic offset (OS) at each night automatically. But we use single DC and OS files, which were

sufficient because the Tube MAX-DOAS worked at a stable detector temperature of 15±0.1 ℃.

Line 168: remove “in the field measurement area”. I don’t think it is needed.

Reply: Agreed. Done.

Line 226: For EA 15 degree measurements, SZA > 75 would result in the sun below the measurement geometry. Under such a condition, geometric approximation is likely not well suited? Should the SZA cutoff be 75 degree instead?

Reply: It should be noted that the ground-based MAX-DOAS observations utilize scattered sun light. As illustrated in the sketch below (http://iup.uni-bremen.de/doas/maxdoas_instrument.htm, accessed date: 23 November 2022), if the scattering point is above the layer of the target species then the geometric approximation is applicable. In this study, SZA < 80 ° is used as one of the filters during the post processing of NO_2 and HCHO DSCDs. According to the aforementioned results about the applicability of the geometric approximation method by radiative transfer simulations, the geometric approximation is still well suited for measured data in the range of 75 °≤SZA < 80 ° without additional significant errors. We prefer to select the threshold of SZA<80 °to balance the quality of the results and skipping not too many data.

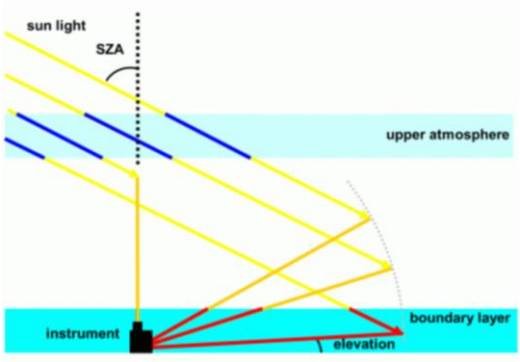

Line 249: change “more exact, but depends on…” to “more accurate, but requires information on…”

Reply: Agreed. Done.

Line 250: change “less correct, but relatively simple …” to “simpler and assumes trace gases are uniformly distributed in the lower troposphere”

Reply: Agreed. Done.

Line 256: add polluted environment.

Reply: Done.

Line 265: Error due to pitch and roll distribution could be easily quantified. Consider quantifying this error rather than saying “errors will cancel out”.

Reply: Many thanks for your kind suggestion. we estimate the error of the elevation angle to be about 2.3 °, based on the median of the mobile platform attitude angle during the effective MAX-DOAS measurement period. The corresponding error of an individual measurement will be up to about 21%. However, it should be noted that on average the positive and negative deviations of the elevation angle will almost cancel each other. Thus the errors of individual measurements will be usually much smaller (except for measurements on continuous strong slopes). For averages of several measurements the errors of the elevation angles lead to much smaller VCD errors with a magnitude smaller than 1% when using geometric approximation method (equation 6):

$\alpha = 15° - 2.3° = 12.7°$, VCD=0.2818×DSCD;

$\alpha = 15°$, VCD=0.3492×DSCD;

$\alpha = 15° + 2.3° = 17.7°$, VCD=0.4232×DSCD;

[(0.2818×DSCD+0.4232×DSCD)÷2-0.3492DSCD] ÷(0.3492×DSCD)×100 =1%

Line 269: change ~ to –. Also in line 362.

Reply: Agreed. Done.

Line 445: Lower NO2 for TROPOMI is likely due to difference in time of measurements.

Reply: Yes. Considering the NO_2 diurnal variations in cities (such as Xining), the lower NO_2 VCDs for TROPOMI in the 'All' situation in Figure 15 were also affected by the differences in time between two measurement methods. This cause has been added to the revised manuscript.

Figure 2: Elevation map of the drive track would be very useful.

Reply: Many thanks for your suggestion. The altitudes along the driving routes have been added in the Figure 2 of the revised manuscript.

Figure 5: Please remove square from measured data for clarity. RMS looks higher than listed in the figure legend especially for NO2. Please consider including fit residual plot as well.

Reply: Per your suggestions, we have amended the figure 5 about the spectral fitting for NO_2 and HCHO.

Figure 6: This information is probably better presented in table 3. Scatter plot between different EA VCDs will be more informative than what is currently presented in Figure 6. With the mean value dominated by few large values, I suggest including bias as well.

Reply: Many thanks for your suggestions. The Figure 6 has been removed in the revised manuscript and the corresponding information has been added to the amended Table 3.

Figure 11-14: It would be better to combine Figures 11 and 13 and Figures 12 and 14.

Reply: Many thanks for your suggestions. However, we prefer not to combine Figures 11 and 13 (Figures 12 and 14), because they include many kinds of colors and

a lot of information besides the spatial distributions of the tropospheric NO_2 VCDs, respectively. For example, the colors of rivers and lakes, roads, and administrative boundaries on the background street map (https://map.baidu.com/, last access: 16 June 2022) in Figure 11 (Figure 12) cannot be modified and will be indistinguishable when we plot all the information of Figures 11 and 13 (Figures 12 and 14) together.

Figure 11: Is the gridded VCDs, mean VCDs over that grid or the median? Since we are dealing with background values, median VCDs might be better for comparison. Also approximately, how many data points are there in each grid?

Reply: We use the mean VCDs for the gridded VCDs. There are no significant differences in the VCD patterns during this campaign. There are typically 2-3 data points in each grid approximately.

Figure 15: Why do you have negative VCDs? Should they be excluded?

Reply: It is possible that there are negative VCDs for the background atmosphere, where the trace gas absorptions are very low. The negative NO_2 and HCHO VCDs are mainly caused by the scatter of the data in this study, which are related to the measurement noises. It is important to keep these negative VCDs. Otherwise we would introduce an artificial positive bias.

Figure S1: Consider including scatterplot between HCHO VCD and temperature in the paper rather than in SI.

Reply: Agreed. Done.

Mobile MAX-DOAS observations of tropospheric NO_2 and HCHO during summer over the Three Rivers' Source region in China

Siyang Cheng[1,2], Xinghong Cheng[1], Jianzhong Ma[1], Xiangde Xu[1], Wenqian Zhang[1], Jinguang Lv[2], Gang Bai[3], Bing Chen[4], Siying Ma[4], Steffen Dörner[5], Sebastian Donner[5], Thomas Wagner[5]

[1]State Key Laboratory of Severe Weather & Institute of Tibetan Plateau Meteorology, Chinese Academy of Meteorological Sciences, Beijing, 100081, China
[2]State Key Laboratory of Applied Optics, Changchun Institute of Optics, Fine Mechanics and Physics, Chinese Academy of Sciences, Changchun, 130033, China
[3]Beijing Remnant Technology Co.,Ltd, Beijing, 100012, China
[4]College of Electronic Engineering, Chengdu University of Information Technology, Chengdu, 610225, China
[5]Max Planck Institute for Chemistry, Mainz, D-55020, Germany

Correspondence to: Jianzhong Ma (majz@cma.gov.cn) and Xinghong Cheng (cxingh@cma.gov.cn)

Abstract. The tropospheric concentrations of nitrogen dioxide (NO_2) and formaldehyde (HCHO) have high spatio-temporal variability, and in situ observations of these trace gases are still scarce especially in remote background areas. We made four similar circling journeys of mobile MAX-DOAS measurements in the Three Rivers' Source region over the Tibetan Plateau in summer (18–30 July) 2021 for the first time. The differential slant column densities (DSCDs) of NO_2 and HCHO were retrieved from the measured spectra with very weak absorptions along the driving routes. The tropospheric NO_2 and HCHO vertical column densities (VCDs) were calculated from their DSCDs by the geometric approximation method, and they were further filtered to form reliable data sets by eliminating the influences of sunlight shelters and vehicle's vibration and bumpiness. The observational data show that the tropospheric NO_2 and HCHO VCDs decreased with the increasing altitude of the driving route, whose background levels were 0.40 $\pm$0.23 $\times10^{15}$ molec cm^{-2} for NO_2 and 2.27 $\pm$0.96 $\times10^{15}$ molec cm^{-2} for HCHO in July 2021 over the Three Rivers' Source region. The NO_2 VCDs show similar geographical distribution patterns between the different circling journeys, but the levels of the HCHO VCDs are different between the different circling journeys. ~~The NO_2 VCDs tended to have peak values in the early morning and late afternoon, while the diurnal variation pattern of HCHO VCDs changed with the driving route.~~ The elevated NO_2 VCDs along the driving routes were usually corresponding to enhanced transport emissions from the towns crossed. However, the spatial distributions of the HCHO VCDs depended significantly on natural and meteorological conditions, such as surface temperature. By comparing TROPOMI satellite products and mobile MAX-DOAS results, we found that ~~TROPOMI is still unable to identify the fine-scale spatial variability in tropospheric NO_2 and HCHO VCDs in the background atmosphere over the Tibetan Plateau~~ TROPOMI NO_2 and HCHO VCDs have large positive offsets in the background atmosphere over the main area of the Three Rivers' Source. Our study provides valuable data sets and information of NO_2 and HCHO over the Tibetan Plateau, benefitting the scientific community in investigating the spatio-temporal evolution of atmospheric composition ~~with high~~

~~spatio-temporal resolution~~ in the background atmosphere at high altitudes, validating and improving the satellite products over mountain terrains, and evaluating the model's ability in simulating atmospheric chemistry over the Tibetan Plateau.

1 Introduction

The Tibetan Plateau, also known as the Qinghai-Tibet Plateau in China, is usually called as "the Third Pole" (or "the Roof of the World") with an average surface altitude of 4000~5000 m, covering a vast region located at 73~105 °E longitude and 26~40 °N latitude (Qiu, 2008). Due to thermal and dynamic processes on the role of high altitude and large terrain, the Tibetan Plateau has an important influence on the atmospheric circulation (such as Asian Summer Monsoon), Asian climate and even global climate, and hydrological cycle (Bolin, 1950; Boos and Kuang, 2010; Dong et al., 2017; Duan et al., 2007; Liu et al., 2007; Yanai et al., 1992; Zhou et al., 2009). As the "Asian Water Towers", there are many water resources in the forms of glaciers, snow packs, lakes and rivers over the Tibetan Plateau, which is the headwaters of major rivers in Asia (such as Indus River, Ganges River, Yangtze River, Yellow River and Lancang River) and influences the economic development and billions of people survival in the downstream region (Xu et al., 2008; Gao et al., 2019). Therefore, the area of "Three Rivers' Source" (i.e. Yangtze River, Yellow River and Lancang River) was established as one of the first five national parks in China in 2021 to better protect the ecological environment. However, we still know very little about the ecological environment including atmospheric environment over this region at present. Almost no observations focus on the abundances and variations of atmospheric composition over the Three Rivers' Source region, limited by the ~~grinding environment,~~ extremely high altitude, topographical heterogeneity, variable weather, and ~~the sparseness of~~ effective techniques and methods. As one of the remote regions in Eurasia, the Tibetan Plateau with low anthropogenic activities and a low population density can be considered as natural laboratory to investigate the background atmospheric chemistry of the inner Eurasian continent (Ma et al., 2021). With increasing emissions of air pollution over the Tibetan Plateau and its surrounding areas (such as tourism in summer), measurements of the background atmosphere with high spatial-temporal resolution are urgent to improve the understanding of the spatio-temporal evolution of the atmospheric composition (Singh, 2021; Yang et al., 2019; Kang et al., 2022).

Nitrogen dioxide (NO_2) and formaldehyde (HCHO) are two important traces gases in the troposphere, participating in the control of the strong atmospheric oxidant of ozone (O_3) (Seinfeld and Pandis, 2016). Nitrogen oxides (NO_x), i.e. the sum of NO_2 and nitric oxide (NO), not only can be released by various anthropogenic emission sources, such as the burning of fossil fuel and biomass, but also can be emitted by natural processes including microbial activities in soils and lightning in the atmosphere (Lee et al., 1997; Granier et al., 2011; Kurokawa et al., 2013). HCHO is produced not only by primary sources (e.g. emissions of industry and transportation in city and biomass burning), but also by photochemical oxidation of methane and non-methane volatile organic compounds (e.g. isoprene emitted from natural vegetation) in the remote atmosphere (Stavrakou et al., 2009). High-accuracy measurements of NO_2 and HCHO with high spatial and temporal resolution are

beneficial to understand their variation characteristics in the background atmosphere, quite useful to validate the satellite products, and very valuable to explore processes of atmospheric chemistry.

The ground-based observations of NO_2 and HCHO concentrations in the background atmosphere at high altitude are relatively scarce at present. Under the frameworks of the Global Atmosphere Watch program of the World Meteorological Organization (WMO/GAW) and the Network for the Detection of Atmospheric Composition Change (NDACC), long-term observations of atmospheric composition have been carried out at some high mountain stations, such as the Waliguan (WLG; 3816 m above sea level) global atmosphere background observatory, located in the northeastern part of the Tibetan Plateau (Xu et al., 2020; Ma et al., 2021). With respect to NO_2 at WLG, previous studies found different levels (5~600 pmol mol^{-1}~~ppt~~) of NO_2 during different periods, leading to a positive or negative sign of net ozone production in the remote troposphere (Xue et al., 2011; Meng et al., 2010; Ma et al., 2020; Ma et al., 2002). Short-term HCHO observations at WLG in 2005 indicated that the possible sources for HCHO were photo-oxidation of biogenic emission of isoprene, animal excrement, and long-distance transportation from polluted air (Mu et al., 2007). The two stations of Qinghai Lake and Menyuan are adjacent to WLG, but the diurnal variations of NO_x (NO_2) are different and possibly influenced by traffic and residential emissions, complex terrain, boundary layer processes, and transport from city air masses (Wang et al., 2015; Zhao et al., 2020). According to the measurements at the Qomolangma Atmospheric and Environmental Observation and Research Station (QOMS; 4276 m above sea level) of the south-central Tibetan Plateau from December 2017 to March 2019, the levels of NO_2 and HCHO were significantly higher than those at WLG station, related to local emissions (e.g. tourism, biomass burning, vegetation) and air pollution transport from the South Asia (Xing et al., 2021; Ma et al., 2020). Increased concentrations of tropospheric NO_2 at QOMS are concentrated in the lower layers with obvious seasonal variations (peak of 1.28 ~~ppb~~ nmol mol^{-1} in autumn) and diurnal variations (two peaks at 11:00~13:00 BJT and after 16:00 BJT; BJT denotes Beijing Time and equals the Coordinated Universal Time plus 8 hours) (Xing et al., 2021). The tropospheric HCHO vertical distribution showed an exponential shape at QOMS with a seasonal peak of 5.20 nmol mol^{-1}~~ppb~~ in autumn, and the peaks of HCHO appeared between 10:00~16:00 BJT in winter and spring and after 16:00 BJT in summer and autumn, respectively (Xing et al., 2021). In recent years, the China National Environmental Monitoring Center (CNEMC) also established several atmospheric composition monitoring stations over the Tibetan Plateau, but they mainly focused on the continuous monitoring of the surface particulate matter with aerodynamic diameter less than 2.5 μm and 10 μm ($PM_{2.5}$ and PM_{10}), NO_2, sulphur dioxide (SO_2), O_3, and carbon oxide (CO) in cities, such as Lhasa and Xining (Chen et al., 2019; He et al., 2017; Yang et al., 2019). As a whole, these station observations cannot meet the demand of detecting the NO_2 and HCHO variations with high spatial resolution over the Tibetan Plateau, which are also crucial to the validation of satellite products over areas with complex terrain. To the best of our knowledge, there are no reports about mobile measurements of NO_2 and HCHO in the background atmosphere over the Tibetan Plateau.

The measurements of NO_2 and HCHO with high spatial and temporal resolution are challenging over the Tibetan Plateau. In the early days, some studies on NO_2 and HCHO were based on the time-consuming air sampling method (Mu et al., 2007; Meng et al., 2010; Ma et al., 2002). The air samplers were analysed by ion chromatography or a spectrophotometer for NO_2

and by a high-performance liquid chromatography and mass spectrometry or gas chromatography for HCHO in the laboratory. With the development of measurement techniques, in-situ methods started to be applied to measure surface concentrations of NO_x (NO_2) and volatile organic compounds (VOCs)~~HCHO concentrations~~ at a few stations (Wang et al., 2006; Xue et al., 2011; Wang et al., 2015; Zhao et al., 2020; Ran et al., 2014; Chen et al., 2019; Yang et al., 2019; Xue et al., 2013; Duo et al., 2018). These in-situ measurements at fixed stations were usually achieved by the chemiluminescence analyser for NO_x (NO_2) and by the gas chromatography for VOCs, respectively. However, there are limitations in the spatio-temporal representation for the sampling and in-situ measurement methods. As an alternative, satellite remote-sensing can perform long-term observations of NO_2 and HCHO and cover large areas with sparse spatio-temporal resolution, but the uncertainties of satellite NO_2 and HCHO products are rather large owing to complex terrain and weather over the Tibetan Plateau (Guo et al., 2016; Zhang et al., 2021). As a kind of advanced ground-based remote-sensing technique, Multi-AXis Differential Optical Absorption Spectroscopy (MAX-DOAS) has been certified in the measurement techniques of NDACC (Mazière et al., 2018). The successful observations of trace gases with very low abundances by MAX-DOAS depend on multi-factors, such as long optical paths, a high signal-to-noise ratio of the instrument, and characteristic spectral absorption features of the target species. According to previous studies, MAX-DOAS has the potential to measure tropospheric trace gases with very low level mixing ratios (pmol ~~m~~mol^{-1}~~ppt~~ order for NO_2 and sub-nmol ~~m~~mol^{-1}~~ppb~~ order for HCHO) in the background atmosphere at high altitude stations (Franco et al., 2015; Gil-Ojeda et al., 2015; Gomez et al., 2014; Marais et al., 2021; Schreier et al., 2016). Also, this technique has been used to measure the levels and monthly variations of NO_2 and HCHO in the global pristine atmosphere at WLG station (Ma et al., 2020). Stratospheric O_3 and its depleting substances (including NO_2) have been successfully retrieved from zenith DOAS spectra at a clean suburb station in the northern Tibetan Plateau (Cheng et al., 2021). Moreover, ground-based MAX-DOAS has been applied to monitor vertical distributions of NO_2 and HCHO in the southern Tibetan Plateau (Xing et al., 2021). Comparing with MAX-DOAS observation at a fixed site, mobile MAX-DOAS measurements in the background atmosphere over the Tibetan Plateau is a greater challenge, because: (1) Vehicle's violent vibration and bumpiness reduce the stability of the signal acquisition and even introduce unknown interference signals; (2) The measured signals can be strongly reduced by shelters due to complex terrain, such as tunnels, bridges, signposts, and mountains (usually such measurements have to be filtered out); and (3) The observations in practice are also controlled by various factors, e.g. variable weather, hypoxic environment in the plateau, geospatial signal loss and problems with the power supply. Although there are challenges in measuring~~Therefore, the~~ NO_2 and HCHO concentrations ~~measured~~ by mobile MAX-DOAS over the Tibetan Plateau, they are useful for studies on ~~are an extremely valuable data sets to characterise~~ the spatio-temporal evolution of the atmospheric composition in the background atmosphere, validation and improvement of satellite products over mountain terrain, and evaluation of the simulation results of atmospheric chemistry models over the Tibetan Plateau.

We made the mobile MAX-DOAS measurements in July 2021 over the plateau terrain for the first time. In this study, the primary objective is to analyse the spectra of scattered sun light collected in the Three Rivers' Source region over the Tibetan Plateau, obtain the data sets of tropospheric NO_2 and HCHO vertical column densities (VCDs) in the background

atmosphere ~~with high spatio-temporal resolution~~ at high altitudes, and investigate the abundances and spatio-temporal variations of tropospheric NO_2 and HCHO VCDs during the field campaign. Large effort was spent on the spectral analysis and data filtering to obtain reliable tropospheric NO_2 and HCHO VCDs, because of the very weak spectral absorptions of the respective trace gases in the background atmosphere at high altitude as well as the influences of shelters and vehicle's vibration and bumpiness along the driving routes. In Section 2, we describe the field experiment in July 2021 over the Tibetan Plateau, including the observation vehicle, MAX-DOAS instrument, experiment region and deployment strategies. Section 3 introduces the spectral analysis as well as the calculation and filtering of the NO_2 and HCHO VCDs. In Section 4, we present the abundances, ~~temporal variation and spatial distribution~~ the spatio-temporal variation of the tropospheric NO_2 and HCHO VCDs during the field campaign, as well as the comparison with TROPOMI products. Summary and conclusions are given in Section 5.

2 Field experiment

2.1 Description of vehicle and instrumentation

A mobile vehicle has been designed and assembled for measurements of atmospheric composition over the Tibetan Plateau (Fig. 1a). The mobile vehicle has been operated by the Chinese Academy of Meteorological Sciences (CAMS) since February 2021. The outside parts of instrumentation are fixed on the roof of the vehicle, which is about 3.5 m above the ground. The outside parts of instrumentation contain the sensors for spatial position (longitude, latitude, altitude) and attitude (yaw, pitch and roll angles) of the mobile vehicle. The units of the system control, data collection, screen display and Uninterruptible Power Supply (UPS) are mounted in the interior of the mobile vehicle. The UPS's battery pack, recharged after the mobile vehicle reaches the destination of observation route, can offer operation time of around 16 h with a power of 2000 W. All instrumentations have been specially reinforced to allow the mobile vehicle to travel over the ~~complex~~ difficult road conditions of the Tibetan Plateau. The mobile vehicle usually runs at a speed of ~60 km/h for motorways and ~40 km/h for ordinary roads, respectively, during our field experiment.

For the field campaign of mobile observations of the atmospheric environment over the Tibetan Plateau, the aforementioned vehicle was equipped with an instrument called Tube MAX-DOAS (Donner, 2016; Cheng et al., 2021), developed by the Max Planck Institute for Chemistry (MPIC), Mainz, Germany. The Tube MAX-DOAS contained two parts, one outside (Fig. 1b) and another inside (Fig. 1c) the vehicle, respectively. (1) The outside part was fixed on the rear of the vehicle's roof and is mainly composed of the telescope, optical fibre, stepper motor, tubular shell, and protective cover. The telescope, pointing to the back of the vehicle, rotated in the vertical plane to achieve the measurement at seven different elevation angles (3°, 6°, 10°, 15°, 20°, 30°, 90° relative to the mobile vehicle) driven by the stepper motor. The scattered sunlight was collected by the telescope and transferred to a spectrograph inside the vehicle via the optical fibre. (2) The inside part was made up of the spectrograph, data collection unit, temperature control unit as well as a laptop which controls

the instrument operation and data collection. For each elevation angle, the Tube MAX-DOAS collected one spectrum at a stable detector temperature of 15 ± 0.1 ℃ with the integration time of ~1 min. The AvaSpec-ULS2048x64-USB2 spectrograph was built by the AVANTES company and covered the wavelength range of 300~466 nm with ~0.6 nm spectral resolution. The Tube MAX-DOAS not only automatically collected the scattered sunlight spectra for the cyclic elevation angle sequences during daytime, but also recorded spectra of dark current (DC) and electronic offset (OS) at night for correcting the daytime spectra of scattered sun light. The laptop coordinated the operation of each module during the measurement procedure. The MPIC Tube MAX-DOAS system has been successfully applied to the ground-based observations of atmospheric composition at the Golmud station over the ~~Northern~~ northern Tibetan Plateau (Cheng et al., 2021).

2.2 Description of the measurement location and deployment strategies

The mobile field observation campaign was performed over the Three Rivers' Source region on the northeast of the Tibetan Plateau in western China (Fig. 2~~a~~). ~~With the average altitude of 3000 ~ 5000 m, this region is the source catchment area of many rivers, such as the Yangtze River, Yellow River and Lancang River (i.e. so-called "Three Rivers' Source"). The Three Rivers' Source region is also one of the regions with the highest concentration of high-altitude biodiversity in the world. As one of five national parks, the establishment of the Three Rivers' Source national park was approved by the China State Council on 30 September 2021.~~ The main vegetation types are alpine steppe and meadows in the region along the observation route, belonging to a unique and typical alpine ecosystem. The main landform is the mountain plain ~~in the field measurement area~~. The Three Rivers' Source region has a typical plateau continental climate, characterized by ~~distinct dry and wet seasons, alternate hot and cold seasons, a small annual temperature difference,~~ a large diurnal temperature difference, long sunshine time~~,~~ and strong solar radiation ~~and four indistinct seasons~~. There are also rapid spatial and temporal variations of the local climate over the Three Rivers' Source region. Yak and sheep grazing in summer is the main industry over the Three Rivers' Source region, isolated from industrial and population centres~~. Therefore, this remote region is an excellent natural laboratory to investigate the background atmosphere~~.

In order to reveal the background abundance and spatio-temporal variation of the atmospheric composition over the Three Rivers' Source region, we took various factors into consideration during the design of the deployment strategies, such as the regional representativeness of the driving routes, the technical requirement of the passive MAX-DOAS measurement, the sunlight shelter and the bumpy condition along the driving route, the reliable electric power safeguard, and first aid for sudden altitude sickness. Finally, the mobile MAX-DOAS field experiment was carried out in the southeast of Qinghai province, China (Fig. 2b). The driving routes traverse the Yangtze River and the Yellow River and are close to the Lancang River. It took three days for one circling journey. Four circling journeys were made during the mobile MAX-DOAS field experiment period in July 2021 (Table 1). We drove from the meteorological bureau of Xining city, the capital of Qinghai province, to the meteorological bureau of Dari county of the Guoluo Tibetan autonomous prefecture, south-eastern Qinghai province, on the first day of each circling journey (~~red curve in~~ Fig. 2~~b~~). We travelled from the meteorological bureau of

Dari county to the meteorological bureau of the Yushu Tibetan autonomous prefecture on the middle day (~~blue curve in~~ Fig. 2~~b~~). We returned to Xining city from the Yushu Tibetan autonomous prefecture on the third day (~~black curve in~~ Fig. 2~~b~~). Hereafter the three segments of the closed-loop journey are referred to as XD, DY, YX, respectively. The durations were about 12 h, 8 h, and 13 h for the XD, DY, and YX segments, respectively. Most of driving routes are motorways, except parts of the national roads in the YX segment. More sunlight shelters occurred in the XD segment, because of the tunnels, bridges, signposts, and mountains. The observed MAX-DOAS data were saved in the laptop, and backed up when arriving at the terminus of each segment of the journey. In addition to troubleshooting by field observers, our MAX-DOAS team also provided the technical support via remote wireless network during the campaign.

3 Spectral retrieval and data filtering

3.1 Spectral analysis

Based on the Beer-Lambert law, the column densities of trace gases can be retrieved from the scattered sunlight spectra by the widely used method of Differential optical absorption spectroscopy (DOAS) (Platt and Stutz, 2008). The basic idea of DOAS is to decompose the atmospheric spectral extinction into two terms, i.e. terms with slow spectral variation (such as atmospheric scattering) and fast variation (mainly trace gas absorptions) with wavelength. The slant column density (SCD) of a trace gas is defined as its concentration integrated along the effective light path (Cheng et al., 2019). The total (from the instrument to the top of atmosphere) SCD can be split into two parts, i.e. so-called tropospheric SCD (SCD_{Trop}) and stratospheric SCD (SCD_{Stra}). For species concentrated in the troposphere or light traversing the same path in the stratosphere for different elevation angles (α), the SCD_{Stra} can be neglected or cancels out respectively, which means $SCD_{\alpha,Stra} \approx SCD_{90,Stra}$ (Ma et al., 2013). In the practice of the MAX-DOAS spectral analysis, a Fraunhofer reference spectrum (FRS) needs to be selected to correct the strong solar Fraunhofer lines. Thus the result of the spectral analysis is the so-called differential slant column density (DSCD) of the target species (such as NO_2 and HCHO in this study), which represents the difference in trace gas absorption between the measured atmospheric spectrum and the FRS (Hönninger et al., 2004). There are two schemes for the FRS selection from measured spectra (Wang et al., 2018): one is using a fixed spectrum (hereafter named "fixed FRS"), usually at the 90°elevation angle during noon to minimize the tropospheric and stratospheric contributions, for all measured spectra; the other is using sequential spectra (hereafter named "sequential FRS"), which are defined as the time interpolated ~~interpolated~~ spectra between two zenith spectra measured before and after the measurement time of the current off-zenith elevation angle~~an off-zenith sequence of elevation angles~~. Due to more similar atmospheric conditions and instrument properties between a specific measured spectrum and the corresponding sequential FRS, higher signal-to-noise ratios and smaller fitting errors are achieved by using a sequential FRS than a fixed FRS. Fig. 3 shows the root mean square (RMS) of the spectral fitting residuals using a fixed FRS and sequential FRS for NO_2 and HCHO, respectively. It is clear that the RMS medians are smaller for using a sequential FRS than that for a fixed FRS. Thus we prefer to use the sequential

FRS for the mobile MAX-DOAS measurement in this study. For NO_2, we can retrieve the DSCD not only in the ultraviolet (UV) region (351~390 nm) but also in the visible region (400~434 nm) (Cheng et al., 2022; Cheng et al., 2019). Fig. 4 compares the NO_2 DSCDs and the RMSs of the spectral fitting residuals for using either the visible and UV spectral interval. The overall trends of the NO_2 DSCDs are consistent between both spectral intervals with the correlation coefficient of R=0.75, but the averaged RMSs of the spectral fitting residuals in the visible wavelength region, i.e. $(6.26 \pm 6.92)\times10^{-4}$, are smaller than those in the UV wavelength interval, i.e. $(7.62 \pm 9.17)\times10^{-4}$. The final settings of the NO_2 and HCHO spectral retrieval parameters, such as cross sections of the target and interference species, Ring spectra, polynomial degree and intensity offset, similar as in previous studies (Cheng et al., 2022; Cheng et al., 2019), see Table 2. The spectral analysis, including DC and OS corrections of the measurement spectra and the spectral calibration of the FRS, was implemented by the QDOAS software based on a non-linear least squares fitting method, developed by the Royal Belgian Institute for Space Aeronomy (BIRA-IASB) (Danckaert et al., 2017). Fig. 5 shows an example of the spectral fitting for the NO_2 and HCHO DSCDs from a spectrum measured at the elevation angle of 15° at 11:02 BJT on 18 July 2021 (SZA = 34.11°). In the post processing of NO_2 and HCHO DSCDs, we applied the following filters: RMS < 0.005; offset (constant) should be between ± 0.03; SZA < 80°. These filters were selected as they provide a good balance between quality of the results and skipping not too many data. These filters almost filtered out all "bad measurements", which were caused by sunlight shelters and bumpy conditions. Finally, relative to measurements with SZA<90°, the percentages of remaining DSCD data were 69% for NO_2 and 74% for HCHO, respectively. We estimated the instrument detection limits of NO_2 and HCHO DSCDs to be twice the medians of the spectral fit errors (Cheng et al., 2021), i.e., 0.68×10^{15} molec cm^{-2} and 2.11×10^{15} molec cm^{-2} at 15° elevation angle respectively. According to the DSCD detection limits divided by the differential air mass factor (DAMF) for 15° elevation angle, the VCD detection limits were estimated to be about 0.24×10^{15} for NO_2 and 0.74×10^{15} for HCHO, respectively. There are 17% and 15% of the retrieved NO_2 and HCHO DSCDs below the detection limits, respectively. Based on the spectral fit errors, we can also calculate the relative errors for each NO_2 and HCHO DSCD. Then the mean relative errors of NO_2 and HCHO DSCDs were about 21% and 12% at 15° elevation angle, respectively.

3.2 NO_2 and HCHO VCDs

Based on the aforementioned filtered NO_2 and HCHO DSCDs retrieved from the spectra, we need to firstly obtain the tropospheric DSCDs at the elevation angle α (i.e., $DSCD_{\alpha,Trop} \equiv SCD_{\alpha,Trop} - SCD_{90,Trop}$), which are used to calculate the NO_2 and HCHO vertical column densities (VCDs) in the troposphere. In the situation of fixed FRS, the $DSCD_{Trop}$ are produced by the DSCDs of off-zenith viewing direction minus that at 90° elevation angle of the same elevation sequence; In the case of sequential FRS in this study, the DSCDs from spectral inversion can be regarded as $DSCD_{Trop}$ (Hönninger et al., 2004).

The SCDs (or DSCDs) depend on the concentration profile of target species, effective light path length, measurement geometry and solar position. Using the air mass factor (AMF), the SCDs (or DSCDs) can be converted to the VCDs, which are independent of the light path and the observation geometry and thus convenient for comparison between different measurements. The tropospheric AMF at the elevation angle α ($AMF_{\alpha,Trop}$) is given by the ratio of the SCD to VCD in the troposphere:

$$AMF_{\alpha,Trop} = \frac{SCD_{\alpha,Trop}}{VCD_{Trop}} \quad (1)$$

If $\alpha = 90^{\circ}$,

$$AMF_{90,Trop} = \frac{SCD_{90,Trop}}{VCD_{Trop}} \quad (2)$$

We define the $DAMF_{\alpha,Trop}$ as the tropospheric differential AMF, i.e.

$$DAMF_{\alpha,Trop} = AMF_{\alpha,Trop} - AMF_{90,Trop} \quad (3)$$

By equation (1) minus equation (2), VCD_{Trop} can be deduced:

$$VCD_{Trop} = \frac{SCD_{\alpha,Trop} - SCD_{90,Trop}}{AMF_{\alpha,Trop} - AMF_{90,Trop}} = \frac{DSCD_{\alpha,Trop}}{DAMF_{\alpha,Trop}} \quad (4)$$

where the AMF can be simulated by an atmospheric radiative transfer model or estimated by the method of geometric approximation. The former method is more accurate~~exact~~, but requires information~~depends~~ on various input parameters, such as the profiles of trace gas and aerosol, which are usually not known. The latter method is simpler and assumes trace gases are uniformly distributed in the lower troposphere~~less correct, but relatively simple and also applicative to get the VCD_{Trop}, if target species are mainly distributed in the lower troposphere~~. Due to the lack of necessary data over the Tibetan Plateau to simulate the correct NO_2 and HCHO AMFs, we adopted the geometric approximation method in this study. Here it should be noted that the errors caused by the geometric approximation method are much smaller for measurements at high altitudes, because the scattering probability is much smaller compared to measurements at sea level. Thus the direct viewing path length becomes longer and is in better agreement with the assumptions of the geometric approximation method. We explored the applicability of the geometric approximation method by radiative transfer simulations. For typical trace gas and aerosol profiles, the errors of the geometric approximation are <20% for NO_2 and HCHO (see Sect. S1). The $AMF_{\alpha,Trop}$ in the condition of geometric approximation in polluted environment can be expressed as:

$$AMF_{\alpha,Trop} \approx \frac{1}{\sin(\alpha)} = \sin^{-1}(\alpha) \quad (5)$$

Therefore, equation (4) becomes

$$VCD_{Trop} = \frac{DSCD_{\alpha,Trop}}{\sin^{-1}(\alpha) - 1}, (\alpha \neq 90^{\circ}, AMF_{90,Trop} = 1) \quad (6)$$

Ideally, the elevation angles should be corrected by the attitude angles of the mobile vehicle when applying the geometric approximation. However, the partial system of the attitude angles of the mobile vehicle did not work well, which may be connected with the special environment of Tibetan Plateau (such as low atmospheric pressure) and bumpiness of the mobile observation platform (leading to instabilities of the data collection). Thus we use the uncorrected elevation angles during the

conversion of DSCD to VCD in equation (6). Of course, the uncorrected elevation angles will cause some errors if the mobile observation vehicle is not on a horizontal surface, but on average these errors will partly cancel out. Also these errors are typically small for the larger elevation angles (for example, 15°, 20°, 30°) and can be neglected when compared to other uncertainties. Based on the mobile platform attitude angles, the elevation angle error is estimated to be about 2.3°. The corresponding error of an individual measurement will be up to about 21%. However, it should be noted that on average the positive and negative deviations of the elevation angle will almost cancel each other. Thus the errors of individual measurements will be usually much smaller (except for measurements on continuous strong slopes). For averages of several measurements the errors of the elevation angles lead to much smaller VCD errors with a magnitude smaller than 1% when using geometric approximation method. To further judge how good the geometric approximation is, the resulting VCDs derived for different elevation angles have been compared (Brinksma et al., 2008). ~~Fig. 6~~Table 3 shows the NO_2 (HCHO) VCDs between the three elevation angles (15°, 20°, 30°). The VCDs are rather consistent at the three elevation angles with correlation coefficients of R=0.91~~–~~0.95 for NO_2 and R=0.66~~–~~0.80 for HCHO, respectively (Table 3). This implies that the geometric approximation method is self-consistent~~has high accuracy~~. The standard deviation of the NO_2 (HCHO) VCDs is small at 15° elevation angles (~~Fig. 6~~Table 3), implying the high reliability of VCDs at 15° elevation angle ($VCD_{15^{\circ}}$). Therefore, to compromise between accuracy of the geometric approximation and signal to noise, the $VCD_{15^{\circ}}$ were treated as the reliable results on a selection criterion (for NO_2, the absolute difference of VCDs between 15° and 20° is $< 1\times10^{15}$ molec cm^{-2} or the relative difference is <5%; for HCHO, the absolute difference of VCDs between 15° and 20° is $< 2\times10^{15}$ molec cm^{-2} or the relative difference is <5%). The filtered NO_2 and HCHO $VCD_{15^{\circ}}$ during the mobile measurement period were kept as the final results to explore the background abundance and spatio-temporal variation of NO_2 and HCHO over the Three Rivers' Source region of the Tibetan Plateau. It spent about 8 min for measurements at two adjacent 15° elevation angle. Therefore, the corresponding spatial resolution was approximately 8 km at a speed of ~60 km/h of the mobile vehicle. Assuming that the trace gas is located in the lowest 1000 m above the surface, we can also estimate the horizontal extent of the line of sight through that layer. For measurements at 15° elevation angle, this extent is about 4km.

From our experience during the measurements, we also suggest that the telescope scans at 15°, 20°, 90° elevation angles in future mobile MAX-DOAS measurements of the background atmosphere over mountain terrain. There are at least two reasons: (1) The relatively large elevation angles are less influenced by the road tilt and obstructions; (2) The measurements at 15° and 20° elevation angles have still an enhanced sensitivity to tropospheric trace gases (increase of sensitivity compared to 90° elevation angle is about a factor 3.8 and 2.9, respectively).

4 Interpretation of the results

4.1 Abundance

Based on filtered final NO_2 and HCHO VCDs, the means ± standard deviations were 0.69 ± 1.13 $\times 10^{15}$ molec cm^{-2} for NO_2 and 2.43 ± 1.66 $\times 10^{15}$ molec cm^{-2} for HCHO in July 2021 along the driving routes. The background levels of NO_2 and HCHO VCDs can be estimated by the maximum frequency method (Cheng et al., 2017). According to the Lorentz fitted curves of the relative frequency distribution of the NO_2 and HCHO VCDs during the field campaign (Fig. ~~7a~~6a), the background levels were 0.40 ± 0.23 $\times 10^{15}$ molec cm^{-2} for NO_2 and 2.27 ± 0.96 $\times 10^{15}$ molec cm^{-2} for HCHO in summer on the northeast of the Tibetan Plateau. The uncertainties of the background levels were estimated by the half width at half maximum of Lorentz fitted curves (Fig. 6a). The~~se values~~ background levels are smaller than those observed in summer 2018~~–~~ at the Qomolangma Atmospheric and Environmental Observation and Research Station of the Chinese Academy of Sciences, located in the south-central Tibetan Plateau (medians of 0.80 $\times 10^{15}$ molec cm^{-2} for NO_2 and 3.13 $\times 10^{15}$ molec cm^{-2} for HCHO, respectively) (Xing et al., 2021). To explore the dependence of the NO_2 and HCHO VCDs on the route altitude (in the range of 2280~4830 m), we divided the mobile route altitudes into vertical bins with intervals of 500 m. Fig. ~~7b~~ 6b shows the means, medians and standard deviations of the NO_2 and HCHO VCDs in each vertical grid cell. There are generally decreasing trends with increasing altitude. This is consistent with our knowledge of the natural background atmosphere, i.e. the higher the altitude, the lower the air density. Different from the nearly constant decreasing rate of the HCHO VCDs with the route altitude, there are at least two segments with significantly different decreasing rates above and below 2750 m altitude. The NO_2 VCDs in the 2000~2500 m grid cell (8.17 $\times 10^{15}$ molec cm^{-2}) were substantially larger because the mobile route was close to the city of Xining (about 2260 m altitude), where there are stronger anthropogenic emission sources of air pollutants, such as increased urban transport emissions leading to higher NO_2 levels. The NO_2 VCDs were quite low in the altitude above 3500 m, partly related to almost no human activities at this altitude. Due to very limited emissions of anthropogenic ~~volatile organic compounds (~~VOCs~~)~~ over the Tibetan Plateau, the changes of the HCHO VCDs with altitude were likely to be primarily connected with the natural process, such as the oxidation of methane and non-methane volatile organic compounds (Stavrakou et al., 2009). Combining the hourly surface air pressure and temperature at 2 m above the land surface with the 0.25 °×0.25 °resolution from ERA5, the profiles of NO_2 and HCHO mixing ratios were also derived from the corresponding mean and median VCDs along driving routes, respectively (Fig. S2). As a whole, the measurements (except close to the cities) at the higher altitudes in summer are able to reflect the background atmosphere with rather low NO_2 and HCHO levels over the Three Rivers' Source region.

4.2 Spatio-temporal variation

4.2.1 NO_2

The ~~daily~~ day-to-day variations of NO_2 VCDs are similar between different circling journeys, characterized by the larger means and 90th percentiles on the first and the third days (i.e. on the days of the XD and YX driving routes) and correspondingly lower values on the second day (i.e. on the day of the DY driving route) of each circling journey (Fig. 7a). The NO_2 means are always larger than the medians on each day, especially in the situation of the XD driving route, partly because the driving route covers small areas with very high NO_2 abundances, such as Xining city, and large background areas with relatively low NO_2 abundances in the XD driving route. For the same driving route of the four circling journeys, the daily NO_2 levels are close to each other, with the NO_2 medians in the range of 0.19~~–~~0.63 $\times 10^{15}$ molec cm^{-2} during the field campaign.

Figure ~~11~~ 8 shows the spatial distributions of the tropospheric NO_2 VCDs along the XD, DY, and YX driving routes in July 2021. For the same segment of four circling journeys (i.e. XD, DY, or YX), the tropospheric NO_2 VCDs present a nearly consistent spatial distribution. It is also clear that the tropospheric NO_2 VCDs were elevated when the mobile observation vehicle passed through counties or cities, such as Xining and Yushu. This can be attributed to increased anthropogenic activities in cities or counties, such as traffic and residential emissions. There are significantly larger NO_2 VCDs on the driving routes of south-eastern Qinghai Lake, which is a famous tourist destination. Moreover, as one of the arterial roads to Tibet, there are many diesel vehicles passing through the basin of Qinghai Lake via national highways surrounding the lake. The touring buses or cars as well as the cargo transport vehicles could lead to the higher NO_2 abundances in summer around the Qinghai Lake. According to previous studies at the northwest section of the Qinghai Lake shore in October of 2010 and 2011, the emissions from diesel vehicles around Qinghai Lake were likely the main source of nitrogen oxides (NO_x) (Wang et al., 2015). The enhanced NO_2 levels could even be found at the highway junction (such as the location of 98.97 °E, 35.20 °N) and the tunnel exit (such as the location of 99.40 °E, 34.92 °N; Note: The telescope of the MAX-DOAS pointed to the backward of the driving direction) (Fig. ~~11a1~~8a1, d1). This situation would not appear once traffic flow was lower~~vehicle flowrate was less~~ at these special locations (Fig. ~~11b1~~8b1, c1). The NO_2 spatial distributions over the main area of the Three Rivers' Source, such as around the counties of Dari, Shiqu, Chenduo, and Maduo during the DY driving route and the first half of the YX driving route, were relatively uniform with very low levels ($<1 \times 10^{15}$ molec cm^{-2}). Previous investigations of the tropospheric ozone chemical budget, simulated and constrained by measured NO_2 concentration at the Waliguan background station located in the north-eastern Tibetan Plateau, showed that the NO_x levels play the vital role in the net sign of ozone production from formation and loss reaction for the tropospheric background atmosphere (Ma et al., 2002; Ma et al., 2020; Xue et al., 2013). Therefore, with the more and more anthropogenic activities, the effects of increasing NO_2 levels on the photochemistry and oxidation capacity of the background atmosphere should be paid more attention to better build an ecological civilization over the remote Three Rivers' Source region in the future.

~~The average daytime diurnal variations of the tropospheric NO_2 VCDs during the mobile MAX-DOAS field campaign in July 2021 over the Three Rivers' Source region of the Tibetan Plateau are presented in Fig. 9.~~ The available time period, confined by the sunshine duration and the distance of the driving routes, is the shortest for the DY driving route. The diurnal cycle of the NO_2 VCD means or medians presents high values in the morning and evening and shows lower levels of ~0.38 $\times 10^{15}$ molec cm^{-2} from 12:00 BJT to 17:00 BJT (Fig. 9a). The means of the NO_2 VCD are also significantly higher than the corresponding medians before 11:00 BJT with larger standard deviations. The NO_2 diurnal variation patterns of the XD, DY, and YX driving routes are different, although the diurnal patterns are rather consistent for different days of the same driving route (Fig. 9b-d). The NO_2 VCDs sharply decreased in the morning during the XD driving route, with larger standard deviations around 16:00 BJT, when the mobile observation vehicle was close to the toll station. For the DY driving route, the NO_2 VCDs stayed at the lower level and then slightly increased in the late afternoon. In the situation of the YX driving route, the diurnal pattern of NO_2 VCDs was a symmetric "U" shape. It should be noted that the mobile observation vehicle reached the destination of the YX driving route around 22:00 BJT and the lacking NO_2 VCDs were due to SZA > 80 ° after 20:00 BJT. The amplitudes of the NO_2 diurnal variation as well as the maxima NO_2 level among different driving routes were decreasing in the order of the segments XD, YX, and DY. Previous studies at the background station of lower altitude showed that ~~a similar "U" shape of~~ the NO_2 diurnal variation~~, which was connected with~~ could be affected by the higher photolysis rate owing to stronger solar irradiance at noon and for a site location far away from emission sources (Cheng et al., 2019). ~~Compared with observations in summer at the Qomolangma station in the south central Tibetan Plateau, the daytime NO_2 diurnal pattern in this study is more continuous (although it is hard to compare quantitatively due to large uncertainties of the NO_2 diurnal pattern at Qomolangma caused by a lot of missing data) (Xing et al., 2021).~~ We also checked whether the enhanced NO_2 VCDs in the morning and evening might be an artefact caused by the effect of stratospheric NO_2 on the derived tropospheric NO_2 VCD. In our data analysis (see section 3.1) it is assumed that the stratospheric NO_2 absorption is independent on the elevation angle. While this is not exactly true, it is a valid assumption for typical measurement situations in polluted or slightly polluted environments. If, however, the tropospheric NO_2 absorption is very weak, the remaining stratospheric influence might be substantial. We tested this potential influence of the stratospheric NO_2 absorption on the retrieved tropospheric NO_2 VCD for our measurements, by performing radiative transfer simulations using a stratospheric NO_2 profile with a stratospheric NO_2 VCD of 4 $\times 10^{15}$ molec cm^{-2}. As a result, we found that for SZA < 80 ° the introduced NO_2 DSCD for an elevation angle of 15 ° is < 1 $\times 10^{15}$ molec cm^{-2} (see Fig. ~~S2~~S3) thus leading to a maximum artificial NO_2 VCD of 3.5×10^{14} molec cm^{-2}. Moreover, for SZA<80 °, the artificial NO_2 VCD shows almost no SZA dependence. Thus the potential influence of the stratospheric NO_2 absorption cannot explain the observed diurnal cycle of the tropospheric NO_2 VCD. From these findings we conclude that the NO_2 diurnal variations were primarily caused by enhanced pollution in the morning and evening when the mobile observation vehicle was located in or close to the cities or county town, i.e. the NO_2 diurnal patterns reflected the differences of the NO_2 spatial distribution. An additional effect on the diurnal variation is probably caused by the enhanced NO_2 photolysis around noon.

4.2.2 HCHO

~~However, the daily variations of the HCHO VCDs are different from those of NO_2.~~ The means and medians of the daily HCHO VCDs are basically consistent on all days, with the maximum mean of 4.63 $\times 10^{15}$ molec cm^{-2} on 21 July 2021 and the minimum mean of 1.15 $\times 10^{15}$ molec cm^{-2} on 27 July 2021 (Fig. 7b). There are obvious differences in the levels of HCHO VCDs between the different circling journeys. The higher and lower HCHO VCDs appeared during the second circling journey (i.e. 21-23 July 2021) and the third circling journey (i.e. 25-27 July 2021), respectively. HCHO has large natural vegetation sources, with the emission strength depending strongly on weather conditions such temperature and solar radiation at the Earth's surface (Borovski et al., 2014). We looked at air temperature at 2 m above the land surface and the downward solar radiation at the surface (SSRD), which are derived from hourly ERA5 reanalysis data with 0.25 °×0.25 ° resolution~~,~~. According to the ERA5 grid cell and hour to which each HCHO measurement belongs, the air temperature and SSRD are extracted and then averaged for each day (Fig. 10a).~~and interpolated them to the geographical and time intervals corresponding to the daily HCHO VCDs.~~ It is shown that the daily variations between air temperature and HCHO VCDs are highly correlated, with the correlation coefficient of R=0.95 (Fig. ~~8b~~7b, ~~S1~~10b). Probably~~This implies that~~ higher temperatures are connected with more VOCs emitted by vegetation, leading to higher HCHO VCDs. The daily HCHO VCDs are also related to surface solar radiation, but with a smaller correlation coefficient of R=0.27 (Fig. 10b), which is probably caused by the higher variability of local solar radiation over the Tibetan Plateau compared to the temperature. ~~For different segments of the specific circling journey, the relative variability in the 90th percentiles of the daily HCHO VCDs is smaller than that of NO_2, implying that the local cities over the Tibetan Plateau (such as Xining) along the driving route have less influence on HCHO compared to NO_2.~~ Therefore, the remarkable HCHO daily variations are mainly connected with the variable weather over the Tibetan Plateau, which affects the natural emissions of HCHO precursors significantly.

Figure ~~12~~ 11 shows the spatial distributions of the HCHO VCDs during the field campaign in July 2021. For the specific driving routes (XD, DY or YX), the HCHO spatial distributions were similar on different days. Normally, the HCHO VCDs were lager at the starting points and ending points of the driving routes (if reaching to the ending points in the condition of SZA < 80 °), which matched with the larger HCHO values in the morning and evening (Fig. ~~10~~12). However, the HCHO levels were significantly different at the same location on different days. For example, the HCHO VCDs on the second circling journey (Fig. 11b1-b3) were obviously larger than those on the other three circling journeys, most probably due to higher surface temperatures on the second circling journey (Fig. ~~12, S3~~S4). From the northeast to the southwest in the region of the mobile observation field experiment, the HCHO VCDs present a decreasing trend. These lower HCHO levels in the main area of Three Rivers' Source reflect the overall conditions of atmospheric HCHO background. The spatial distributions of HCHO column observed by the OMI satellite from 2009 to 2019 over the Tibetan Plateau also found that the regions with sparse population and less human activities were frequently affected by natural factors, such as air temperature and precipitation (Zhang et al., 2021). The elevated HCHO VCDs around Maqin county of the XD driving route were partly related to anthropogenic HCHO emissions, such as biomass burning and fossil fuel combustion (Fig. 11a1, b1, c1, d1)

(Zhang et al., 2021). Comparing the HCHO VCDs before and after Maduo county on the YX driving route, the former was larger than the later, corresponding to the jump of the HCHO diurnal variation before and after 13:00 BJT (Fig. 12d). Besides the differences in human activities, the spatial step changes in the HCHO VCDs were also partly connected with the decreasing altitudes on the YX driving route (Fig. 2ba).

~~The diurnal variation of the tropospheric hourly HCHO VCDs for the entire campaign, each day, and three segments of the circling journey are shown in Fig. 10.~~ With respect to the total means and medians of the HCHO VCDs in the range of 1.92~~–~~4.36 $\times 10^{15}$ molec cm^{-2} (Fig. ~~10a~~12a), their diurnal variations are rather consistent during the whole day. They slightly decrease before 10:00 BJT and increase after 18:00 BJT, and also have no significant differences in the standard deviations. However, the diurnal variations of the HCHO VCDs are obviously different both for different days of the same driving route or among different driving routes (Fig. ~~10b~~12b-d). On average, the diurnal pattern of the HCHO VCDs during the XD driving route presents a weak "U" shape, i.e. slightly higher HCHO levels in the morning and evening. For the DY driving route, the total averaged HCHO VCDs almost maintain the level around 2 $\times 10^{15}$ molec cm^{-2} before 14:00 BJT, and then gradually increase until the end of the DY journey. The diurnal pattern of the HCHO VCDs for the YX driving route presents a "W" shape, i.e. higher HCHO VCDs occur around 13:00 BJT, in the morning and in the evening. The variable diurnal cycles of HCHO VCDs were also found by ship-based MAX-DOAS measurements over the middle and lower Yangtze River in winter, where the both primary sources and photochemical secondary formation have large influences (Hong et al., 2018). ~~The daytime HCHO diurnal patterns in this study are also distinguished from those observed by ground-based MAX-DOAS at the Qomolangma station in the south central Tibetan Plateau in summer, where HCHO peaks appeared around 12:30, 15:00, and 18:00 BJT (Xing et al., 2021).~~ Even at the starting and ending points of the driving route, there were almost no strong HCHO primary sources caused by anthropogenic activities over the Three Rivers' Source region. Thus we infer that the variable diurnal patterns of HCHO were mainly connected with the secondary photochemical formation of active VOCs emitted from vegetation (Mu et al., 2007). Meanwhile, due to the varying local microclimates over the Tibetan Plateau as well as different types and amounts of vegetation at different altitudes, the ~~temporal~~ diurnal variations of secondary HCHO production are quite changeable and closely related to the specific property of a location. More comprehensive observations are needed over the Tibetan Plateau in the future to deeply understand the HCHO spatio-temporal evolution.

4.~~4~~ 3 Comparison with TROPOMI observations

The TROPOspheric Monitoring Instrument (TROPOMI) is the sole payload on the Copernicus Sentinel-5 Precursor (Sentinel-5P or S5P) satellite, which provides measurements of multiple atmospheric trace species including NO_2 and HCHO at high spatial and temporal resolutions (Veefkind et al., 2012). The S5P reference orbit is a near-polar sun-synchronous orbit with a mean Local Solar Time of 13:30 at Ascending Node. TROPOMI covers the wavelength ranges of ultraviolet-visible (270~495 nm), near infrared (675~775 nm), and shortwave infrared (2305~2385 nm) with a 108°

Field-of-View in nadir view. TROPOMI achieves daily global coverage with a spatial resolution of 5.5×3.5 km^2 at nadir since the along-track pixel size reduction on August 6, 2019. The NO_2 retrieval consists of a three-step procedure: (1) The total NO_2 SCDs are retrieved from the Level-1b spectra measured by TROPOMI using the DOAS method; (2) The total NO_2 SCDs are separated into stratospheric SCDs and tropospheric SCDs on the basis of information coming from a data assimilation system; (3) The tropospheric NO_2 SCDs are converted into VCDs through a look-up table of tropospheric AMFs. The 1st and 3rd steps also apply to HCHO, but in addition, a bias of the HCHO SCDs needs to be corrected before the conversion of the HCHO SCDs to VCDs. In this study, we use the TROPOMI level-2 NO_2 and HCHO products (i.e. S5P_L2__NO2____HiR and S5P_L2__HCHO___HiR) downloaded from the NASA Goddard Earth Sciences Data and Information Services Center (GES-DISC) (ESA and KNMI, 2021; ESA and DLR, 2020). For comparison between the mobile MAX-DOAS and TROPOMI observations, their NO_2 and HCHO VCDs are gridded into 0.25 °×0.25 ° cells (Fig. 13, 14). The reason for averaging two data sets into 0.25 °×0.25 ° grid is to balance the spatial resolution and the amount of observed NO_2 and HCHO VCDs at specific grid cell.

Figure 13 shows the spatial distributions of the tropospheric gridded NO_2 VCDs from TROPOMI on each day of the field campaign. The spatial distributions of the tropospheric NO_2 VCDs are basically consistent on different days, i.e. higher values are found in the northeast and lower values in the southwest. Similar as for the mobile MAX-DOAS, the TROPOMI NO_2 VCDs are larger around Xining city than in the main area of Three Rivers' Source region. But the elevated trends of the tropospheric NO_2 VCDs around the counties, which are clearly observed by the mobile MAX-DOAS, are nearly not captured by TROPOMI. To validate the fine-scale (0.25 °×0.25 °) spatial variability in tropospheric NO_2 VCDs, we made a linear regression analysis between both data sets (Fig. 15a). When using all tropospheric NO_2 VCDs at the same grid cell on the same day during the field campaign (referred to 'All' in Fig. 15a, corresponding to the white circles in Fig. 13), the consistency is good with a correlation coefficient of R=0.67 between the two data sets. However, the slope is much lower than unity indicating that ~~TROPOMI systematically underestimates~~ the NO_2 VCDs from TROPOMI are systematically lower than those from mobile MAX-DOAS over the polluted areas~~, in agreement with previous studies~~. Besides of the probable underestimation of TROPOMI, the lower TROPOMI NO_2 VCDs are also connected with the time differences between the two observation methods at the same grid cell. Interestingly, there is almost no correlation of the two data sets, if we only use the tropospheric NO_2 VCDs within the 1.5 h time difference between mobile MAX-DOAS and TROPOMI at the same grid (referred to '$\Delta T_{1.5}$' in Fig. 15a, corresponding to the red pluses in Fig. 13). Comparing the situations of 'All' and '$\Delta T_{1.5}$', significant differences in the correlation are connected with the former including the larger NO_2 VCDs close to the cities, inferred by the locations of the grid cell in Fig. 13. For the '$\Delta T_{1.5}$' comparison, mostly the low background values are included. These results indicate the TROPOMI can distinguish the differences in tropospheric NO_2 VCDs between city and background atmosphere~~, but can't identify the fine-scale spatial variability in the tropospheric NO_2 VCDs in background atmosphere~~ over the Tibetan Plateau. Relative to the NO_2 VCDs by mobile MAX-DOAS during the field campaign, the relative differences of the NO_2 VCDs by TROPOMI are -12% and 40% for 'All' and '$\Delta T_{1.5}$' on average, respectively. The positive bias for '$\Delta T_{1.5}$' is probably related to the mountain terrains over the main area of the Three Rivers' Source. As a

whole, in contrast to routine TROPOMI validation based on site observations (Verhoelst et al., 2021), the mobile MAX-DOAS observations can serve as a supplement to quantify the impact of the fine-scale NO_2 horizontal variability on satellite products.

In contrast to NO_2, the spatial distributions of the tropospheric gridded HCHO VCDs from TROPOMI are not uniform among different days of the field campaign (Fig. 14). The higher HCHO VCDs appear more in the second circling journey and the lower HCHO VCDs in the third and fourth circling journey, consistent with the aforementioned results derived from mobile MAX-DOAS. The HCHO levels around the city of Xining are also not significantly enhanced, even lower than those in the main area of the Three Rivers' Source region on some days, such as 25 July 2021. We also perform a linear regression analysis of tropospheric HCHO VCDs derived from mobile MAX-DOAS and TROPOMI, respectively. Whether for 'All' (corresponding to the white circles in Fig. 14) situation or for '$\Delta T_{1.5}$' (corresponding to the red pluses in Fig. 14) situation, the correlation coefficients are the same (R=0.26 in Fig. 15b), indicating that there are no strong anthropogenic HCHO sources along the driving routes even in the city of Xining. The rather small correlation coefficient between the two data sets is also related to the rather small variability of the HCHO VCDs and the relatively ~~large noise in~~ low signal-to-noise ratio of the TROPOMI satellite product~~, which prevents to monitor the fine-scale spatial variability in tropospheric HCHO VCDs~~ in background atmosphere over the Tibetan Plateau. Comparing the '$\Delta T_{1.5}$' situation between NO_2 and HCHO, the correlation of the tropospheric HCHO VCDs is higher than that of NO_2, which is probably related to the stronger HCHO daily variations in the background atmosphere influenced by natural factors, such as air temperature and precipitation (Zhang et al., 2021). Similar to the validations of TROPOMI at remote sites by ground-based solar-absorption Fourier-transform infrared (FTIR) measurements (Vigouroux et al., 2020), an overestimation of the true HCHO VCD by TROPOMI is also found during the field campaign, with significantly larger relative differences of 104% and 87% for 'All' and '~~'~~$\Delta T_{1.5}$' on average, respectively (Fig. 15b). This large positive offset of the TROPOMI HCHO VCDs is probably connected with the horizontal HCHO inhomogeneity, caused by mountain terrain and varying local microclimates over the Tibetan Plateau. Therefore, although TROPOMI significantly improves the precision of the HCHO observations at short temporal scales and for low HCHO columns (De Smedt et al., 2021), it is still ~~very difficult~~a challenge for satellite instruments to detect the ~~fine-scale spatial and~~ spatio-temporal variations of HCHO over the Tibetan Plateau.

5 Summary and conclusions

In this study we performed mobile MAX-DOAS measurements over the Tibetan Plateau in summer (18–30 July) 2021 for the first time. We analysed spectra of scattered sun light collected in the Three Rivers' Source region over the Tibetan Plateau, and obtained the data sets of tropospheric NO_2 and HCHO VCDs in the background atmosphere ~~with high spatio-temporal resolution~~; We further investigated the abundances and spatio-temporal variations of the tropospheric NO_2 and HCHO VCDs, and validated the TROPOMI satellite products during the field campaign.

We tested the influences of different Fraunhofer reference spectra (FRSs) and different spectral intervals on the spectral retrieval, and found that the fitting residuals are smaller when using the sequential FRSs in the NO_2 visible wavelength region for mobile MAX-DOAS measurements in the background atmosphere over mountain terrain. After investigating the optimal filters to eliminate the "bad measurements" caused by sunlight shelters and vehicle's vibration and bumpiness, the NO_2 and HCHO DSCDs were retained with the conditions of (1) RMS < 0.005, (2) offset (constant) between ± 0.03, and (3) SZA < 80 °. The qualified NO_2 and HCHO DSCDs were converted to the corresponding VCDs based on the air mass factor (AMF) estimated by the geometric approximation method. Through comparing the resulting NO_2 and HCHO VCDs at three different elevation angles (15°, 20°, 30°), the $VCD_{15°}$ were further filtered and kept as the final data sets of tropospheric NO_2 and HCHO VCDs when absolute and relative VCD differences (ΔVCD) between 15 °and 20 °are < 10^{15} molec cm^{-2} or <5% for NO_2 and < 2×10^{15} molec cm^{-2} or <5% for HCHO, respectively.

The background levels of tropospheric NO_2 and HCHO VCDs, estimated by the maximum frequency method, were 0.40 ± 0.23 × 10^{15} molec cm^{-2} for NO_2 and 2.27 ± 0.96 ×10^{15} molec cm^{-2} for HCHO in July 2021 over the Three Rivers' Source region. We also determined the dependence of the tropospheric NO_2 and HCHO VCDs on altitude, which generally presents a decreasing trend with the increasing altitude. This characteristic for natural background atmosphere is probably mainly related to the lower air density at higher altitude. However, different from the nearly constant decreasing rate of HCHO VCDs with increasing altitude, the differences of decreasing rate above and below the 2750 m altitude for NO_2 VCDs are significant, which is highly connected with different contributions of anthropogenic sources and natural sources for NO_2 and HCHO.

~~The NO_2 daily means were always larger than the corresponding medians on each day, but the daily means and medians for HCHO were very close to each other. The day-to-day variations of the NO_2 VCDs between different circling journeys were similar, i.e. similar geographical distributions of the NO_2 VCDs were observed for each circling journey. However, the daily HCHO VCDs varied from the minimum mean of 1.15 ×10^{15} molec cm^{-2} on 27 July 2021 to the maximum mean of 4.63 ×10^{15} molec cm^{-2} on 21 July 2021. The obvious differences of the daily HCHO VCDs between different circling journeys were highly related to the air temperature, which affects the levels of VOCs emitted by natural vegetation. The daytime diurnal cycles of NO_2 VCDs presented higher values in the morning and evening, and the amplitudes of the NO_2 diurnal variation changed with the driving routes. The simulations of stratospheric NO_2 absorption cannot explain the observed diurnal cycle of the tropospheric NO_2 VCD. Besides the enhanced NO_2 photolysis around noon, the enhanced NO_2 VCDs in the morning and evening were primarily caused by enhanced pollution when the mobile observation vehicle was located in or close to the cities or county town.~~

With respect to the ~~spatial~~ spatio-temporal distributions, the day-to-day variations of the NO_2 VCDs between different circling journeys were similar, i.e. similar geographical distributions of the NO_2 VCDs were observed for each circling journey. ~~the~~ The tropospheric NO_2 VCDs over the main area of Three Rivers' Source were relatively uniform with very low levels (<1×10^{15} molec cm^{-2}), but they were usually elevated in cities or counties, around the Qinghai Lake, even

occasionally at the highway junction and the tunnel exit, where there were enhanced transport emissions. The daytime diurnal patterns of NO_2 VCDs, i.e. higher values in the morning and evening, could also reflect the differences of the NO_2 spatial distribution. Based on radiative transfer simulations we can rule out that the stratospheric NO_2 absorption can explain the observed diurnal cycle of the tropospheric NO_2 VCD. Besides the enhanced NO_2 photolysis around noon, the enhanced NO_2 VCDs in the morning and evening were primarily caused by enhanced pollution levels when the mobile observation vehicle was located in or close to the cities or county towns. However, the day-to-day variations of the HCHO VCDs were highly correlated to the air temperature and significantly different between different circling journeys. Overall, the HCHO VCDs presented a decreasing trend from the northeast to the southwest in the region of the field experiment. The HCHO VCDs were elevated at the starting points and ending points of the driving routes, corresponding to larger HCHO VCDs in the morning and evening. The levels of the HCHO VCDs were variable on different days at the same location, implying that natural factors, such as air temperature, significantly influenced the atmospheric HCHO photochemical formation.

TROPOMI NO_2 clearly presents the obvious influences of anthropogenic sources on enhanced NO_2 VCDs around Xining city, i.e. it can distinguish the differences in tropospheric NO_2 VCDs between the city and the background atmosphere over the region of the field campaign. But the elevated trends of the tropospheric NO_2 VCDs around the counties over the main area of the Three Rivers' Source region, which are clearly observed by the mobile MAX-DOAS, are nearly not captured by TROPOMI. In contrast, the stronger influences of natural factors on HCHO lead to larger daily variation of HCHO, which causes inconsistent and variable spatial distributions of TROPOMI HCHO VCDs on different days but also a higher correlation between mobile MAX-DOAS and TROPOMI than NO_2 for the background atmosphere. ~~In addition, through comparing NO_2 and HCHO VCDs between mobile MAX-DOAS and TROPOMI, we found that TROPOMI can distinguish the differences in tropospheric NO_2 VCDs between city and background atmosphere, but cannot identify the fine scale spatial variability in tropospheric NO_2 and HCHO VCDs in the background atmosphere over the Tibetan Plateau.~~The positive offsets of TROPOMI NO_2 and HCHO VCDs are 40% and 87% on average, respectively. This is probably caused by mountain terrains and varying local microclimates over the main area of the Three Rivers' Source region.

As a whole, we obtained valuable data sets and information of the spatio-temporal variation of NO_2 and HCHO over the Tibetan Plateau, which have the great potential in investigating the evolution of the atmospheric composition ~~with high spatio temporal resolution~~ in the background atmosphere at high altitude, validating and improving the satellite products over mountain terrain, and evaluating atmospheric chemistry model over the Tibetan Plateau.

Code and data availability. The filtered final NO_2 and HCHO VCDs for the field campaign by mobile MAX-DOAS observations on 18-30 July 2021 over the Three Rivers' Source region of the Tibetan Plateau in China are available upon request.

Supplement. The supplement related to this article is available online.

Author contributions. X.H. Cheng and X.D. Xu designed the field experiment. S.Y. Cheng and J.Z. Ma set up the mobile MAX-DOAS measurement platform under discussions with X.H. Cheng, J.G. Lv, S. Dörner, S. Donner, and T. Wagner. W.Q. Zhang, G. Bai, B. Chen, and S.Y. Ma contributed to the field measurements. S.Y. Cheng performed the spectra retrieval and data analysis with contributions from T. Wagner, S. Dörner, S. Donner, and J.Z. Ma. S.Y. Cheng, J.Z. Ma, and T. Wagner prepared the manuscript with consent by all co-authors.

Competing interests. The authors declare that they have no conflict of interest.

Acknowledgements. We thank the staff at the Qinghai Meteorological Administration for supporting the measurements. We thank BIRA-IASB for QDOAS spectral analysis software. We also thank ESA, KNMI, DLR and NASA for the TROPOMI satellite products.

Financial support. This research is supported by grants from the Fundamental Research Funds for Central Public-interest Scientific Institution from Chinese Academy of Meteorological Sciences (No. 2021Z013), the National Natural Science Foundation of China (No. 41875146), and the Fund of State Key Laboratory of Applied Optics (No. SKLAO2021001A02).

References

Bolin, B.: On the Influence of the Earth's Orography on the General Character of the Westerlies, Tellus, 2, 184-195, 10.3402/tellusa.v2i3.8547, 1950.

Boos, W. R. and Kuang, Z.: Dominant control of the South Asian monsoon by orographic insulation versus plateau heating, Nature, 463, 218-222, 10.1038/nature08707, 2010.

Borovski, A. N., Dzhola, A. V., Elokhov, A. S., Grechko, E. I., Kanaya, Y., and Postylyakov, O. V.: First measurements of formaldehyde integral content in the atmosphere using MAX-DOAS in the Moscow Region, International Journal of Remote Sensing, 35, 5609-5627, 10.1080/01431161.2014.945011, 2014.

Brinksma, E. J., Pinardi, G., Volten, H., Braak, R., Richter, A., Schönhardt, A., van Roozendael, M., Fayt, C., Hermans, C., Dirksen, R. J., Vlemmix, T., Berkhout, A. J. C., Swart, D. P. J., Oetjen, H., Wittrock, F., Wagner, T., Ibrahim, O. W., de Leeuw, G., Moerman, M., Curier, R. L., Celarier, E. A., Cede, A., Knap, W. H., Veefkind, J. P., Eskes, H. J., Allaart, M., Rothe, R., Piters, A. J. M., and Levelt, P. F.: The 2005 and 2006 DANDELIONS NO_2 and aerosol intercomparison campaigns, Journal of Geophysical Research, 113, D16S46, 10.1029/2007jd008808, 2008.

Chen, P., Kang, S., Yang, J., Pu, T., Li, C., Guo, J., and Tripathee, L.: Spatial and Temporal Variations of Gaseous and Particulate Pollutants in Six Sites in Tibet, China, during 2016–2017, Aerosol and Air Quality Research, 19, 516-527, 10.4209/aaqr.2018.10.0360, 2019.

Cheng, S., Wang, Y., and An, X.: Temporal Variation and Source Identification of Black Carbon at Lin'an and Longfengshan Regional Background Stations in China, Journal of Meteorological Research, 31, 1070-1084, 10.1007/s13351-017-7030-5, 2017.

Cheng, S., Jin, J., Ma, J., Lv, J., Liu, S., and Xu, X.: Temporal Variation of NO_2 and HCHO Vertical Profiles Derived from MAX-DOAS Observation in Summer at a Rural Site of the North China Plain and Ozone Production in Relation to $HCHO/NO_2$ Ratio, Atmosphere, 13, 860, 10.3390/atmos13060860, 2022.

Cheng, S., Ma, J., Cheng, W., Yan, P., Zhou, H., Zhou, L., and Yang, P.: Tropospheric NO_2 vertical column densities retrieved from ground-based MAX-DOAS measurements at Shangdianzi regional atmospheric background station in China, J Environ Sci (China), 80, 186-196, 10.1016/j.jes.2018.12.012, 2019.

Cheng, S., Ma, J., Zheng, X., Gu, M., Donner, S., Dörner, S., Zhang, W., Du, J., Li, X., Liang, Z., Lv, J., and Wagner, T.: Retrieval of O_3, NO_2, BrO and OClO Columns from Ground-Based Zenith Scattered Light DOAS Measurements in Summer and Autumn over the Northern Tibetan Plateau, Remote Sensing, 13, 4242, 10.3390/rs13214242, 2021.

Danckaert, T., Fayt, C., Roozendael, M. V., Smedt, I. D., Letocart, V., Merlaud, A., and Pinardi, G.: QDOAS Software user manual, Belgian Institute for Space Aeronomy, Brussels, Belgium, 2017.

De Smedt, I., Pinardi, G., Vigouroux, C., Compernolle, S., Bais, A., Benavent, N., Boersma, F., Chan, K.-L., Donner, S., Eichmann, K.-U., Hedelt, P., Hendrick, F., Irie, H., Kumar, V., Lambert, J.-C., Langerock, B., Lerot, C., Liu, C., Loyola, D.,

Piters, A., Richter, A., Rivera Cárdenas, C., Romahn, F., Ryan, R. G., Sinha, V., Theys, N., Vlietinck, J., Wagner, T., Wang, T., Yu, H., and Van Roozendael, M.: Comparative assessment of TROPOMI and OMI formaldehyde observations and validation against MAX-DOAS network column measurements, Atmospheric Chemistry and Physics, 21, 12561-12593, 10.5194/acp-21-12561-2021, 2021.

Dong, W., Lin, Y., Wright, J. S., Xie, Y., Xu, F., Xu, W., and Wang, Y.: Indian Monsoon Low-Pressure Systems Feed Up-and-Over Moisture Transport to the Southwestern Tibetan Plateau, Journal of Geophysical Research: Atmospheres, 122, 12,140-112,151, 10.1002/2017jd027296, 2017.

Donner, S.: Mobile MAX-DOAS measurements of the tropospheric formaldehyde column in the Rhein-Main region, Master thesis, University of Mainz, Mainz, 2016.

Duan, A., Zhang, Q., Liu, Y., Wu, G., Wang, T., Wan, R., Liu, X., Li, W., Wang, Z., and Liang, X.: The Influence of Mechanical and Thermal Forcing by the Tibetan Plateau on Asian Climate, Journal of Hydrometeorology, 8, 770-789, 10.1175/jhm609.1, 2007.

Duo, B., Cui, L., Wang, Z., Li, R., Zhang, L., Fu, H., Chen, J., Zhang, H., and Qiong, A.: Observations of atmospheric pollutants at Lhasa during 2014-2015: Pollution status and the influence of meteorological factors, J Environ Sci (China), 63, 28-42, 10.1016/j.jes.2017.03.010, 2018.

ESA and DLR: Sentinel-5P TROPOMI Tropospheric Formaldehyde HCHO 1-Orbit L2 5.5km x 3.5km, Goddard Earth Sciences Data and Information Services Center (GES DISC) [dataset], 10.5270/S5P-vg1i7t0, 2020.

ESA and KNMI: Sentinel-5P TROPOMI Tropospheric NO_2 1-Orbit L2 5.5km x 3.5km, Goddard Earth Sciences Data and Information Services Center (GES DISC) [dataset], 10.5270/S5P-9bnp8q8, 2021.

Franco, B., Hendrick, F., Van Roozendael, M., Müller, J. F., Stavrakou, T., Marais, E. A., Bovy, B., Bader, W., Fayt, C., Hermans, C., Lejeune, B., Pinardi, G., Servais, C., and Mahieu, E.: Retrievals of formaldehyde from ground-based FTIR and MAX-DOAS observations at the Jungfraujoch station and comparisons with GEOS-Chem and IMAGES model simulations, Atmospheric Measurement Techniques, 8, 1733-1756, 10.5194/amt-8-1733-2015, 2015.

Gao, J., Yao, T., Masson-Delmotte, V., Steen-Larsen, H. C., and Wang, W.: Collapsing glaciers threaten Asia's water supplies, Nature, 565, 19-21, 10.1038/d41586-018-07838-4, 2019.

Gil-Ojeda, M., Navarro-Comas, M., Gómez-Martín, L., Adame, J. A., Saiz-Lopez, A., Cuevas, C. A., González, Y., Puentedura, O., Cuevas, E., Lamarque, J. F., Kinninson, D., and Tilmes, S.: NO_2 seasonal evolution in the north subtropical free troposphere, Atmospheric Chemistry and Physics, 15, 10567-10579, 10.5194/acp-15-10567-2015, 2015.

Gomez, L., Navarro-Comas, M., Puentedura, O., Gonzalez, Y., Cuevas, E., and Gil-Ojeda, M.: Long-path averaged mixing ratios of O_3 and NO_2 in the free troposphere from mountain MAX-DOAS, Atmospheric Measurement Techniques, 7, 3373-3386, 10.5194/amt-7-3373-2014, 2014.

Granier, C., Bessagnet, B., Bond, T., D'Angiola, A., Denier van der Gon, H., Frost, G. J., Heil, A., Kaiser, J. W., Kinne, S., Klimont, Z., Kloster, S., Lamarque, J.-F., Liousse, C., Masui, T., Meleux, F., Mieville, A., Ohara, T., Raut, J.-C., Riahi, K., Schultz, M. G., Smith, S. J., Thompson, A., van Aardenne, J., van der Werf, G. R., and van Vuuren, D. P.: Evolution of

anthropogenic and biomass burning emissions of air pollutants at global and regional scales during the 1980–2010 period, Climatic Change, 109, 163-190, 10.1007/s10584-011-0154-1, 2011.

Guo, F., Bao, M., Mu, Y., Liu, Z., Li, Y., and Shi, H.: Temporal and spatial characteristics of lightning-produced nitrogen oxides in China, Journal of Atmospheric and Solar-Terrestrial Physics, 149, 100-107, 10.1016/j.jastp.2016.10.007, 2016.

He, J., Gong, S., Yu, Y., Yu, L., Wu, L., Mao, H., Song, C., Zhao, S., Liu, H., Li, X., and Li, R.: Air pollution characteristics and their relation to meteorological conditions during 2014–2015 in major Chinese cities, Environmental Pollution, 223, 484-496, 10.1016/j.envpol.2017.01.050, 2017.

Hong, Q., Liu, C., Chan, K. L., Hu, Q., Xie, Z., Liu, H., Si, F., and Liu, J.: Ship-based MAX-DOAS measurements of tropospheric NO_2, SO_2, and HCHO distribution along the Yangtze River, Atmospheric Chemistry and Physics, 18, 5931-5951, 10.5194/acp-18-5931-2018, 2018.

Hönninger, G., Friedeburg, C. v., and Platt, U.: Multi axis differential optical absorption spectroscopy (MAX-DOAS), Atmospheric Chemistry and Physics, 4, 231-254, 10.5194/acp-4-231-2004, 2004.

Kang, S., Zhang, Q., Zhang, Y., Guo, W., Ji, Z., Shen, M., Wang, S., Wang, X., Tripathee, L., Liu, Y., Gao, T., Xu, G., Gao, Y., Kaspari, S., Luo, X., and Mayewski, P.: Warming and thawing in the Mt. Everest region: A review of climate and environmental changes, Earth-Science Reviews, 225, 103911, 10.1016/j.earscirev.2021.103911, 2022.

Kurokawa, J., Ohara, T., Morikawa, T., Hanayama, S., Janssens-Maenhout, G., Fukui, T., Kawashima, K., and Akimoto, H.: Emissions of air pollutants and greenhouse gases over Asian regions during 2000–2008: Regional Emission inventory in ASia (REAS) version 2, Atmospheric Chemistry and Physics, 13, 11019-11058, 10.5194/acp-13-11019-2013, 2013.

Lee, D. S., Köhler, I., Grobler, E., Rohrer, F., Sausen, R., Gallardo-Klenner, L., Olivier, J. G. J., Dentener, F. J., and Bouwman, A. F.: Estimations of global NO_x emissions and their uncertainties, Atmospheric Environment, 31, 1735-1749, 10.1016/s1352-2310(96)00327-5, 1997.

Liu, Y., Hoskins, B., and Blackburn, M.: Impact of Tibetan Orography and Heating on the Summer Flow over Asia, Journal of the Meteorological Society of Japan. Ser. II, 85B, 1-19, 10.2151/jmsj.85B.1, 2007.

Ma, J., Zhou, X., Xu, X., Xu, X., Gromov, S., and Lelieveld, J.: Ozone and aerosols over the Tibetan Plateau, in: Asian Atmospheric Pollution: Sources, Characteristics and Impacts, edited by: Singh, R. P., Elsevier, Amsterdam, Netherlands, 287-302, 2021.

Ma, J., Dörner, S., Donner, S., Jin, J., Cheng, S., Guo, J., Zhang, Z., Wang, J., Liu, P., Zhang, G., Pukite, J., Lampel, J., and Wagner, T.: MAX-DOAS measurements of NO_2, SO_2, HCHO, and BrO at the Mt. Waliguan WMO GAW global baseline station in the Tibetan Plateau, Atmospheric Chemistry and Physics, 20, 6973-6990, 10.5194/acp-20-6973-2020, 2020.

Ma, J. Z., Tang, J., Zhou, X. J., and Zhang, X. S.: Estimates of the chemical budget for ozone at Waliguan Observatory, Journal of Atmospheric Chemistry, 41, 21-48, Doi 10.1023/A:1013892308983, 2002.

Ma, J. Z., Beirle, S., Jin, J. L., Shaiganfar, R., Yan, P., and Wagner, T.: Tropospheric NO_2 vertical column densities over Beijing: results of the first three years of ground-based MAX-DOAS measurements (2008-2011) and satellite validation, Atmospheric Chemistry and Physics, 13, 1547-1567, 10.5194/acp-13-1547-2013, 2013.

Marais, E. A., Roberts, J. F., Ryan, R. G., Eskes, H., Boersma, K. F., Choi, S., Joiner, J., Abuhassan, N., Redondas, A., Grutter, M., Cede, A., Gomez, L., and Navarro-Comas, M.: New observations of NO_2 in the upper troposphere from TROPOMI, Atmospheric Measurement Techniques, 14, 2389-2408, 10.5194/amt-14-2389-2021, 2021.

Mazière, M. D., Thompson, A. M., Kurylo, M. J., Wild, J. D., Bernhard, G., Blumenstock, T., Braathen, G. O., Hannigan, J. W., Lambert, J.-C., Leblanc, T., McGee, T. J., Nedoluha, G., Petropavlovskikh, I., Seckmeyer, G., Simon, P. C., Steinbrecht, W., and Strahan, S. E.: The Network for the Detection of Atmospheric Composition Change (NDACC): history, status and perspectives, Atmos. Chem. Phys., 18, 4935–4964, 10.5194/acp-18-4935-2018, 2018.

Meng, Z.-Y., Xu, X.-B., Wang, T., Zhang, X.-Y., Yu, X.-L., Wang, S.-F., Lin, W.-L., Chen, Y.-Z., Jiang, Y.-A., and An, X.-Q.: Ambient sulfur dioxide, nitrogen dioxide, and ammonia at ten background and rural sites in China during 2007–2008, Atmospheric Environment, 44, 2625-2631, 10.1016/j.atmosenv.2010.04.008, 2010.

Mu, Y., Pang, X., Quan, J., and Zhang, X.: Atmospheric carbonyl compounds in Chinese background area: A remote mountain of the Qinghai-Tibetan Plateau, Journal of Geophysical Research, 112, 10.1029/2006jd008211, 2007.

Platt, U. and Stutz, J.: Differential Optical absorption spectroscopy, Principles and Applications, Springer, Berlin, 2008.

Qiu, J.: China: The third pole, Nature, 454, 393-396, 10.1038/454393a, 2008.

Ran, L., Lin, W. L., Deji, Y. Z., La, B., Tsering, P. M., Xu, X. B., and Wang, W.: Surface gas pollutants in Lhasa, a highland city of Tibet-current levels and pollution implications, Atmospheric Chemistry and Physics, 14, 10721-10730, 10.5194/acp-14-10721-2014, 2014.

Schreier, S. F., Richter, A., Wittrock, F., and Burrows, J. P.: Estimates of free-tropospheric NO_2 and HCHO mixing ratios derived from high-altitude mountain MAX-DOAS observations at midlatitudes and in the tropics, Atmospheric Chemistry and Physics, 16, 2803-2817, 10.5194/acp-16-2803-2016, 2016.

Seinfeld, J. H. and Pandis, S. N.: Atmospheric Chemistry and Physics: From Air Pollution to Climate Change, 3rd Edn., John Wiley & Sons, Inc., Hoboken, New Jersey, USA, 2016.

Singh, R. P.: Asian Atmospheric Pollution: Sources, Characteristics and Impacts, Elsevier, Amsterdam, Netherlands, 2021.

Stavrakou, T., Müller, J. F., De Smedt, I., Van Roozendael, M., van der Werf, G. R., Giglio, L., and Guenther, A.: Evaluating the performance of pyrogenic and biogenic emission inventories against one decade of space-based formaldehyde columns, Atmospheric Chemistry and Physics, 9, 1037-1060, 10.5194/acp-9-1037-2009, 2009.

Veefkind, J. P., Aben, I., McMullan, K., Förster, H., Vries, J. d., Otter, G., Claas, J., Eskes, H. J., Haan, J. F. d., Kleipool, Q., Weele, M. v., Hasekamp, O., Hoogeveen, R., Landgraf, J., Snel, R., Tol, P., Ingmann, P., Voors, R., Kruizinga, B., Vink, R., Visser, H., and Levelt, P. F.: TROPOMI on the ESA Sentinel-5 Precursor: A GMES mission for global observations of the atmospheric composition for climate, air quality and ozone layer applications, Remote Sensing of Environment, 120, 70-83, 10.1016/j.rse.2011.09.027, 2012.

Verhoelst, T., Compernolle, S., Pinardi, G., Lambert, J.-C., Eskes, H. J., Eichmann, K.-U., Fjæraa, A. M., Granville, J., Niemeijer, S., Cede, A., Tiefengraber, M., Hendrick, F., Pazmiño, A., Bais, A., Bazureau, A., Boersma, K. F., Bognar, K., Dehn, A., Donner, S., Elokhov, A., Gebetsberger, M., Goutail, F., Grutter de la Mora, M., Gruzdev, A., Gratsea, M., Hansen, G.

H., Irie, H., Jepsen, N., Kanaya, Y., Karagkiozidis, D., Kivi, R., Kreher, K., Levelt, P. F., Liu, C., Müller, M., Navarro Comas, M., Piters, A. J. M., Pommereau, J.-P., Portafaix, T., Prados-Roman, C., Puentedura, O., Querel, R., Remmers, J., Richter, A., Rimmer, J., Rivera Cárdenas, C., Saavedra de Miguel, L., Sinyakov, V. P., Stremme, W., Strong, K., Van Roozendael, M., Veefkind, J. P., Wagner, T., Wittrock, F., Yela González, M., and Zehner, C.: Ground-based validation of the Copernicus Sentinel-5P TROPOMI NO_2 measurements with the NDACC ZSL-DOAS, MAX-DOAS and Pandonia global networks, Atmospheric Measurement Techniques, 14, 481-510, 10.5194/amt-14-481-2021, 2021.

Vigouroux, C., Langerock, B., Aquino, C. A. B., Blumenstock, T., Cheng, Z., Mazière, M. D., Smedt, I. D., Grutter, M., Hannigan, J. W., Jones, N., Kivi, R., Loyola, D., Lutsch, E., Mahieu, E., Makarova, M., Metzger, J.-M., Morino, I., Murata, I., Nagahama, T., Notholt, J., Ortega, I., Palm, M., Pinardi, G., Röhling, A., Smale, D., Stremme, W., Strong, K., Sussmann, R., Té, Y., Roozendael, M. v., Wang, P., and Winkler, H.: TROPOMI–Sentinel-5 Precursor formaldehyde validation using an extensive network of ground-based Fourier-transform infrared stations, Atmos. Meas. Tech., 13, 3751–3767, 10.5194/amt-13-3751-2020, 2020.

Wang, Q. Y., Gao, R. S., Cao, J. J., Schwarz, J. P., Fahey, D. W., Shen, Z. X., Hu, T. F., Wang, P., Xu, X. B., and Huang, R. J.: Observations of high level of ozone at Qinghai Lake basin in the northeastern Qinghai-Tibetan Plateau, western China, Journal of Atmospheric Chemistry, 72, 19-26, 10.1007/s10874-015-9301-9, 2015.

Wang, T., Wong, H. L. A., Tang, J., Ding, A., Wu, W. S., and Zhang, X. C.: On the origin of surface ozone and reactive nitrogen observed at a remote mountain site in the northeastern Qinghai-Tibetan Plateau, western China, Journal of Geophysical Research, 111, 10.1029/2005jd006527, 2006.

Wang, Y., Puķīte, J., Wagner, T., Donner, S., Beirle, S., Hilboll, A., Vrekoussis, M., Richter, A., Apituley, A., Piters, A., Allaart, M., Eskes, H., Frumau, A., Van Roozendael, M., Lampel, J., Platt, U., Schmitt, S., Swart, D., and Vonk, J.: Vertical Profiles of Tropospheric Ozone From MAX-DOAS Measurements During the CINDI-2 Campaign: Part 1-Development of a New Retrieval Algorithm, Journal of Geophysical Research: Atmospheres, 123, 10637-10670, 10.1029/2018jd028647, 2018.

Xing, C., Liu, C., Wu, H., Lin, J., Wang, F., Wang, S., and Gao, M.: Ground-based vertical profile observations of atmospheric composition on the Tibetan Plateau (2017–2019), Earth System Science Data, 13, 4897-4912, 10.5194/essd-13-4897-2021, 2021.

Xu, X., Lu, C., Shi, X., and Gao, S.: World water tower: An atmospheric perspective, Geophysical Research Letters, 35, 10.1029/2008gl035867, 2008.

Xu, X., Lin, W., Xu, W., Jin, J., Wang, Y., Zhang, G., Zhang, X., Ma, Z., Dong, Y., Ma, Q., Yu, D., Li, Z., Wang, D., and Zhao, H.: Long-term changes of regional ozone in China: implications for human health and ecosystem impacts, Elementa: Science of the Anthropocene, 8, Art. 13, 10.1525/elementa.409, 2020.

Xue, L. K., Wang, T., Guo, H., Blake, D. R., Tang, J., Zhang, X. C., Saunders, S. M., and Wang, W. X.: Sources and photochemistry of volatile organic compounds in the remote atmosphere of western China: results from the Mt. Waliguan Observatory, Atmospheric Chemistry and Physics, 13, 8551-8567, 10.5194/acp-13-8551-2013, 2013.

Xue, L. K., Wang, T., Zhang, J. M., Zhang, X. C., Deliger, Poon, C. N., Ding, A. J., Zhou, X. H., Wu, W. S., Tang, J., Zhang, Q. Z., and Wang, W. X.: Source of surface ozone and reactive nitrogen speciation at Mount Waliguan in western China: New insights from the 2006 summer study, Journal of Geophysical Research, 116, 10.1029/2010jd014735, 2011.

Yanai, M., Li, C., and Song, Z.: Seasonal Heating of the Tibetan Plateau and Its Effects on the Evolution of the Asian Summer Monsoon, Journal of the Meteorological Society of Japan. Ser. II, 70, 319-351, 10.2151/jmsj1965.70.1B_319, 1992.

Yang, J., Ji, Z., Kang, S., Zhang, Q., Chen, X., and Lee, S.-Y.: Spatiotemporal variations of air pollutants in western China and their relationship to meteorological factors and emission sources, Environmental Pollution, 254, 112952, 10.1016/j.envpol.2019.07.120, 2019.

Zhang, Y., Ju, T., Shi, Y., Wang, Q., Li, F., and Zhang, G.: Analysis of spatiotemporal variation of formaldehyde column concentration in Qinghai-Tibet Plateau and its influencing factors, Environ Sci Pollut Res Int, 28, 55233-55251, 10.1007/s11356-021-14719-3, 2021.

Zhao, R., Dou, X., Zhang, N., Zhao, X., Yang, W., Han, B., Yu, H., Azzi, M., Wang, Y., and Bai, Z.: The characteristics of inorganic gases and volatile organic compounds at a remote site in the Tibetan Plateau, Atmospheric Research, 234, 104740, 10.1016/j.atmosres.2019.104740, 2020.

Zhou, X., Zhao, P., Chen, J., Chen, L., and Li, W.: Impacts of thermodynamic processes over the Tibetan Plateau on the Northern Hemispheric climate, Science in China Series D: Earth Sciences, 52, 1679-1693, 10.1007/s11430-009-0194-9, 2009.

Table 1. Observation periods and routes of the mobile MAX-DOAS field experiment over the Three Rivers' Source region of the Tibetan Plateau in July 2021.

Cycles	Xining to Dari (XD)	Dari to Yushu (DY)	Yushu to Xining (YX)
1	2021-07-18 9:00~22:49BJT[a]	2021-07-19 9:05~17:40BJT	2021-07-20 8:17~21:48BJT
2	2021-07-21 8:09~21:40BJT	2021-07-22 8:20~16:07BJT	2021-07-23 8:18~21:38BJT
3	2021-07-25 8:29~20:08BJT	2021-07-26 8:08~15:20BJT	2021-07-27 8:18~21:48BJT
4	2021-07-28 8:27~18:56BJT	2021-07-29 9:00~16:00BJT	2021-07-30 8:21~22:35BJT

[a] BJT denotes the Beijing time, corresponding to Universal Time Coordinated (UTC) + 8 h.

Table 2. Fit settings for the NO_2 and HCHO spectral analyses.

Parameters	Setting for NO_2	Setting for HCHO
Fraunhofer reference spectrum	sequential spectra	sequential spectra
fitting interval (nm)	400~434	324~359
DOAS polynomial	degree: 5	
intensity offset	degree: 2 (constant and order 1)	
shift and stretch	spectrum	
Ring spectra	original and wavelength-dependent Ring spectra	
NO_2 cross section	Vandaele et al. (1998), 294 K, I_o correction (10^{17} molec•cm^{-2})	
H_2O cross section	Polyansky et al. (2018), 293 K	/
O_3 cross section	Serdyuchenko et al. (2014), 223 K, I_o correction (10^{20} molec•cm^{-2})	Serdyuchenko et al. (2014), 223 K, 243 K, I_o correction (10^{20} molec•cm^{-2})
O_4 cross section	Thalman and Volkamer (2013), 293 K	Thalman and Volkamer (2013), 293 K
HCHO cross section	/	Meller and Moortgat (2000), 298 K

~~**Table 3.** Correlation for the NO_2 and HCHO VCDs between the three elevation angles (15°, 20°, 30°).~~

~~Correlation Coefficient~~	~~NO_2~~	~~HCHO~~
~~$R_{15°,20°}$~~	~~0.95~~	~~0.80~~
~~$R_{15°,30°}$~~	~~0.91~~	~~0.66~~
~~$R_{20°,30°}$~~	~~0.94~~	~~0.73~~

Table 3. Statistics for the NO_2 and HCHO VCDs at the three elevation angles (15°, 20°, 30°).

Parameters	Mean (Median) ± Standard deviation (10^{15} molec cm^{-2})			Correlation Coefficient		
	15°	20°	30°	15° vs. 20°	15° vs. 30°	20° vs. 30°
NO_2	1.40 (0.57) ±2.61	1.42 (0.63) ±2.52	1.59 (0.82) ±2.70	0.95	0.91	0.94
HCHO	2.53 (2.35) ±1.97	2.81 (2.69) ±2.60	3.25 (3.20) ±4.09	0.80	0.66	0.73

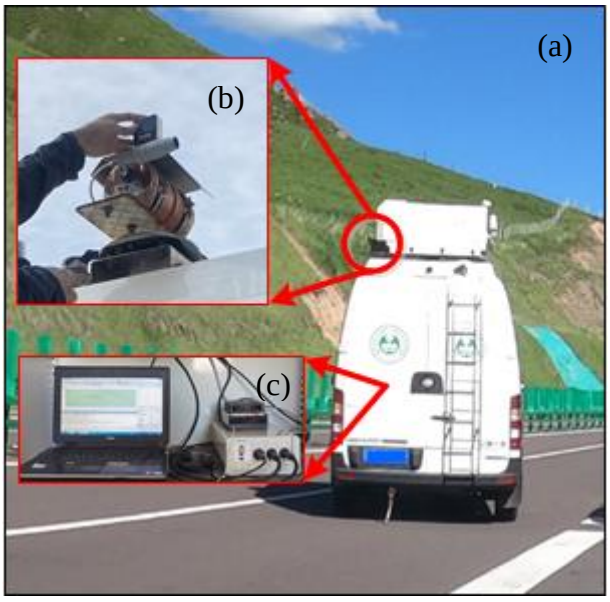

Figure 1. (a) Mobile observation vehicle of atmospheric composition and meteorological parameters. Two parts of the Tube MAX-DOAS instrument are installed **(b)** on the rear of the vehicle's roof and **(c)** inside the vehicle, respectively.

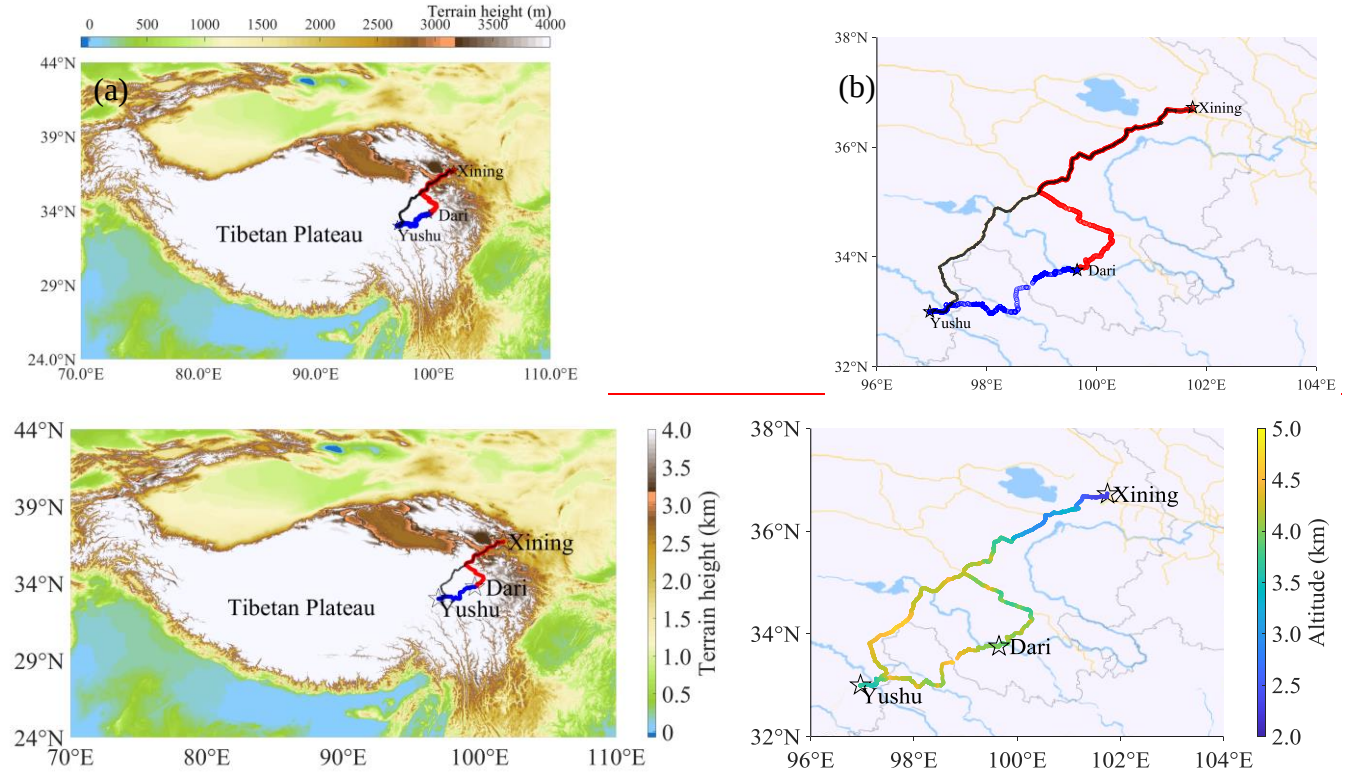

Figure 2. Driving routes ~~(red, blue and black lines)~~ of the mobile observation vehicle. The driving routes are added to **(a)** the terrain height map over the Tibetan Plateau (red, blue and black lines) and **(b)** the street map (https://map.baidu.com/, last access: 16 June 2022) in the

experiment region as an overlay, respectively. The altitudes along the driving routes are marked by coloured dotted curves in figure (b). Light blue lines and areas in figure (b) indicate rivers and lakes.

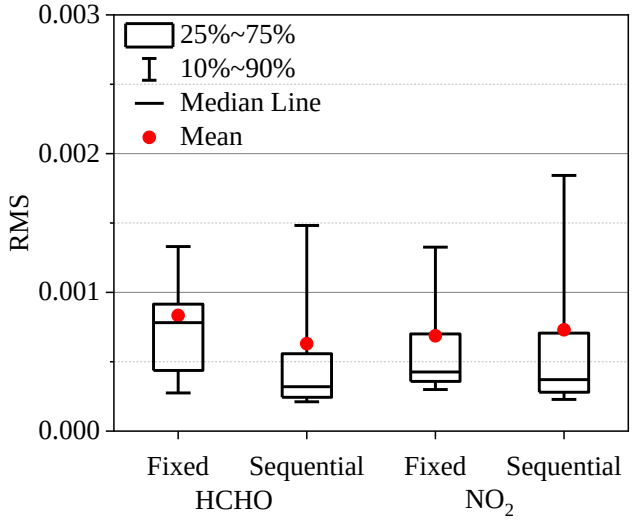

Figure 3. Statistics of the root mean square (RMS) of the NO_2 and HCHO spectral fitting residuals using a sequential FRS or fixed FRS (for RMS<0.005 and SZA<80 °) during the field campaign. Lower (upper) error bars and boxes are the 10th (90th), 25th (75th) percentiles, respectively. Lines inside the boxes and dots denote the medians and the mean values.

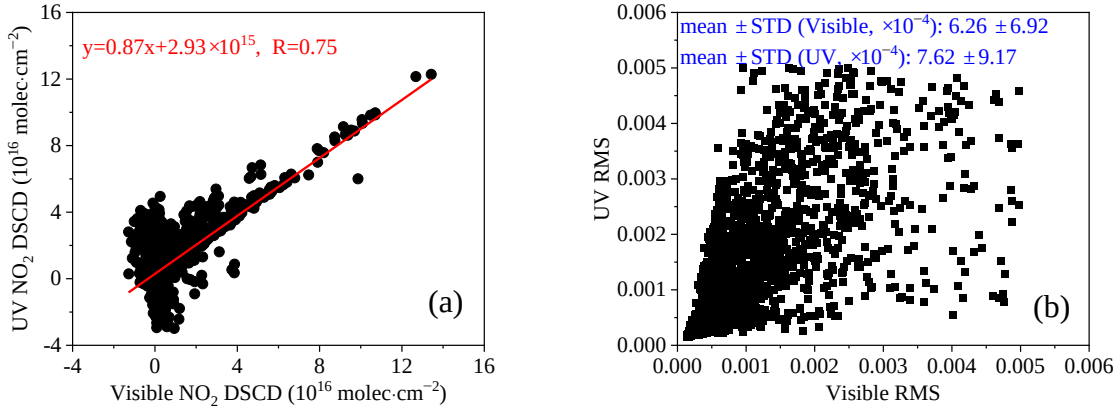

Figure 4. Comparison of NO_2 spectral fitting results using the visible and UV wavelength intervals (for RMS<0.005 and SZA<80 °) during the field campaign. **(a)** Linear fit of corresponding NO_2 DSCDs between visible and UV spectral intervals. **(b)** Corresponding NO_2 RMS between visible and UV spectral intervals. The red lines denote the results of the regression analyses and the corresponding equations and correlation coefficients are displayed in the figure (a). The numbers in figure (b) indicate the mean ± standard deviation (STD) in the visible and UV spectral intervals.

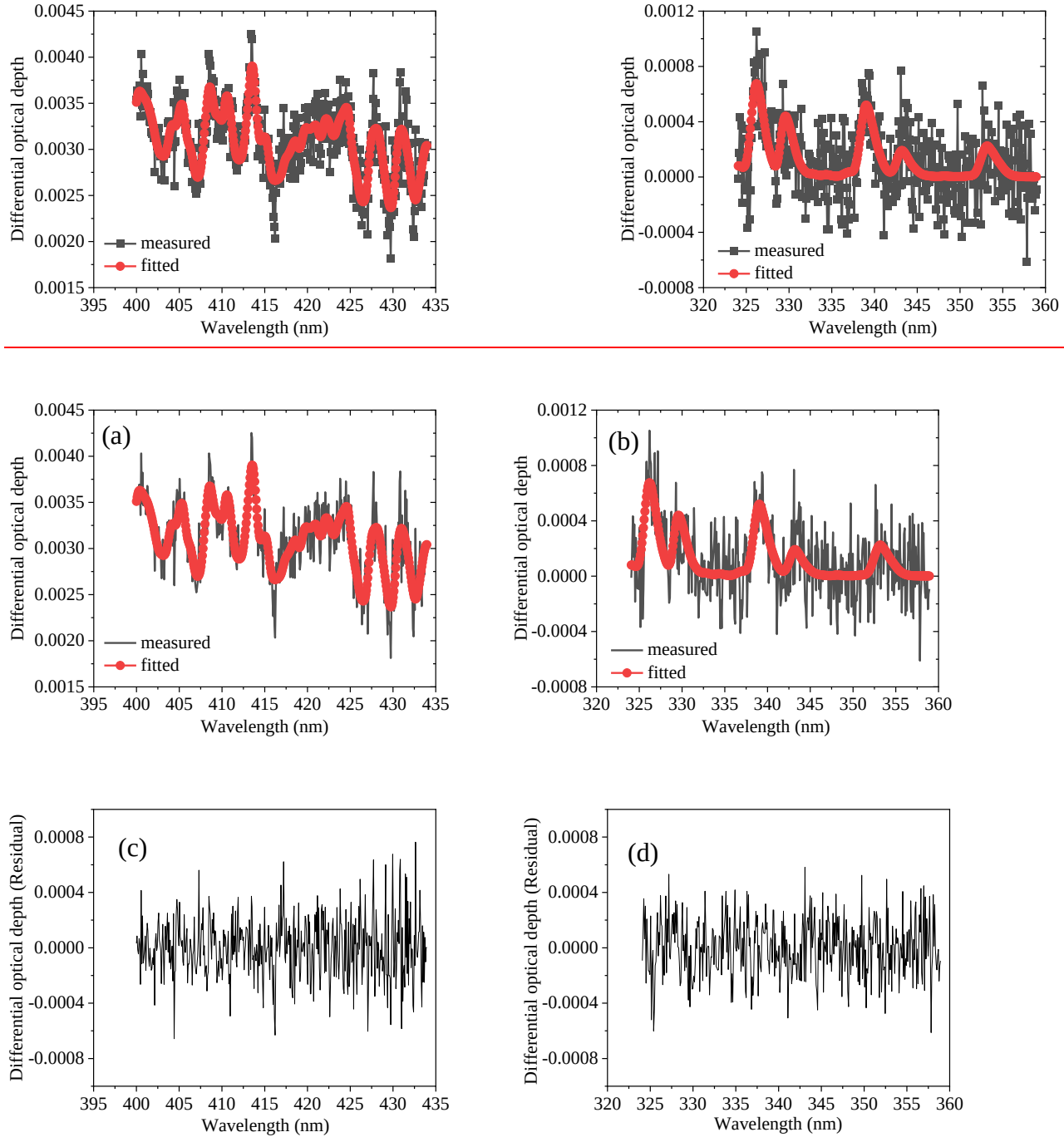

Figure 5. Examples of DOAS spectral analyses for ~~**(a)**~~ NO_2 and ~~**(b)**~~ HCHO. Black curves ~~with squares~~ and red curves with dots indicate the measured and fitted differential optical depth for **(a)** NO_2 and **(b)** HCHO, respectively. The NO_2 and HCHO DSCDs are 5.27×10^{15} molec cm^{-2} and 9.36×10^{15} molec cm^{-2}, respectively. The RMSs of the spectral fitting residuals between measured and fitted spectra are 2.17×10^{-4} for **(c)** NO_2 and 2.09×10^{-4} for **(d)** HCHO, respectively.

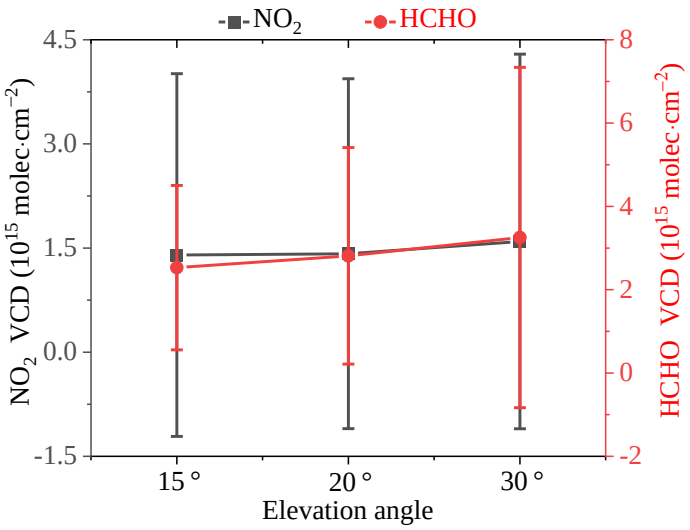

Figure 6. Mean NO_2 (line with squares) and HCHO (line with dots) VCDs calculated by the geometric approximation method for different elevation angles during the effective observation period. The error bars indicate the standard deviations of NO_2 and HCHO VCDs for different elevation angles.

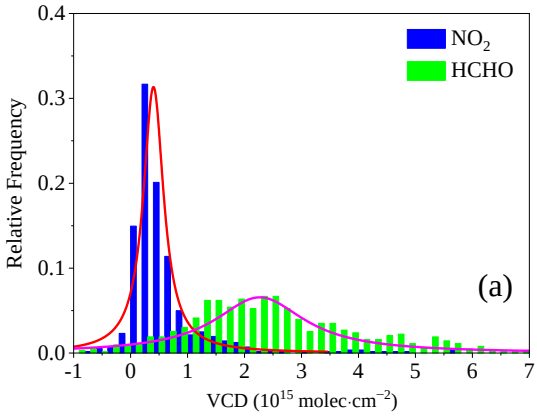

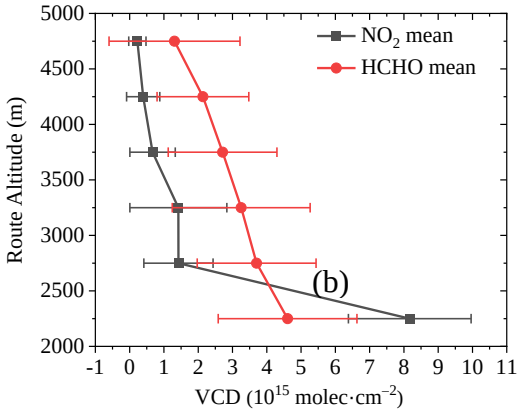

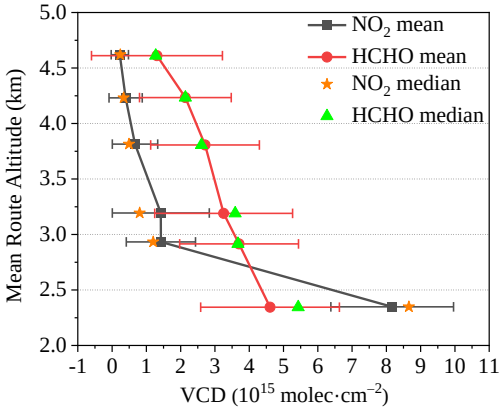

Figure ~~7~~6. Overall characteristics of NO_2 and HCHO VCDs during the field campaign. **(a)** Frequency distributions of NO_2 (blue column) and HCHO (green column) VCDs as well as their Lorentz distribution curves for NO_2 (red curve) and HCHO (magenta curve), respectively. **(b)** Dependence of the NO_2 and HCHO VCDs on mean altitude of driving route from 2000 m to 5000 m at vertical intervals of 500 m. The black (red) lines with squares (dots), ~~symbols~~ stars (triangles) and error bars denote the means, medians and standard deviations of the NO_2 (HCHO) VCDs for each altitude range.

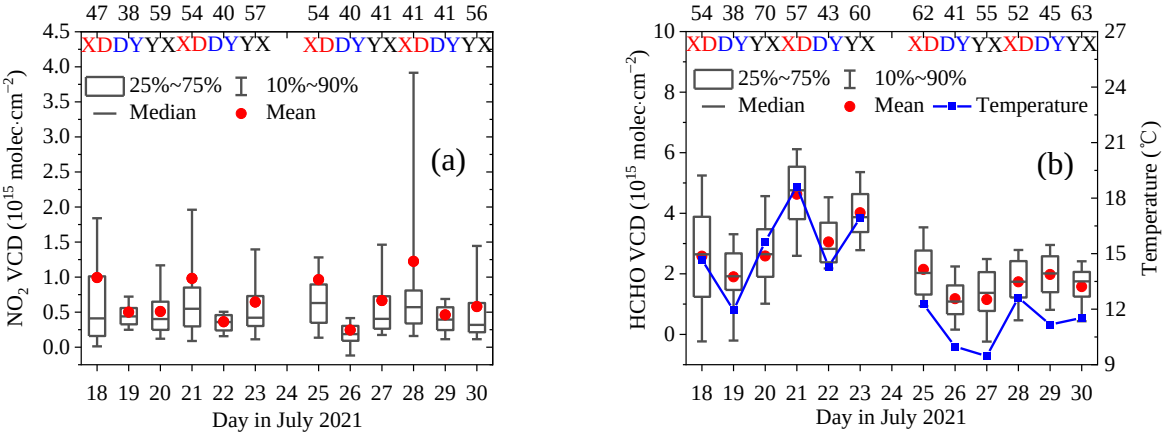

845 **Figure ~~8~~7.** Day-to-day variations of the daily averaged **(a)** NO_2 and **(b)** HCHO VCDs over the mobile observation routes (XD, DY, YX). Lower (upper) error bars and boxes are the 10th (90th), 25th (75th) percentiles of the data. Lines inside the boxes and red dots denote the medians and the mean values, respectively. The integrated sampling numbers for specific day are labelled at the top axis. The blue curves with squares in Figure (b) denote the daily air temperature at 2 m above the land surface.

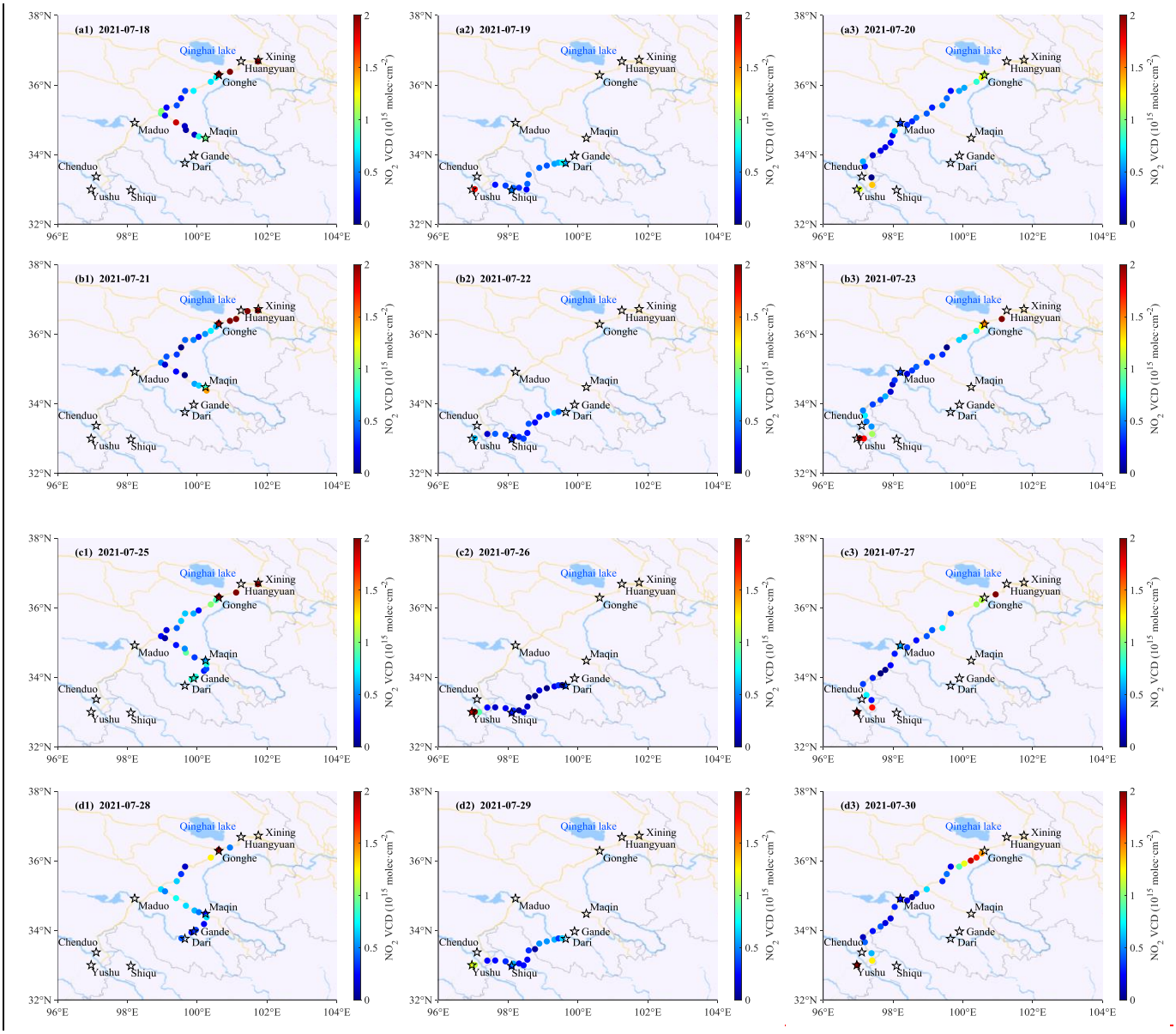
(a1) 2021-07-18
(a2) 2021-07-19
(a3) 2021-07-20
(b1) 2021-07-21
(b2) 2021-07-22
(b3) 2021-07-23
(c1) 2021-07-25
(c2) 2021-07-26
(c3) 2021-07-27
(d1) 2021-07-28
(d2) 2021-07-29
(d3) 2021-07-30
Qinghai lake
Xining
Huangyuan
Gonghe
Maduo
Maqin
Gande
Dari
Chenduo
Yushu
Shiqu
38°N
36°N
34°N
32°N
96°E
98°E
100°E
102°E
104°E
NO2 VCD (10^15 molec·cm^-2)
0
0.5
1
1.5
2

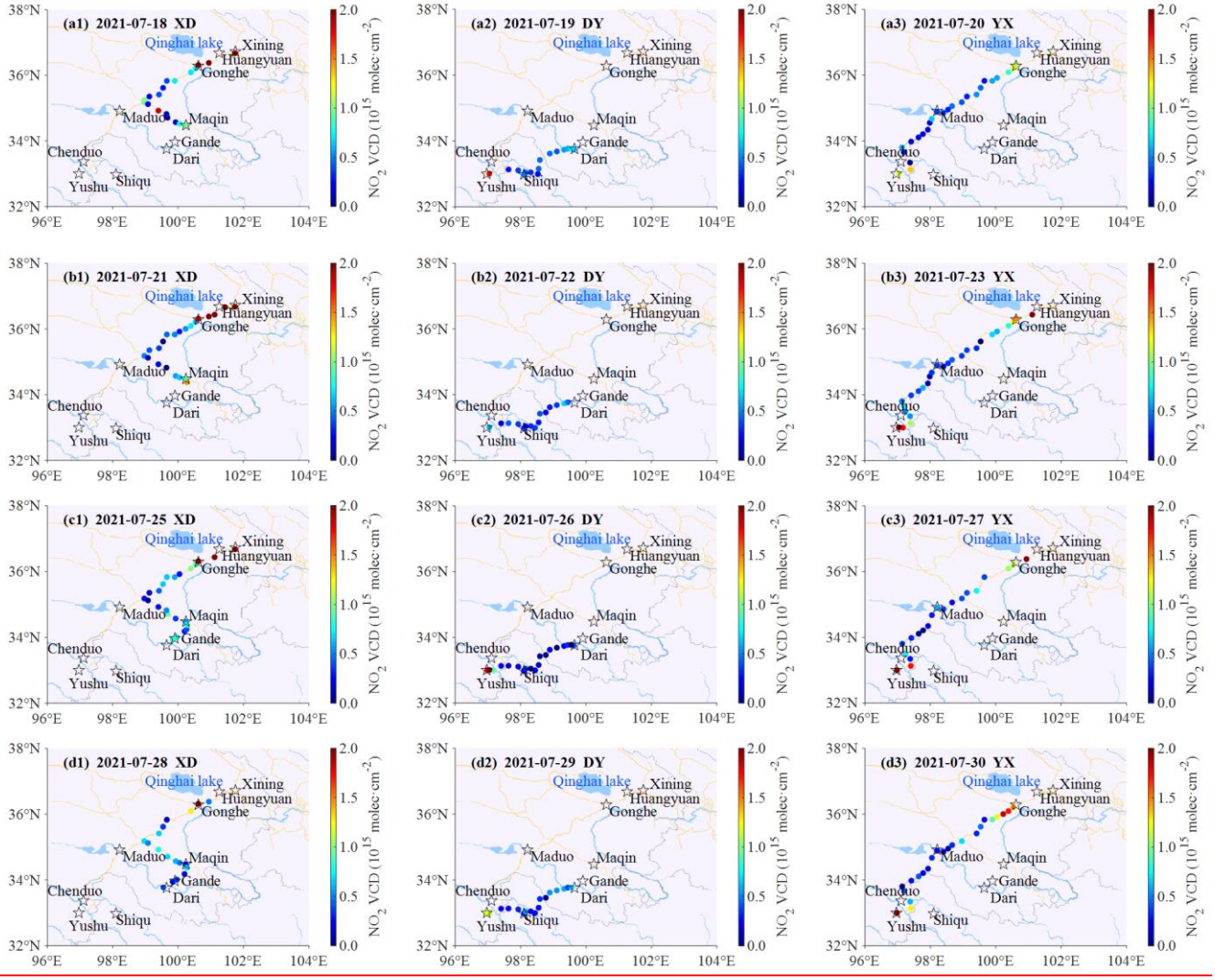

Figure ~~11~~8. Spatial distributions of gridded NO_2 VCDs with 0.25 °×0.25 °resolution. The observed NO_2 VCDs in each spatial grid cell are averaged for three segments **(1, 2, 3)** of four circling journeys **(a, b, c, d)**. The main cities and counties on the driving routes are marked by the black stars. On the background map, the light blue lines and areas represent rivers and lakes (such as, Qinghai Lake), the yellow lines denote the roads, and the grey lines indicate the administrative boundaries.

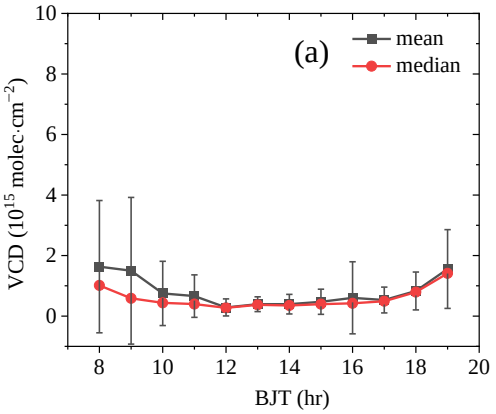
(a)
mean
median
VCD (10^{15} molec·cm^{-2})
BJT (hr)

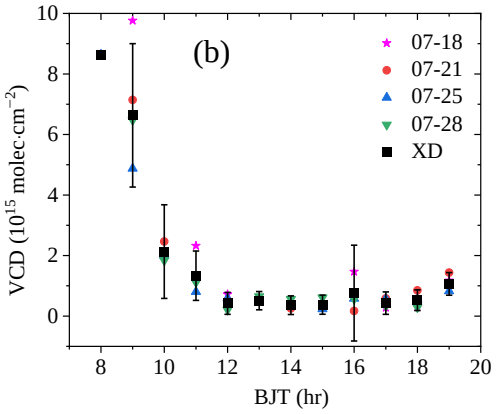
(b)
07-18
07-21
07-25
07-28
XD
VCD (10^{15} molec·cm^{-2})
BJT (hr)

855

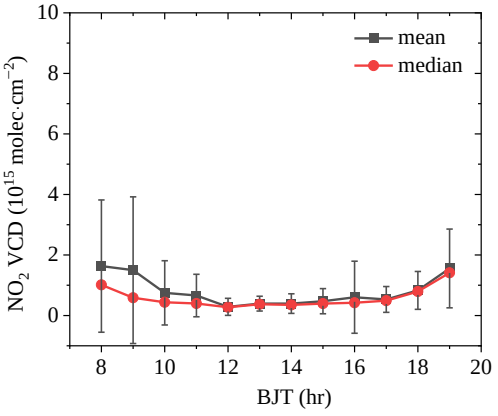
mean
median
NO_2 VCD (10^{15} molec·cm^{-2})
BJT (hr)

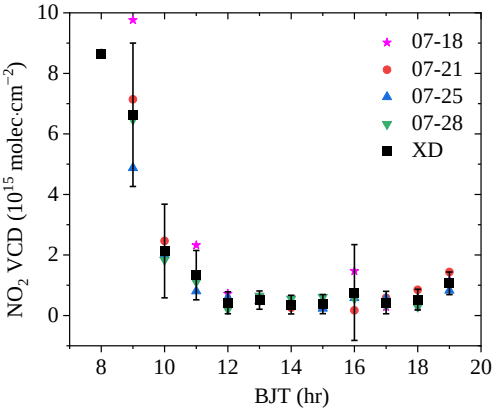
07-18
07-21
07-25
07-28
XD
NO_2 VCD (10^{15} molec·cm^{-2})
BJT (hr)

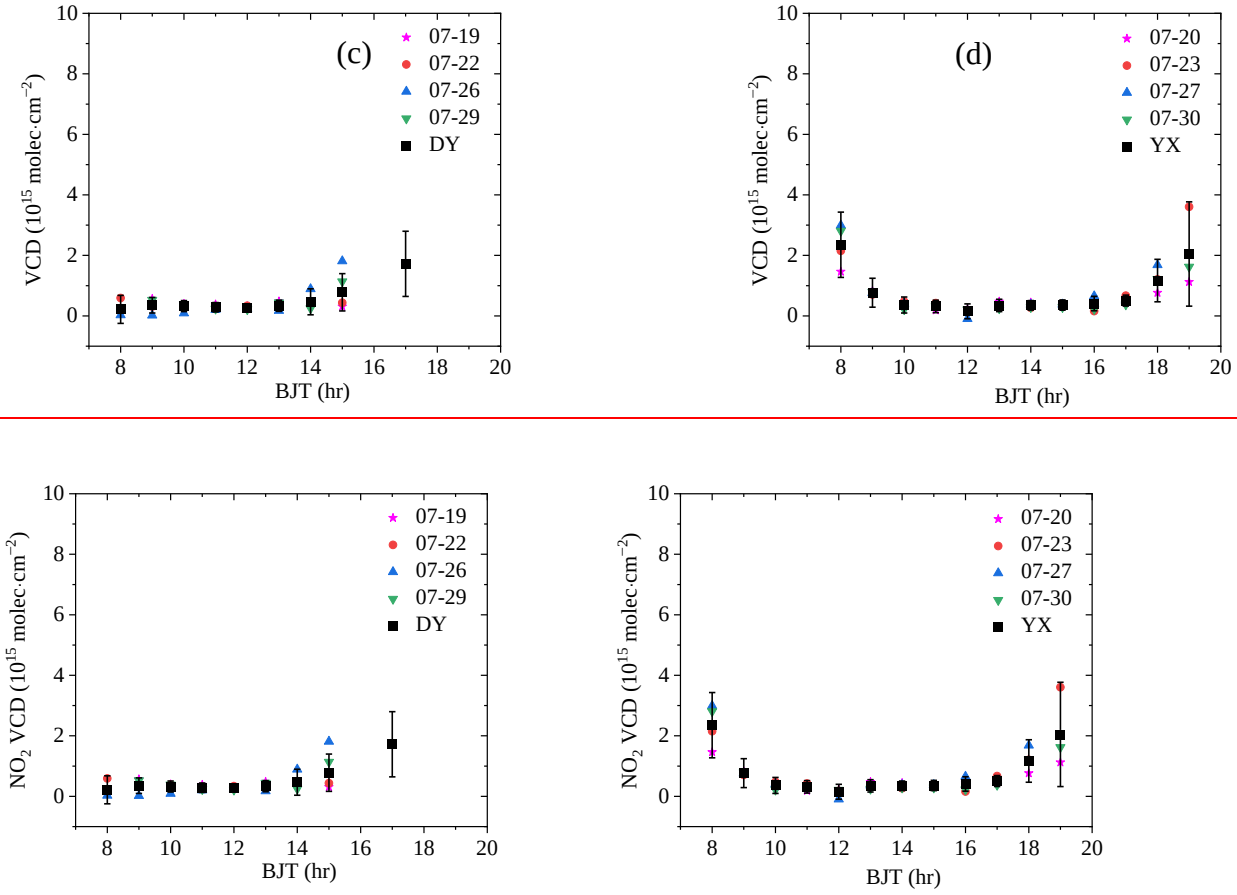

Figure 9. Diurnal variations of the NO_2 VCDs over the mobile observation routes. **(a)** Diurnal variations of the overall means (black curve with squares), medians (red curves with dots), and standard deviations (error bars) of the NO_2 VCDs. **(b)** Diurnal variations of the mean NO_2 VCDs on selected days (18/21/25/28 July 2021) as well as the means and standard deviations of the NO_2 VCDs on the XD driving route. **(c, d)** Same as (b), but for the DY and YX driving routes during the field campaign.

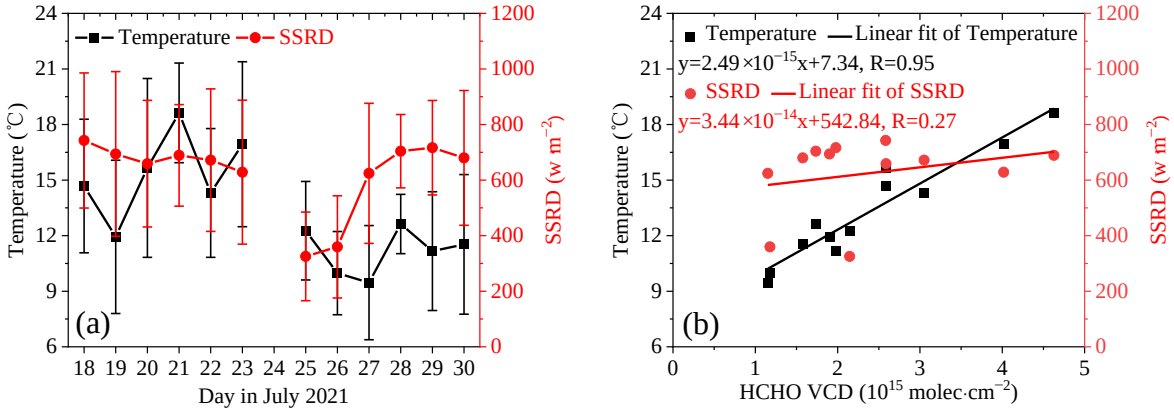

Figure 10. Comparison of the HCHO VCDs with other data sets. **(a)** Day-to-day variations of the mean air temperature at 2 m above the land surface (black curves with squares) and the downward solar radiation at the surface (SSRD, red curves with dots) as well as **(b)** linear fits between the two parameters and the daily averaged HCHO VCDs over the mobile observation routes. The error bars denote the standard deviations of the air temperature and SSRD in figure (a). The lines denote the results of the regression analyses, and the corresponding equations and correlation coefficients are displayed in the figure (b).

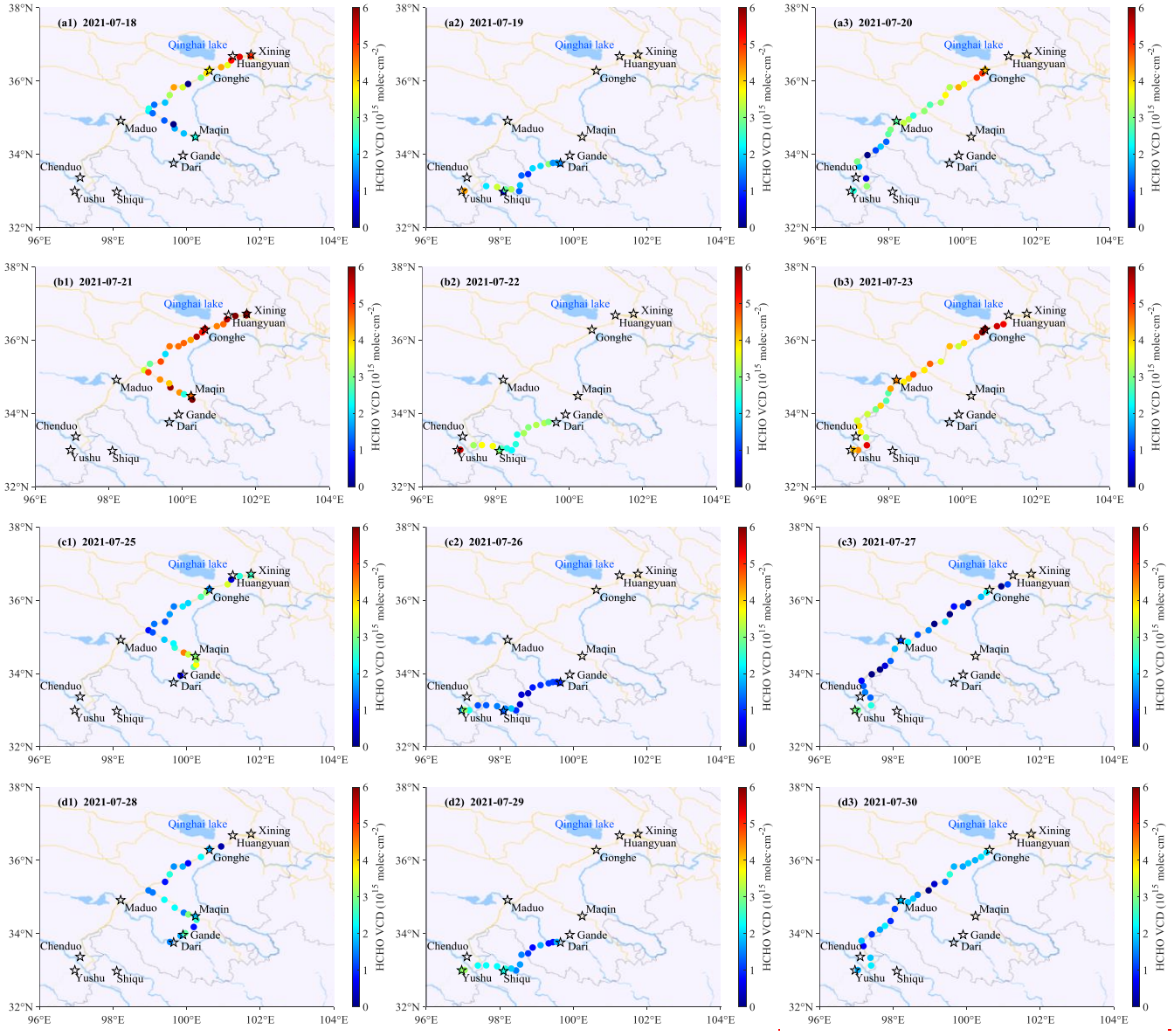
(a1) 2021-07-18
(a2) 2021-07-19
(a3) 2021-07-20
(b1) 2021-07-21
(b2) 2021-07-22
(b3) 2021-07-23
(c1) 2021-07-25
(c2) 2021-07-26
(c3) 2021-07-27
(d1) 2021-07-28
(d2) 2021-07-29
(d3) 2021-07-30
Qinghai lake
Xining
Huangyuan
Gonghe
Maduo
Maqin
Gande
Dari
Chenduo
Yushu
Shiqu
38°N
36°N
34°N
32°N
96°E
98°E
100°E
102°E
104°E
HCHO VCD (10^{15} molec·cm^{-2})
0
1
2
3
4
5
6

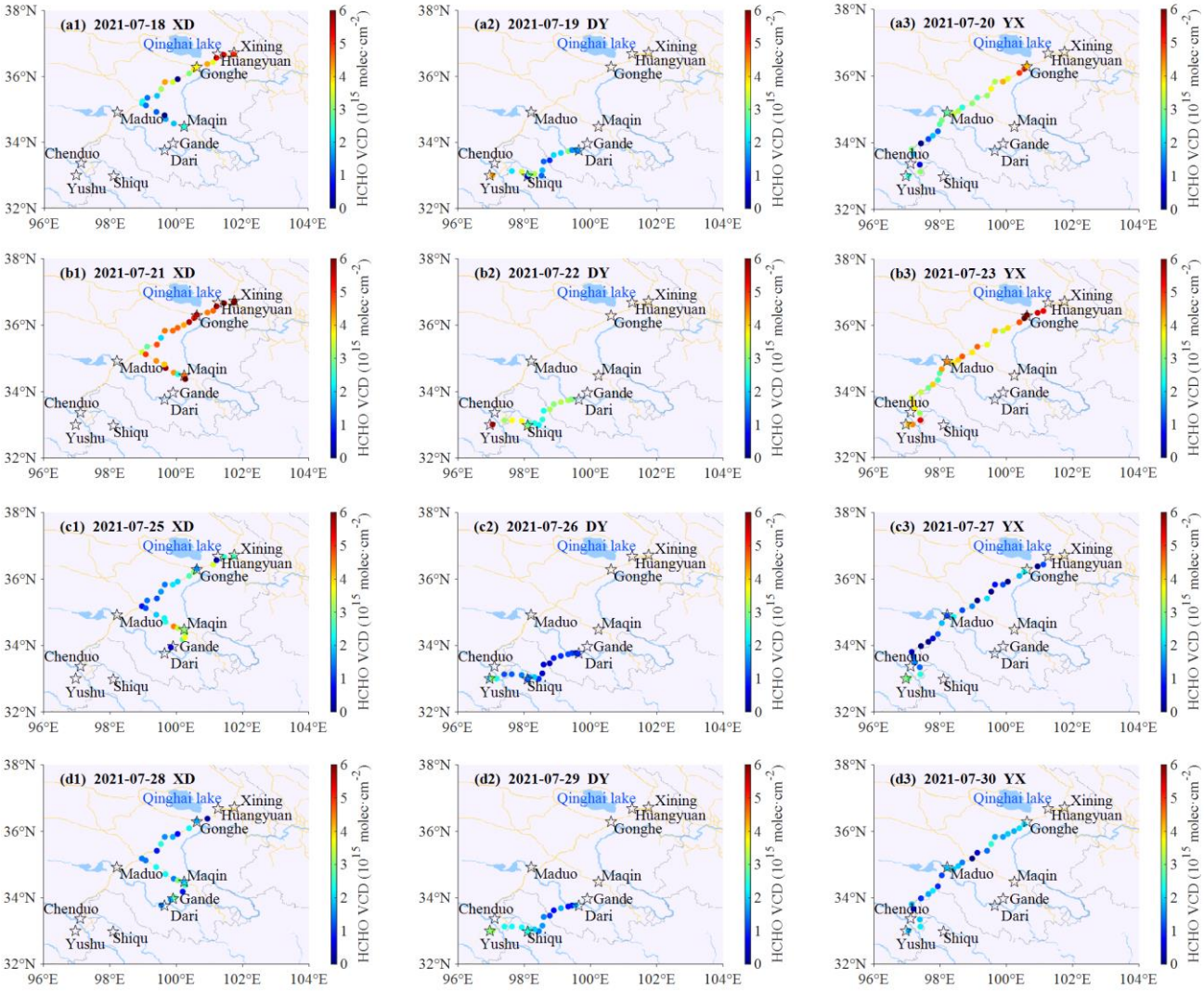

Figure ~~12~~11. Same as figure ~~11~~8, but for HCHO.

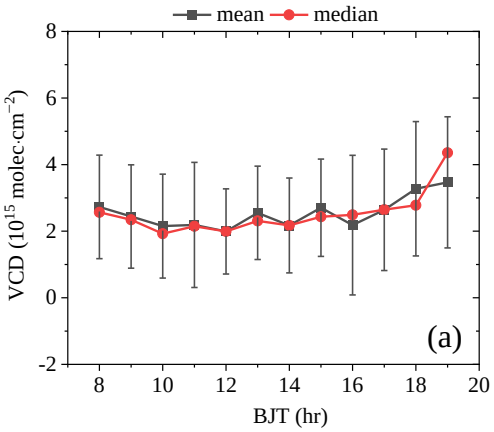
mean
median
VCD (10^{15} molec·cm^{-2})
BJT (hr)
(a)

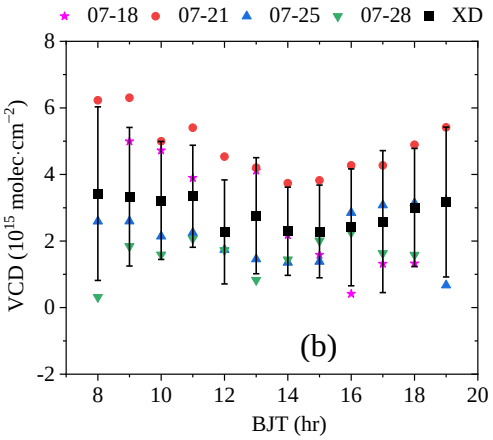
07-18
07-21
07-25
07-28
XD
VCD (10^{15} molec·cm^{-2})
BJT (hr)
(b)

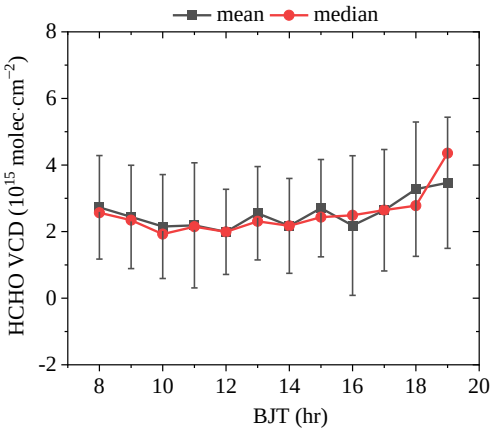
mean
median
HCHO VCD (10^{15} molec·cm^{-2})
BJT (hr)

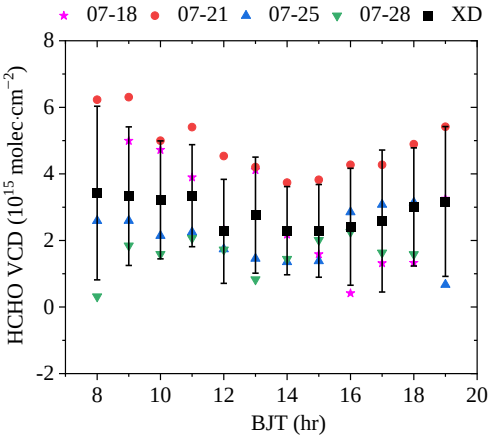
07-18
07-21
07-25
07-28
XD
HCHO VCD (10^{15} molec·cm^{-2})
BJT (hr)

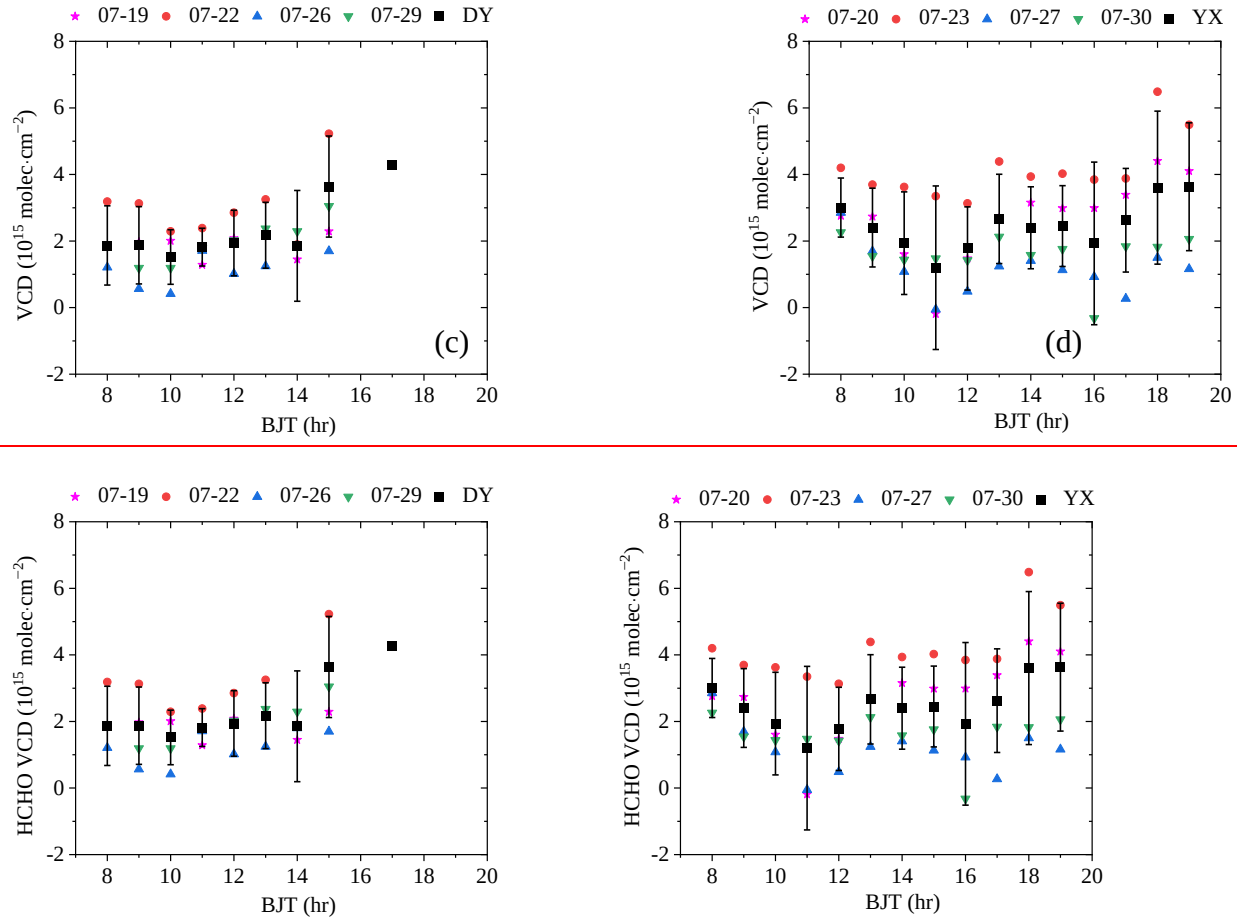

875

Figure ~~10~~12. Same as figure 9, but for HCHO.

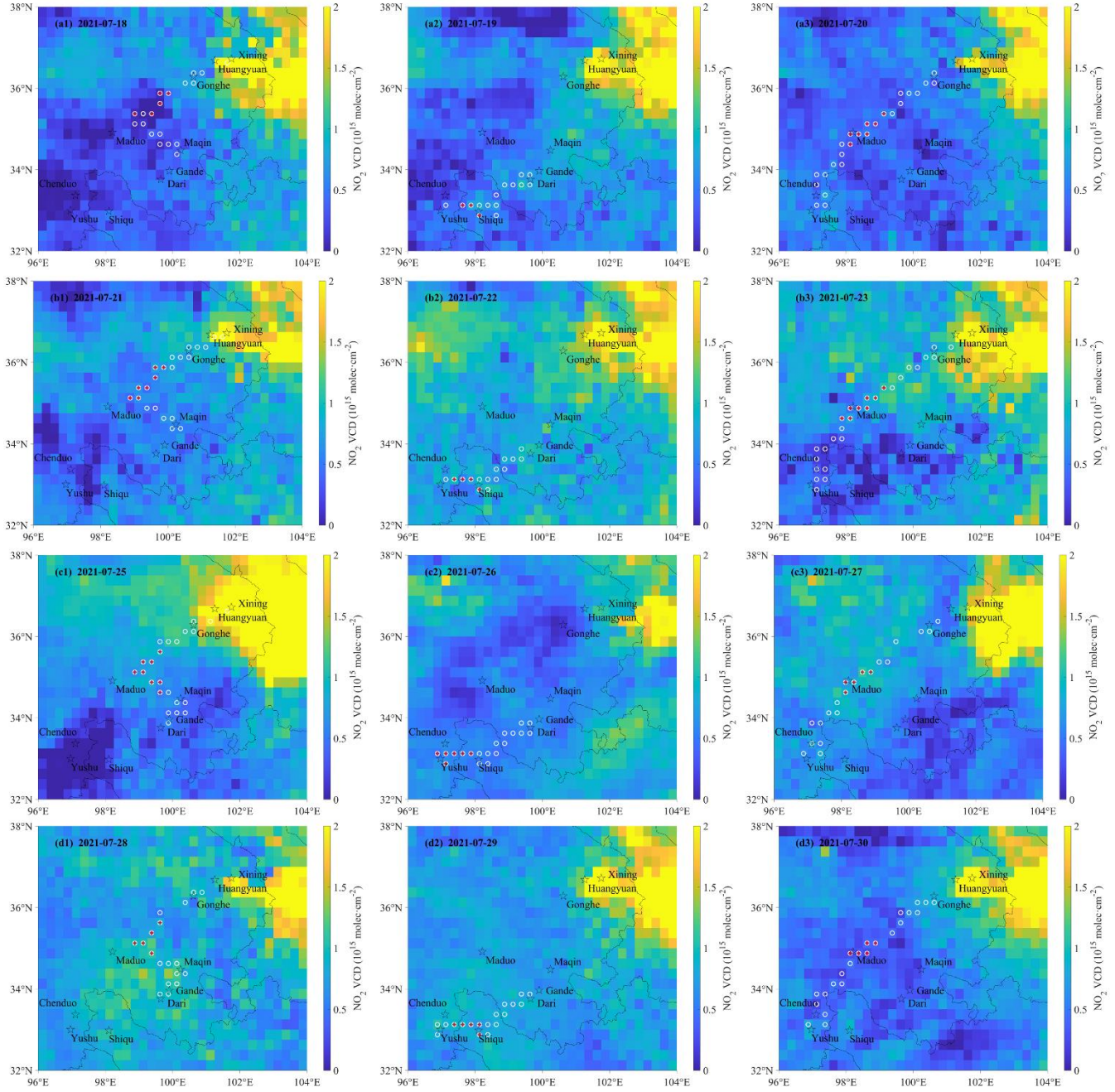

Figure 13. Spatial distributions of the tropospheric NO_2 VCDs observed by TROPOMI on each day of the field campaign. The TROPOMI S5P_L2__NO2____HiR product has been gridded to 0.25 °×0.25 ° cells. The main cities and counties on the driving routes of the field campaign are marked by the black stars. The black curves indicate the administrative boundaries. The white circles and red plus symbols show the grid cell where the data of both TROPOMI and MAX-DOAS are available on the same day or within a 1.5 h time difference, respectively.

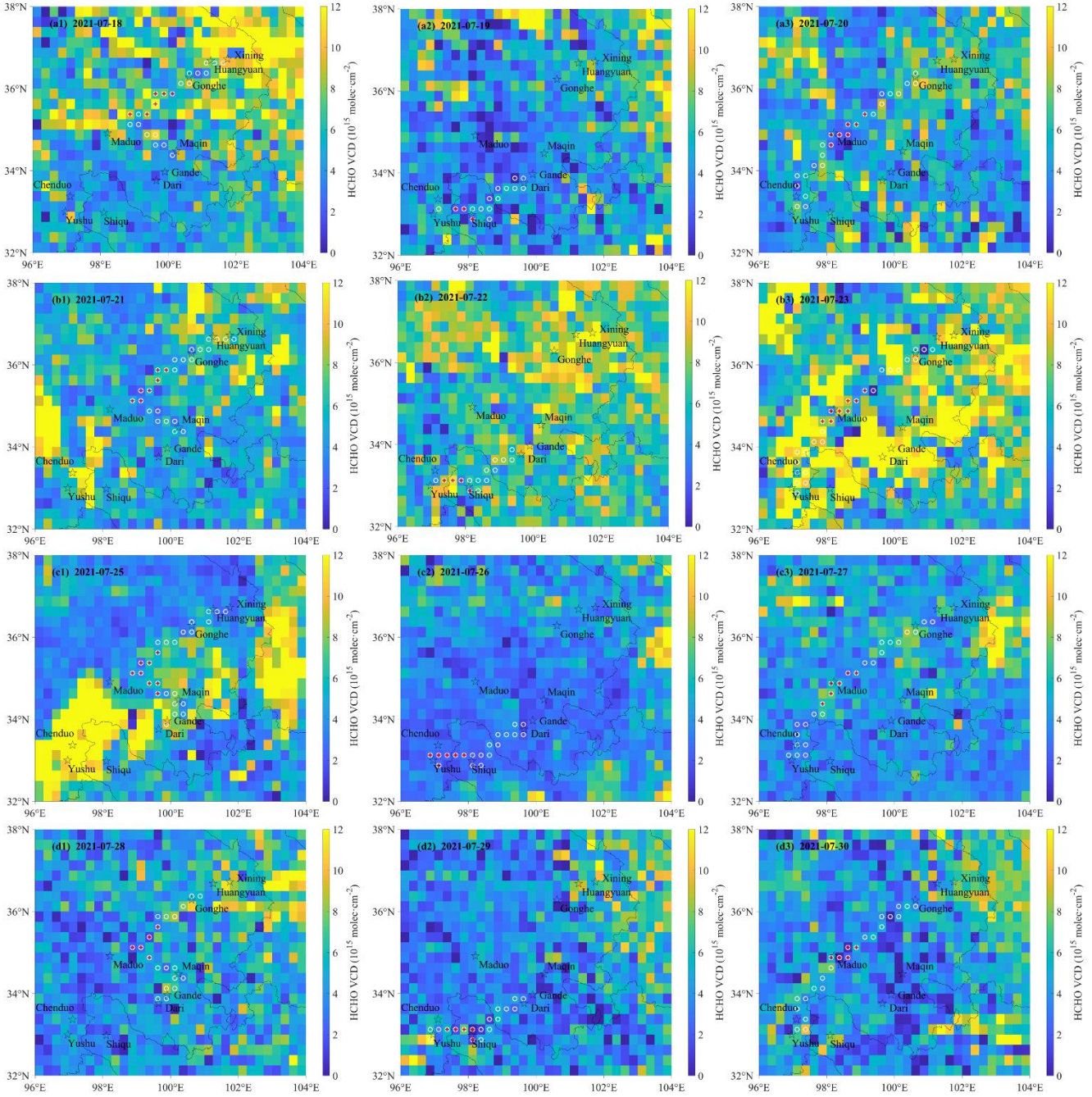

Figure 14. Same as figure 13, but for HCHO.

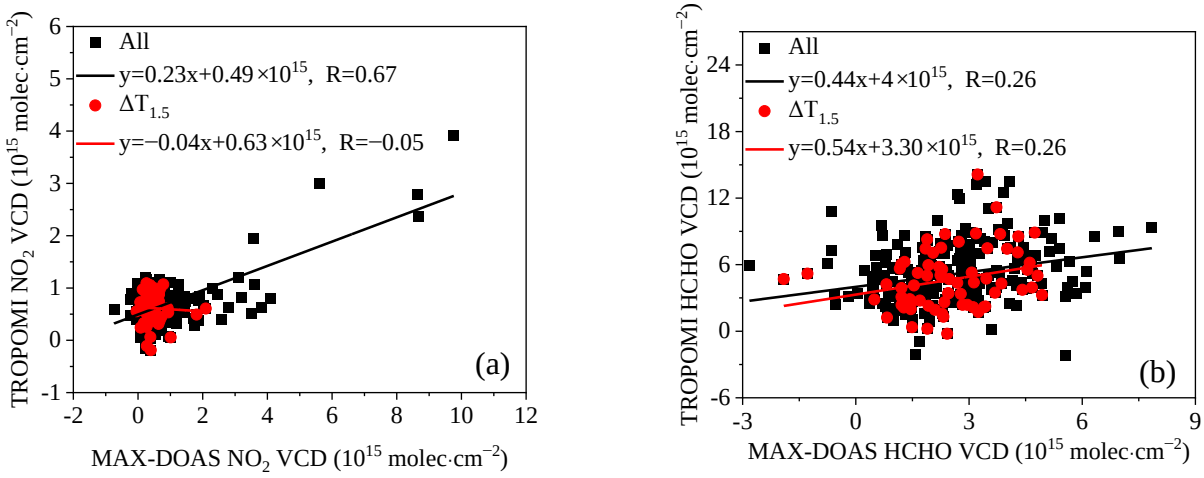

885

Figure 15. Linear fit between the tropospheric **(a)** NO_2 and **(b)** HCHO VCDs measured by the mobile MAX-DOAS and TROPOMI. The black squares and red dots represent the available VCDs of both data sets at the same grid cell on the same day or within a 1.5 h time difference, respectively. The black (red) lines denote the results of the regression analyses and the corresponding equations and correlation coefficients are displayed in the figures.

890